Nanonetworks as Innovative Platforms for Therapeutic Solubilization and Delivery

By

David Michael Stevens

Dissertation

Submitted to the Faculty of the

Graduate School of Vanderbilt University

in partial fulfillment of the requirements

for the degree of

DOCTOR OF PHILOSOPHY

in

Pharmacology

August, 2014

Nashville, Tennessee

Approved:

Eva M. Harth, Ph.D.

W. Scott Akers, Ph.D., Pharm. D.

Joey V. Barnett, Ph.D.

Heidi E. Hamm, Ph.D.

Craig W. Lindsley, Ph.D.

To Jenny and Boethius

ACKNOWLEDGEMENTS

Foremost, I would like to sincerely thank Dr. Eva Harth for her mentorship, guidance, advice, and her willingness to take on a pharmacology student. As my mentor, she has provided invaluable knowledge and opportunities that have helped me grow as both a scientist and a person. Words cannot fully express my gratitude.

Likewise, I would like to thank my committee members for their personal and professional guidance throughout the years. I have appreciated all of the constructive criticisms and advice as their insights have taught me a great deal about scientific research and what to expect as a scientist in the future. I would especially like to thank Dr. Joey Barnett, chairman of my committee, for his extensive advice and discussions dating back to my first year as a graduate student. By example, he has shown me how a good scientist and administrator should act in order to get effective results.

I am extremely grateful to all of the members of the Harth group as they have played a significant role in both my personal and professional life. The group provided a very welcoming and pleasant working atmosphere and made the graduate research experience that much more memorable.

My success would not be possible without the unconditional love and encouragement from my family. I would like to thank my parents for encouraging me to pursue my greatest aspirations and providing the opportunity to make those aspirations become reality. I would also

like to thank my brother, Charlie, who I believe has had the greatest impact on my life and who first challenged me to think critically and outside-the-box.

Lastly, I offer my thanks to anyone who helped or supported me in any way during the completion of my scientific research.

LIST OF FIGURES

TABLE OF CONTENTS

CHAPTER I

INTRODUCTION

Poor water solubility, toxicity, off-target effects, and lack of sustained release formulas are the most significant barriers limiting drug development and drug delivery.[1, 2, 3, 4] Not surprisingly, many promising chemotherapeutics, antibiotics, and peptide therapeutics have failed clinically due to these issues. As a consequence, expensive and time-consuming medicinal chemistry approaches are used to increase solubility of these drugs but often at the expense of drug efficacy. Alternatively, many drugs are shelved, and efforts are used to develop new therapies. A superior, more time- and cost-effective approach is to develop and apply nanoformulations of these promising drugs. This is accomplished using biodegradable nanoparticles or hydrogels that can aid in drug solubilization, have the ability to target the therapeutic cargo to a specific site in the body, and allow for a sustained release of the drug at a defined rate.

While nanotechnology continues to make significant advances in the diagnosis, prevention, and treatment of various diseases[5, 6], significant time and money are expended every year to develop new therapeutics, and the majority fail to enter the market due to solubility. Developed drug delivery vehicles possess the ability to encapsulate or incorporate therapeutic cargo within their networks. In the case of hydrophobic drugs, the drugs are confined to the nanoscale which decreases crystallinity thereby increasing water solubility. In this way, hydrophobic drugs can potentially overcome their solubility issues through encapsulation into a platform drug delivery vehicle.

Biodegradable polymers are widely investigated for their potential as building blocks for advanced drug delivery vehicles. Polyesters remain the most studied class of polymer due to its low immunogenicity, low toxicity, biocompatibility, and hydrolytically cleavable ester bonds.[7] Recently, polycarbonates have garnered significant attention as drug delivery materials due to their low toxicity, amorphous characteristic at room and body temperature, and very slow degradation rates.[8, 9, 10] The ability to utilize these polymers as building blocks for supramolecular drug delivery vehicles is dependent on the ability to consistently synthesize well-defined polymer precursors. Therefore, methods to synthesize functionalized polymers in a well-controlled manner are paramount for the advancement of polymeric drug delivery applications.

Organocatalysts for ring opening polymerization of ester and carbonate monomers are well studied and have received much attention due to their metal-free conditions. This class of catalyst has proven useful for the successful formation of well-defined, functionalized polyesters and polycarbonates which can be used to synthesize supramolecular structures such as hydrogels and nanoparticles.[11, 12] However, most organocatalysts are sensitive to moisture and require very pure monomers thus requiring the use of a glovebox and extensive purification steps.[13, 14] Because of this, time and materials become limiting factors for the synthesis of polymer precursors. Alternatively, metal catalysts for ring opening polymerizations offer significantly less strict reaction conditions. Tin octanoate is one of the most popular of the metal catalysts due to its low toxicity and effectiveness for synthesizing various types of polymers.[15, 16, 17] However, high temperatures, long polymerization times, and high dispersities limit the applicability of this catalyst for well-defined, functionalized polymer precursors. Tin triflate, on the other hand, is not as well studied for the polymerization of functionalized polyesters and polycarbonates but was

2

determined to be an effective catalyst to yield predictable polymers with low dispersities without excessive heat or reaction times.

Of the many obstacles that limit drug effectiveness and applicability, solubility is the most essential factor. Poor water-solubility of drugs is a significant limitation for many promising therapeutics causing low bioavailability, inability to cross membranes, and poor efficacy. Drugs in classes II and IV of the BCS classification system are characterized by poor solubility. For example, paclitaxel is a powerful chemotherapeutic classified as a class IV drug meaning poor solubility as well as poor permeability.[18] Numerous approaches have been utilized to improve the bioavailability and effectiveness of paclitaxel such as attaching to albumin (Abraxane) and administering with Cremophor oil (Taxol). However, toxic side effects and inability for tumor targeting impose significant limitations.[19] Alternatively, drug delivery approaches have been developed to improve the solubility and efficacy of paclitaxel. For example, micelles are capable of loading hydrophobic drugs, but typically result in quick and rapid drug release and accumulation in the liver.[20, 21, 22] Polymeric nanoparticles are heavily investigated for the delivery of hydrophobic drugs such as paclitaxel. However, many lack necessary characteristics such as biodegradability, controlled release, and targeting capabilities.[23, 24, 25] Therefore, a need still remains for the development of a platform drug delivery vehicle capable of tunable and controlled drug release as well as targeting capabilities. An ideal vehicle would have the following characteristics: biodegradable and amorphous structures that can be scaled from 20 nm to 800 nm, have the ability to allow predictable and controlled linear drug release kinetics, achieve efficient encapsulation of hydrophobic drugs that would decrease drug crystallinity and increase solubility, possess functional groups capable of orthogonal chemistries for the attachment of imaging dyes and targeting moieties, and can be

combined with other delivery methods for combined drug delivery therapies. Collectively, the ability to incorporate these unique properties into a single nanoparticle drug delivery system allows for optimization of many drug therapies including cancer, diabetes, and bone healing. The development of this technology allows for the advanced progress of the treatments of these diseases by addressing the critical clinical barrier of drug solubility, sustained release formulas, and targeting.

Of all therapeutic routes, oral delivery is by far the most convenient but also perhaps the most difficult and complex. Therapeutics must be able to survive the acid and enzyme rich conditions of the stomach and gastrointestinal tract, have favorable uptake capability in the intestines, and pass through the metabolic liver before entering systemic blood flow. However, overcoming any one of these barriers can significantly increase the oral bioavailability of a drug. Solubility remains a major issue since solubilization is typically required for intestinal transport.[26] Although nanoparticles can help solubilize hydrophobic drugs, polyester vehicles are believed to degrade rapidly in the stomach due to acid-catalyzed hydrolysis. Also, nanoparticle size plays a significant role in its ability to be taken up intestinally.[27] Lipid-based particles have shown great ability to encapsulate drugs and enhance lipophilicity of the drug for better intestinal uptake, but the lipid makeup of the vehicle leads to secretion of lipase enzyme which breaks down the vehicle in the intestines.[28] Thus, there remains a need for an advanced drug delivery vehicle that will not significantly degrade or release therapeutic cargo in the acidic stomach and also possess an ideal size that can be taken up by the intestines. The advancement of such a vehicle could significantly improve the oral bioavailability of drugs with low solubility and low intestinal uptake.

Combination therapies offer intriguing approaches to treat complex diseases in which multiple signaling pathways are affected. Since drug delivery vehicles are often designed for the delivery of a single class of therapeutic, the delivery of two different classes of therapeutics such as a small molecule and peptide imposes a major challenge. For example, bone morphogenetic protein 2 (BMP2) has become a popular therapeutic due to its ability to improve the bone healing process for numerous orthopedic applications.[29, 30, 31] However, the delivery of peptide and protein therapeutics are particularly challenging since they are often cleared or degraded within hours upon administration. Larger biologically active cargo is also more difficult to incorporate into nano and macro delivery devices. Methods to improve protein therapeutic half-lives primarily rely on pegylation strategies that often lead to decreased efficacy.[32] However, a non-covalent incorporation into a PEG-like environment would mediate a slower degradation/clearance rate and not affect therapeutic efficacy which could significantly improve the use of protein and peptide therapeutics. Therefore, novel delivery systems that are capable of entrapping and delivering various combinations of drugs are necessary and would provide a major impact on the treatment of critical diseases. For example, skeletal disorders associated with neurofibromatosis 1 (NF1), which can result in reduced bone mineral density, long bone dysplasia, and morbidity associated with focal bony lesions, remain difficult to treat despite advances in medicine and technology, and combination therapies may be required to treat these disorders.[33] Noninvasive approaches are limited as most options include surgery, amputation, or open fracture treatments. Ideally, patients could be treated through a single, noninvasive injection. Since solubility remains a major hurdle for most pharmacologically active drugs and sustained release formulas are desired to circumvent frequent dosing, a novel formulation that allows the sustained release of a protein and small molecule drug could prove useful.

A multi-functional nanoparticle that is capable of both imaging dye and targeting ligand attachment would allow not only the potential to act as a way to image specific cells, but also allow for the restricted, targeted delivery of drugs to these cells. For example, two of the primary goals of diabetes research are the development of technology that allows for the tracking of beta cells in the pancreatic islets and technology to deliver therapeutic agents specifically to pancreatic islet cells. Currently, there are a number of interventional strategies under development that seek to promote beta cell regeneration, halt or slow beta cell apoptosis, and protect islets from autoimmune attack. However, these approaches often suffer from undesirable off target effects on other cell types that share common pathways or targets with the pancreatic islet. The ability to specifically target and image these cells remains a major goal for scientists and doctors, and this ability would allow the potential delivery of therapeutic agents such as small molecule drugs or even siRNA specifically to these cells for the improved treatment of patients.

Hydrogels remain an attractive biomaterial for the application of implants and sustained drug release formulas due to their biocompatibility, mechanical properties, and simple synthetic methods. One of the hallmarks of traditional hydrogels is the ability to swell several times their own volume with water, but because of this, drug release through diffusion is often faster than desired. Also, polymers such as acrylates are nondegradable and therefore must be surgically removed after implantation. Alternatively, degradable, more hydrophobic polymers such as polycarbonates could be used to form hydrogels that could allow less water swelling and potentially a slower release of drug over time. Therefore, an appropriate balance of hydrophobic and hydrophilic components within a hydrogel network must be achieved in order to improve the limitation of rapid drug release typically seen in traditional hydrogel systems. The ability to

easily tune the swelling and degradation of a gel would allow for a customizable design that could potentially meet any sustained drug release application.

Dissertation Overview

Nanonetwork strategies have been developed to overcome the issues of drug solubility, toxicity, targeting, sustained release, and combination treatments. Amine-epoxide and thiolene-click intermolecular crosslinking chemistries were used to synthesize supramolecular structures from functionalized polycarbonates and polyesters. Although organocatalysts were initially utilized to synthesize polycarbonates, more practical polymerization conditions were developed utilizing tin triflate to afford well-defined, functionalized polycarbonates and polyesters.

Using epoxide-functionalized polyesters and 2,2'-ethylenedioxy-bis(ethylamine), polyesters underwent an intermolecular crosslinking reaction to form 3-dimensional, nano-sized architectures containing hydrophobic components from the polyester and hydrophilic components from the ethylene-oxide crosslinker. Particles with different crosslinking densities were synthesized and were used to encapsulate and nanosolubilize small molecule drugs such as paclitaxel. The crosslinking density has a critical effect on drug release and can be tailored to release a drug at a defined rate. The ability to withhold the majority of the therapeutic cargo after several hours in simulated gastric fluid indicates the possibility of these polyester nanosponges to act as oral drug delivery vehicles.

In order to treat complex bone disorders by acting on two different signaling pathways, polyester nanoparticles containing a water-insoluble MEK inhibitor was formulated with a polyglycidol matrix containing a protein growth factor, bone morphogenetic protein 2 (BMP2). This combined, injectable formulation allowed for the sustained release of the two different

classes of therapeutics simultaneously, and its usefulness and efficacy were investigated for bone healing applications *in vivo*.

Pendant functional groups on the nanoparticle surface such as allyls and amines were utilized for post-modification reactions, including thiolene-click reactions to attach targeting moieties. For applications that utilized targeting peptides, orthogonal approaches were developed in order to successfully attach both the targeting peptide and an imaging dye without side reactions.

The same concept of using intermolecular crosslinking reactions to form nanoparticles was used to form hydrogels under concentrated conditions. Using allyl-functionalized polycarbonates and PEG-dithiol crosslinkers, polycarbonates underwent intermolecular crosslinking reactions via thiolene-click to form insoluble hydrogel materials. Hydrogels were formed using crosslinkers of different sizes as well as incorporating hydrophilic components (polyglycidol) in the hydrogel network. Gels could also be formed in the presence of drugs such as paclitaxel, thereby entrapping the drug within the gel network. Crosslinker size and presence of polyglycidol both had significant impacts on mechanical properties such as swelling and also significant effects on drug release rates.

References

1. Gewirtz, D.; Bristol, M.; Yalowich, J., Toxicity issues in cancer drug development. *Current Opinion in Investigational Drugs* **2010,** *11* (6), 612-614.

2. Stegemann, S.; Leveiller, F.; Franchi, D.; de Jong, H.; Linden, H., When poor solubility becomes an issue: From early stage to proof of concept. *European Journal of Pharmaceutical Sciences* **2007,** *31* (5), 249-261.

3.   Zhang, Y.; Hong, H.; Cai, W., Tumor-Targeted Drug Delivery with Aptamers. *Current Medicinal Chemistry* **2011,** *18* (27), 4185-4194.

4.   Dey, N.; Majumadar, S.; Rao, M., Multiparticulate Drug Delivery Systems for Controlled Release. *Tropical Journal of Pharmaceutical Research* **2008,** *7* (3), 1067-1075.

5.   Davis, M.; Zuckerman, J.; Choi, C.; Seligson, D.; Tolcher, A.; Alabi, C.; Yen, Y.; Heidel, J.; Ribas, A., Evidence of RNAi in humans from systemically administered siRNA via targeted nanoparticles. *Nature* **2010,** *464* (7291), 1067-U140.

6.   Dimond, P., Using nanotechnologies in biotech and medicine. *Genetic Engineering News* **2005,** *25* (6), 1-+.

7.   Mohamed, F.; van der Walle, C., Engineering biodegradable polyester particles with specific drug targeting and drug release properties. *Journal of Pharmaceutical Sciences* **2008,** *97* (1), 71-87.

8.   Zhu, K.; Hendren, R.; Jensen, K.; Pitt, C., Synthesis, properties, and biodegradation of poly(1,3-trimethylene carbonate). *Macromolecules* **1991,** *24* (8), 1736-1740.

9.   Edlund, U.; Albertsson, A.; Singh, S.; Fogelberg, I.; Lundgren, B., Sterilization, storage stability and in vivo biocompatibility of poly(trimethylene carbonate)/poly(adipic anhydride) blends. *Biomaterials* **2000,** *21* (9), 945-955.

10.   Suyama, T.; Tokiwa, Y., Enzymatic degradation of an aliphatic polycarbonate poly(tetramethylene carbonate). *Enzyme and Microbial Technology* **1997,** *20* (2), 122-126.

11.   Truong, V.; Barker, I.; Tan, M.; Mespouille, L.; Dubois, P.; Dove, A., Preparation of in situ-forming   poly(5-methyl-5-allyloxycarbonyl-1,3-dioxan-2-one)-poly(ethylene   glycol) hydrogels with tuneable swelling, mechanical strength and degradability. *Journal of Materials Chemistry B* **2013,** *1* (2), 221-229.

12.   Stevens, D.; Tempelaar, S.; Dove, A.; Harth, E., Nanosponge Formation from Organocatalytically Synthesized Poly(carbonate) Copolymers. *Acs Macro Letters* **2012,** *1* (7), 915-918.

13.   Nederberg, F.; Lohmeijer, B.; Leibfarth, F.; Pratt, R.; Choi, J.; Dove, A.; Waymouth, R.; Hedrick, J., Organocatalytic ring opening polymerization of trimethylene carbonate. *Biomacromolecules* **2007,** *8* (1), 153-160.

14.   Tempelaar, S.; Mespouille, L.; Dubois, P.; Dove, A. P., Organocatalytic Synthesis and Postpolymerization Functionalization of Allyl-Functional Poly(carbonate)s. *Macromolecules* **2011,** *44* (7), 2084-2091.

15.   Weiser, J.; Zawaneh, P.; Putnam, D., Poly(carbonate-ester)s of Dihydroxyacetone and Lactic Acid as Potential Biomaterials. *Biomacromolecules* **2011,** *12* (4), 977-986.

16.   Zawaneh, P.; Doody, A.; Zelikin, A.; Putnam, D., Diblock copolymers based on dihydroxyacetone and ethylene glycol: Synthesis, characterization, and nanoparticle formulation. *Biomacromolecules* **2006,** *7* (11), 3245-3251.

17.   Zelikin, A.; Zawaneh, P.; Putnam, D., A functionalizable biomaterial based on dihydroxyacetone, an intermediate of glucose metabolism. *Biomacromolecules* **2006,** *7* (11), 3239-3244.

18.   Reddy, B. B. K.; Karunakar, A., Biopharmaceutics Classification System: A Regulatory Approach. *Dissolut Technol* **2011,** *18* (1), 31-37.

19.   Rowinsky, E.; Jiroutek, M.; Bonomi, P.; Johnson, D.; Baker, S., Paclitaxel steady-state plasma concentration as a determinant of disease outcome and toxicity in lung cancer patients treated with paclitaxel and cisplatin. *Clinical Cancer Research* **1999,** *5* (4), 767-774.

20. Gong, C.; Xie, Y.; Wu, Q.; Wang, Y.; Deng, S.; Xiong, D.; Liu, L.; Xiang, M.; Qian, Z.; Wei, Y., Improving anti-tumor activity with polymeric micelles entrapping paclitaxel in pulmonary carcinoma. *Nanoscale* **2012,** *4* (19), 6004-6017.

21. Wang, H.; Tang, L.; Tu, C.; Song, Z.; Yin, Q.; Yin, L.; Zhang, Z.; Cheng, J., Redox-Responsive, Core-Cross-Linked Micelles Capable of On-Demand, Concurrent Drug Release and Structure Disassembly. *Biomacromolecules* **2013,** *14* (10), 3706-3712.

22. McCarley, R.; Forsythe, J.; Loew, M.; Mendoza, M.; Hollabaugh, N.; Winter, J., Release Rates of Liposomal Contents Are Controlled by Kosmotropes and Chaotropes. *Langmuir* **2013,** *29* (46), 13991−13995.

23. Richard, R.; Schwarz, M.; Ranade, S.; Chan, A.; Matyjaszewski, K.; Sumerlin, B., Evaluation of acrylate-based block copolymers prepared by atom transfer radical polymerization as matrices for paclitaxel delivery from coronary stents. *Biomacromolecules* **2005,** *6* (6), 3410-3418.

24. Potineni, A.; Lynn, D.; Langer, R.; Amiji, M., Poly(ethylene oxide)-modified poly(beta-amino ester) nanoparticles as a pH-sensitive biodegradable system for paclitaxel delivery. *Journal of Controlled Release* **2003,** *86* (2-3), 223-234.

25. Smulders, W.; Monteiro, M., Seeded emulsion polymerization of block copolymer core-shell nanoparticles with controlled particle size and molecular weight distribution using xanthate-based RAFT polymerization. *Macromolecules* **2004,** *37* (12), 4474-4483.

26. Mathot, F.; van Beijsterveldt, L.; Preat, V.; Brewster, M.; Arien, A., Intestinal uptake and biodistribution of novel polymeric micelles after oral administration. *Journal of Controlled Release* **2006,** *111* (1-2), 47-55.

27.   Singh, R.; Singh, S.; Lillard, J., Past, present, and future technologies for oral delivery of therapeutic proteins. *Journal of Pharmaceutical Sciences* **2008,** *97* (7), 2497-2523.

28.   Dahan, A.; Hoffman, A., Rationalizing the selection of oral lipid based drug delivery systems by an in vitro dynamic lipolysis model for improved oral bioavailability of poorly water soluble drugs. *Journal of Controlled Release* **2008,** *129* (1), 1-10.

29.   Misch, C., The Use of Recombinant Human Bone Morphogenetic Protein-2 for the Repair of Extraction Socket Defects: A Technical Modification and Case Series Report. *International Journal of Oral & Maxillofacial Implants* **2010,** *25* (6), 1246-1252.

30.   Pradhan, B.; Bae, H.; Dawson, E.; Patel, V.; Delamarter, R., Graft resorption with the use of bone morphogenetic protein: Lessons from anterior lumbar interbody fusion using femoral ring allografts and recombinant human bone morphogenetic protein-2. *Spine* **2006,** *31* (10), E277-E284.

31.   Gerszten, P.; Tobler, W.; Nasca, R., Retrospective analysis of L5-S1 axial lumbar interbody fusion (AxiaLIF): a comparison with and without the use of recombinant human bone morphogenetic protein-2. *Spine Journal* **2011,** *11* (11), 1027-1032.

32.   Veronese, F., Peptide and protein PEGylation: a review of problems and solutions. *Biomaterials* **2001,** *22* (5), 405-417.

33.   Elefteriou, F.; Kolanczyk, M.; Schindeler, A.; Viskochil, D.; Hock, J.; Schorry, E.; Crawford, A.; Friedman, J.; Little, D.; Peltonen, J.; Carey, J.; Feldman, D.; Yu, X.; Armstrong, L.; Birch, P.; Kendler, D.; Mundlos, S.; Yang, F.; Agiostratidou, G.; Hunter-Schaedle, K.; Stevenson, D., Skeletal Abnormalities in Neurofibromatosis Type 1: Approaches to Therapeutic Options. *American Journal of Medical Genetics Part a* **2009,** *149A* (10), 2327-2338.

CHAPTER II

POLYCARBONATE NANOSPONGES SYNTHESIZED FROM ORGANOCATALYZED

CARBONATE COPOLYMERS

Introduction

The synthesis and engineering of biomaterials for applications in tissue engineering, wound healing, and drug delivery are the driving forces in the development of defined and functionalized materials. While the preparation of polyester and polycarbonate based particles has been mainly driven by precipitation processes, chemically driven nanoparticle formation has given the opportunity to control sizes and the architectural nature of the particles. Intramolecular[1, 2] and inter chain-crosslinking processes[3, 4] have been developed into suitable methods to form versatile supramolecular structures. In particular, intermolecular chain cross-linking of side-chain functional polyesters derived by ring-opening polymerization of substituted δ-valerolactone monomers[5, 6, 7] affords controlled nanoparticle sizes that can be varied via the percentiles of side-chain functionalities into the linear polyester precursor. Furthermore, the morphology and size can be controlled with the amount of difunctionalized cross-linking units which react with the side-chain functionality of the polymer. With this, functionalized particles that are further post-modified with targeting units, and upon drug encapsulation, can be tested for their biological response as drug delivery systems.[8, 9] A wide range of degradable polymers have been investigated for *in vivo* applications.[10, 11, 12, 13] Polyesters are most commonly studied due to their degradability and non-toxic degradation products; however, the introduction of side-chain

13

functional groups is typically challenging and can limit their applicability in advanced applications.[11, 14]

Polycarbonates prepared by the ring-opening polymerization (ROP) of 6-membered cyclic monomers have been widely explored for these applications, and organocatalysis has provided efficient routes to realize a range of functionalized polymer structures.[15, 16, 17] Recently, a range of functional monomers and polymers have been explored from simple precursors giving access to unprecedented levels of functional group incorporation.[18, 19, 20] Importantly, polycarbonate materials display slower degradation profiles with less toxic byproducts than polyesters thus making them ideal candidates as one of the building blocks for advanced nanomaterials.[14] Herein, we demonstrate that synthesized allyl-functional aliphatic polycarbonates can be transformed into epoxide-functional aliphatic polycarbonates and can be employed in the intermolecular chain crosslinking process for the synthesis of polycarbonate nanosponges.

Results and Discussion

Advanced organocatalytic synthesis methods were employed to prepare linear polycarbonates with control over functional group incorporation and molecular weight. The incorporation of the allyl group allows for immediate nanosponge formation via thiolene click reactions or further modification through full conversion of the allyl to an epoxide. Pendant allyl or epoxide groups served as reaction partners in thiolene click or epoxide-amine reactions with ethylene oxide-containing crosslinkers to form a panel of six novel polycarbonate nanosponges with crosslinking densities containing 5, 10, or 20% via an intermolecular chain crosslinking approach.

Synthesis of ethyl and allyl functionalized carbonate monomers
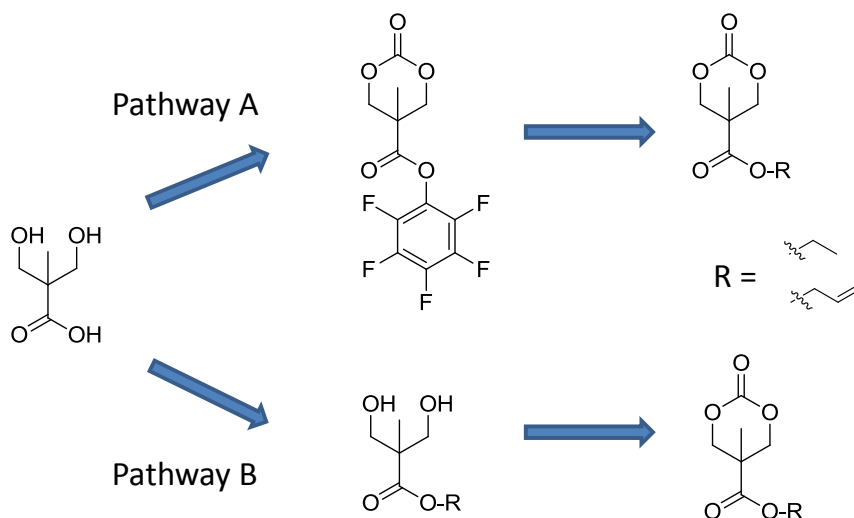
Figure II-1. Two reported synthetic pathways to form allyl and ethyl functionalized cyclic carbonate monomers.

The ability to synthesize cyclic monomers with various functional groups in a cost-effective and high yielding manner is paramount for the production and application of advanced polymer systems. To achieve this, numerous approaches have focused on the use of cyclic carbonate monomers derived from 1,3-diols. For example, a simple, two-step synthesis has been utilized to synthesize cyclic carbonate monomers with a wide variety of functional groups.[18] In this approach, 2,2-bis(hydroxymethyl)-propionic acid undergoes both ring-closing and a pentafluorophenyl attachment at the carboxylic acid in a single step. In the second step, nucleophilic substitution is utilized to attach various functionalities since pentafluorophenyl is an excellent leaving group (Figure II-1 pathway A). This pathway is advantageous since it requires only two steps and the reactive intermediate after the first step can be utilized to form various other functionalized monomers in the second step such as bromo, chloro, and alkyne

functionalities. However, this pathway is also quite expensive and yields are generally low (less than 50%).

An alternative two-step synthesis pathway can be used to form the same functionalized monomers but at significantly lower costs and higher yields. In this approach, 2,2-bis(hydroxymethyl)-propionic acid first undergoes esterification followed by ring-closing in the second step (Figure II-1 pathway B). For example, 2,2-bis(hydroxymethyl)-propionic acid can react with ethanol using heat and Amberlyst-15 resin to form ethyl 3-hydroxy-2-(hydroxymethyl)-2-methylpropanoate (88% yield) followed by a ring closure reaction using triethylamine and ethyl chloroformate (71% yield). Although each functionalized monomer must undergo its own individual synthetic route as opposed to using a single reactive intermediate seen in pathway A, the yields are significantly higher while keeping costs significantly lower.

Synthesis of functionalized, linear polycarbonates

Extension of the organocatalytic methods for ROP of 5-methyl-5-allyloxycarbonyl-1,3-dioxane-2-one (MAC) was undertaken to prepare a series of novel copolymers with 5-methyl-5-ethyloxycarbonyl-1,3-dioxane-2-one (MEC) to provide a series of three copolymers (Figure II-3) initiated from benzyl alcohol using the (−)-sparteine/thiourea catalyst system with controlled functional group densities.[21] The observed copolymers showed good control in molecular weight but slightly broad dispersities that are a consequence of high molecular weight tailing of the polymer distributions at high conversions (Figure II-3). It was decided that these polymers were suitable to test the ability and performance in nanoparticle formation since the incorporation of the MAC monomer, which contains the allyl functionality, was consistent with the monomer feed ratios as confirmed by ^{1}H NMR spectroscopy. As an alternative methodology, particle

formation using epoxide-amine crosslinking chemistry was also employed. As previously demonstrated by Storey and coworkers[22], the oxidation of allyl-functional polycarbonates with meta-chloroperoxybenzoic acid (mCPBA) results in the formation of the epoxide-functional polymers. This provides an alternative group that is very valuable to the synthesis of nanoparticles and functionalization reactions for surface labeling.
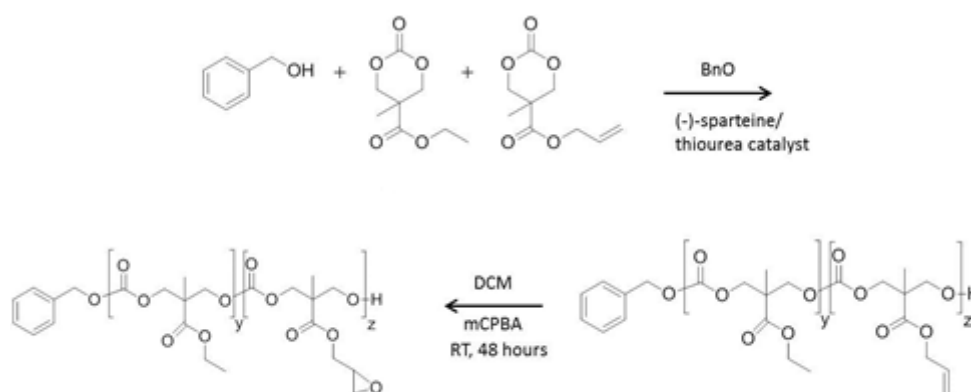
Figure II-2. Synthesis of allyl-functionalized polycarbonate copolymers and their subsequent conversion to epoxide groups.

The MAC-containing copolymers were fully epoxidized (100% conversion as indicated by ^{1}H NMR analysis) by treatment with 1.2 equivalents mCPBA in CH_2Cl_2 to form the suitable linear precursor. The disappearance of the characteristic alkene resonances in the range $\delta = 5.9-5.3$ ppm was observed with the appearance of resonances that are clearly attributable to the formation of epoxide-functional polymers at $\delta = 3.19$, 2.82, and 2.63 ppm. Other resonances in the ^{1}H NMR spectra of the polymers did not change and the same chain length was determined by end group analysis.
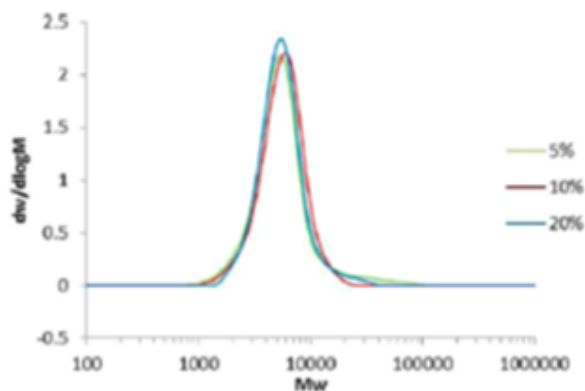
Polymer Composition (MEC:MAC)	Monomer Conversion (%)	Mn (GPC) (Da)	Mn (NMR) (Da)	PDI
95:5	> 95	4700	5000	1.56
90:10	> 95	5000	5300	1.25
80:20	> 95	4900	6400	1.39

Figure II-3. Molecular weight and PDI were determined using GPC calibrated with poly(styrene) standards in chloroform. Conversion and molecular weight were determined by NMR. The legend for the GPC traces refers to the percentile of MAC monomer in the copolymer.

Polycarbonate nanosponge formation via thiolene-click chemistry

The ability of the copolymers to form nanoparticles was investigated initially via the previously developed thiolene-click chemistry. To investigate polycarbonate-based nanosponge formation, a panel of three copolymers containing 5, 10, and 20% MAC was planned to react with the dithiolethyleneoxide crosslinker. We sought to keep the equivalents of the difunctionalized crosslinker constant to investigate the control of size dimensions with a variation of the cross-linking density in the linear precursor; therefore, all reactions were completed using 4 equivalents of respective difunctionalized crosslinker (8 equivalents thiol/allyl). Transmission electron microscopy (TEM) and dynamic light scattering (DLS) analysis demonstrated that polycarbonate-based nanosponges could be successfully prepared employing intermolecular crosslinking reactions. The increasing amount of allyl functionality in

18

the polymer backbone led to larger particles for the series as displayed by the number-average

hydrodynamic diameters, D_h = 220 nm for the 20% crosslinker-containing particles, in contrast

to smaller particle sizes of D_h = 150 nm for the particles prepared with 5% MAC comonomer

incorporated. The DLS data shown in Figure II-5 in logarithmic scale underlined the chemically

driven nanoparticle formation via the intermolecular chain collapse process using the cross-

linking density to control the nanoparticle formation. In comparison to thiolene-click reactions

with analogous polyester linear polymers[7], the polycarbonate-derived particles are smaller than

expected, attributed to a lower degree of polymerization (DP) of the polycarbonate copolymers

Figure II-4. Intermolecular chain crosslinking with either amine-epoxide or thiolene-click
chemistries to form nanosponges.

(DP = 20) than those reported from the polyester polymers and its analogs (DP = 50). Regardless, particles of increasing diameter could be synthesized between 150 nm and 220 nm by increasing the percentage of allyl functionality between the range of 5% and 20% present in the polycarbonate precursor.

Polycarbonate nanosponge formation via amine-epoxide chemistry
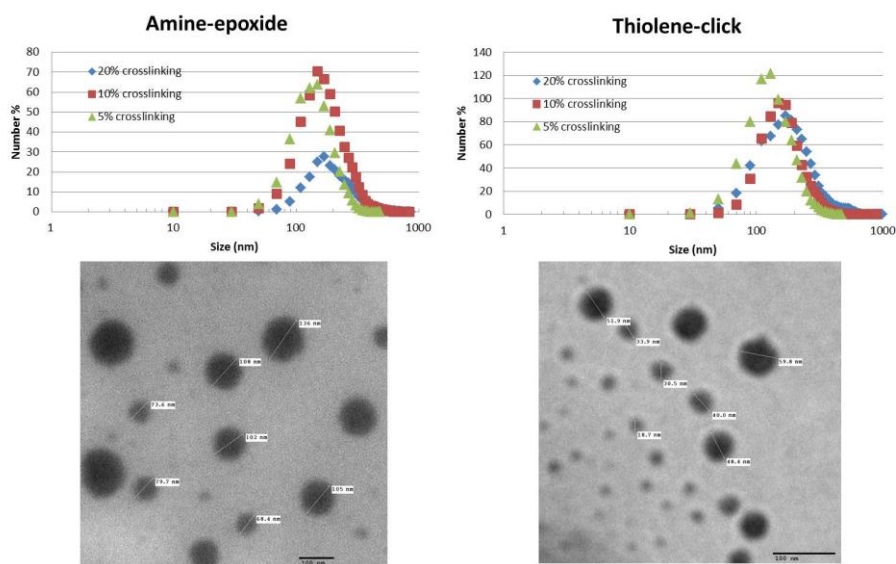
Figure II-5. Top row: DLS analysis data for both particle series derived from the two panels of copolymer precursors with amine-epoxide and the thiolene-click reactions. TEM images of two representative polycarbonate nanosponges: left, 5% amine−epoxide; right, 5% thiolene-click.

Reaction of the panel of functionalized copolymers containing 5, 10, and 20% epoxide pendant functional groups with 4 equivalents diaminoethyleneoxide (8 equivalents amine/epoxide) was performed to crosslink the polymers. Analysis of the resultant nanosponges, again by TEM and DLS, demonstrated that particle size was dependent on crosslinking density

as can be seen for sizes of $D_h = 230$ nm for the particles with 20% cross-linking in contrast to D_h = 160 nm for particles prepared from the lowest crosslinking density available in the study (Figure II-5). In comparison to analogous polyester materials, the particle sizes are again smaller, attributed to the lower degree of polymerization in contrast to the previously investigated polyester materials. Notably, however, the different preparation methods have resulted in comparably sized particles, demonstrating the versatile synthesis of these nanomaterials. Therefore, polycarbonate nanoparticles can be synthesized using either thiolene-click or amine-epoxide to achieve similar sized particles.

Conclusion

In summary, for the first time, we have demonstrated the formation of a range of novel functionalized polycarbonate nanoparticles using two different chemistries with the established intermolecular cross-linking process. We have prepared functionalized polycarbonate copolymers of 5-methyl-5-allyl-oxycarbonyl-1,3-dioxan-2-one (MAC) and 5-methyl-5-ethyloxycarbonyl-1,3-dioxane-2-one (MEC) via organocatalytic synthesis under mild conditions using a thiourea and (−)-sparteine catalyst system. The pendant allyl groups were utilized as cross-linking partners in thiolene click reactions forming nanosponges in the sizes of 150−220 nm depending on the cross-linking density of the linear precursor with 5, 10, and 20% of pendant allyl groups incorporated. The oxidation of the allyl groups in the copolymers to epoxides was successful, and the following crosslinking reaction with diamines enabled the synthesis of the nanosponge particles in size ranges of 160−230 nm using the alternative epoxide-amine chemistry. The ability to synthesize particles of similar size from two different chemistries demonstrates the versatility of this technology to be used for advanced materials. These studies

demonstrate the potential to form a basis for complex degradable nanoparticle syntheses for controlled release applications.

Experimental

Materials

CDCl$_3$ and (-)-sparteine were dried over CaH$_2$, distilled, degassed and stored under inert atmosphere. Benzyl alcohol was dried and stored over 4 Å molecular sieves under inert atmosphere. Methylene chloride was purified over an Innovative Technology SPS alumina solvent column and degassed before use. 5-Methyl-5-allyloxycarbonyl-1,3-dioxan-2-one (MAC) and 5-methyl-2-oxo-1,3-dioxane-5-carboxylate (MEC) were synthesized as reported previously[23], [24] and recrystallized several times before use and dried over CaH$_2$ in dry THF at 50-60 °C. 1-(3,5-Bis(trifluoromethyl)phenyl)-3-cyclohexylthiourea was synthesized as previously reported[25] then dried over calcium hydride in dry tetrahydrofuran and recrystallized from dry methylene chloride. Silica Gel (pore size = 40 Å) was obtained from Fisher Scientific and used as received. All other solvents and chemicals were obtained from Sigma Aldrich or Fisher Scientific and used as received.

Characterization

Polymerizations were performed under inert atmosphere in a glovebox. ^{1}H NMR and ^{13}C NMR spectra at Warwick were recorded on a Bruker DPX-300, DPX-400, DRX-500 or AV II-700 spectrometer at 293K. Chemical shifts are reported as δ in parts per million (ppm) and referenced to the residual solvent signal (CDCl3: ^{1}H, δ = 7.26 ppm; 13C, δ = 77.16 ppm; (CD$_3$)$_2$SO: 1H, δ = 2.50; 13C, δ = 39.52). Gel-permeation chromatography (GPC) was used to determine the

molecular weights and polydispersities of the synthesized polymers. GPC in THF was conducted on a system composed of a Varian 390-LC-Multi detector suite fitted with differential refractive index (DRI), light scattering (LS), and ultraviolet (UV) detectors equipped with a guard column (Varian Polymer Laboratories PLGel 5 μM, 50 × 7.5 mm) and two mixed D columns (Varian Polymer Laboratories PLGel 5 μM, 300 × 7.5 mm). The mobile phase was either tetrahydrofuran eluent or tetrahydrofuran with 5% triethylamine eluent at a flow rate of 1.0 mL/min, and samples were calibrated against Varian Polymer Laboratories Easi-Vials linear poly(styrene) standards (162-3.7 × 105 g mol^{-1}) using Cirrus v3. The dymamic light scattering (DLS) measurements were performed by Mr. Jerry Cabiness from Nanosight Inc. and were measured in CH_2Cl_2 as solvent. Samples for transmission electron microscopy (TEM) imaging were prepared by dissolving 0.5 mg nanoparticles in a solution of 1 mL isopropanol, 0.3 mL acetonitrile and 0.2 mL toluene. The samples were sonicated for 5 min and stained with 3 drops of 3% phosphotungstic acid. The carbon grids were prepared by slowly dipping an Ultrathin Carbon Type-A 400 Mesh Copper Grid (Ted Pella, Inc., Redding, CA) into the particle solution three times and air drying the grid at room temperature. A Philips CM20T transmission electron microscope operating at 200 kV in bright-field mode was used to obtain TEM micrographs of the polymeric nanoparticles.

General procedure for Ring–Opening Polymerization

Polymerizations were completed in glovebox. A solution of ethyl 5-methyl-2-oxo-1,3-dioxane-5-carboxylate (397 mg, 2.112 mmol) and allyl 5-methyl-2-oxo-1,3-dioxane-5-carboxylate (106 mg, 0.528 mmol) in CH_2Cl_2 (0.84 mL) was added to a stirred solution of 1-(3,5-bis(trifluoromethyl)phenyl)-3-cyclohexylthiourea (97.8 mg, 0.264 mmol), benzyl alcohol (13.7

μL, 0.132 mmol) and sparteine (30.3 μL, 0.132 mmol) in CH_2Cl_2 (0.84 mL). After the allotted period of time, the reaction was twice precipitated from CH_2Cl_2 into hexanes and dried under reduced pressure. Residual catalyst impurities were removed by column chromatography on silica (80% hexanes, 20% ethyl acetate). Purified polymer was dried under reduced pressure. ^{1}H NMR (400MHz, CDCl$_3$/TMS, ppm) δ: 7.37 (m, OBn-ArH), 5.9 (m, CHvinyl), 5.3 (m, CH$_2$-vinyl), 5.15 (s, OBn-CH$_2$), 4.64 (m, O*CH$_2$*CHCH$_2$), 4.40-4.18 (m, MAC & MEC, OC(O)OCH$_2$), 1.30-1.22 (m, MAC, CH$_3$; MEC, OCH$_2$*CH$_3$*)

General procedure for oxidation of copolymers

3-Chloroperoxybenzoic acid (30.4 mg, 0.176 mmol) was added to a stirred solution of poly(MEC, MAC) (0.200 g, 0.214 mmol) in CH_2Cl_2 (3.7 mL). The mixture stirred for 48 hours at room temperature. Residual 3-chloroperoxybenzoic acid was removed by dialysis against dichloromethane using Spectra/Por Dialysis Membrane (MWCO = 2,000) to yield pure polymer (0.180 g). ^{1}H NMR (400MHz, CDCl$_3$/TMS, ppm) δ: The significant change is the disappearance of the allylic protons at 5.9 and 5.3 ppm and the emergence of small broad peaks at 3.19, 2.82, and 2.63 ppm due to formation of the epoxide ring.

Poly(5% MAC, 95% MEC) nanoparticle formation using thiolene crosslinking

3,6-dioxa-1,8-octane-dithiol (18.4 μL, 0.113 mmol) was added to a solution of poly(5% MAC, 95% MEC) (100 mg, Mn = 5.0 kDa, PDI = 1.56) in CH_2Cl_2 (8.7 mL). The reaction mixture refluxed for 12 hours at 45 °C. Residual crosslinker was removed by dialyzing with SnakeSkin Pleated Dialysis Tubing (MWCO = 10,000) against CH_2Cl_2 to yield particles (96 mg). ^{1}H NMR (400MHz, CDCl$_3$/TMS, ppm) δ: The significant change is the disappearance of the allylic

protons at 5.9 and 5.3 ppm and the emergence of peaks at 3.64 ppm due to the methylene protons adjacent to the oxygens in the crosslinker and 2.73-2.68 ppm due to methylene protons adjacent to the sulfide functionality.

Poly(10% MAC, 90% MEC) nanoparticle formation using thiolene crosslinking

3,6-dioxa-1,8-octane-dithiol (34.3 μL, 0.209 mmol) was added to a solution of poly(10% MAC, 90% MEC) (100 mg, Mn = 5.3 kDa, PDI = 1.25) dissolved in CH_2Cl_2 (16.2 mL). The reaction mixture refluxed at 12 hours at 45 °C. Residual dithiol was removed by dialyzing with SnakeSkin Pleated Dialysis Tubing (MWCO = 10,000) against CH_2Cl_2 to yield particles (90 mg). ^{1}H NMR (400MHz, CDCl$_3$/TMS, ppm) δ: The significant change is the disappearance of the allylic protons at 5.9 and 5.3 ppm and the emergence of peaks at 3.64 ppm due to the methylene protons adjacent to the oxygens in the crosslinker and 2.73-2.68 ppm due to methylene protons adjacent to the sulfide functionality.

Poly(20% MAC, 80% MEC) nanoparticle formation using thiolene crosslinking

3,6-dioxa-1,8-octane-dithiol (70.1 μL, 0.428 mmol) was added to a solution of poly(20% MAC, 80% MEC) (100 mg, Mn = 6.4 kDa, PDI = 1.39) in CH_2Cl_2 (33.0 mL). The reaction mixture refluxed at 12 hours at 45 °C. Residual dithiol was removed by dialyzing with SnakeSkin Pleated Dialysis Tubing (MWCO = 10,000) against CH_2Cl_2 to yield particles (90 mg). ^{1}H NMR (400MHz, CDCl$_3$/TMS, ppm) δ: The significant change is the disappearance of the allylic protons at 5.8 and 5.3 ppm and the emergence of peaks at 3.64 ppm due to the methylene protons adjacent to the oxygens in the crosslinker and 2.73-2.68 ppm due to methylene protons adjacent to the sulfide functionality.

Poly(5% MTC-epox, 95% MEC) nanoparticle formation using epoxide-amine crosslinking

2,2'-ethylenedioxy-bis(ethylamine) (22.9 μL, 0.157 mmol) was added to a solution of poly(5% MTC-epox, 95% MEC) (140 mg, Mn = 5.0 kDa, PDI = 1.56) dissolved in CH_2Cl_2 (12.1 mL). The reaction mixture refluxed at 12 hours at 45 °C. Residual bisamine was removed by dialyzing with Snakeskin Pleated Dialysis Tubing (MWCO = 10,000) against CH_2Cl_2 to yield particles (130 mg). 1H NMR (400MHz, CDCl$_3$/TMS, ppm) δ: The significant change is the disappearance of the epoxide ring protons at 3.19, 2.82, and 2.63 ppm and the emergence of peaks at 3.62-3.56 ppm due to the methylene protons adjacent to the oxygens in the crosslinker and 3.36 ppm corresponding to the protons neighboring the secondary amine of the PEG linker after crosslinking.

Poly(10% MTC-epox, 90% MEC) nanoparticle formation using epoxide-amine crosslinking

2,2'-ethylenedioxy-bis(ethylamine) (27.0 μL, 0.187 mmol) was added to a solution of poly(10% MTC-epox, 90% MEC) (90 mg, Mn = 5.3 kDa, PDI = 1.25) dissolved in CH_2Cl_2 (14.4 mL). The reaction mixture refluxed at 12 hours at 45 °C. Residual bisamine was removed by dialyzing with Snakeskin Pleated Dialysis Tubing (MWCO = 10,000) against CH_2Cl_2 to yield particles (71 mg). ^{1}H NMR (400MHz, CDCl$_3$/TMS, ppm) δ: The significant change is the disappearance of the epoxide ring protons at 3.19, 2.82, and 2.63 ppm and the emergence of peaks at 3.62-3.56 ppm due to the methylene protons adjacent to the oxygens in the crosslinker and 3.36 ppm corresponding to the protons neighboring the secondary amine of the PEG linker after crosslinking.

Poly(20% MTC-epox, 80% MEC) nanoparticle formation using epoxide-amine crosslinking

2,2'-ethylenedioxy-bis(ethylamine) (61.8 μL, 0.420 mmol) was added to a solution of poly(20% MTC-epox, 80% MEC) (100 mg, Mn = 6.6 kDa, PDI = 1.39) dissolved in CH_2Cl_2 (32.5 mL). The reaction mixture refluxed at 12 hours at 45 °C. Residual bisamine was removed by dialyzing with Snakeskin Pleated Dialysis Tubing (MWCO = 10,000) against CH_2Cl_2 to yield particles (74 mg). ^{1}H NMR (400MHz, $CDCl_3$/TMS, ppm) δ: The significant change is the disappearance of the epoxide ring protons at 3.19, 2.82, and 2.63 ppm and the emergence of peaks at 3.62-3.56 ppm due to the methylene protons adjacent to the oxygens in the crosslinker and 3.36 ppm corresponding to the protons neighboring the secondary amine of the PEG linker after crosslinking.

References

1.   Beck, J. B.; Killops, K. L.; Kang, T.; Sivanandan, K.; Bayles, A.; Mackay, M. E.; Wooley, K. L.; Hawker, C. J., Facile Preparation of Nanoparticles by Intramolecular Cross-Linking of Isocyanate Functionalized Copolymers. *Macromolecules* **2009,** *42* (15), 5629-5635.

2.   Seo, M.; Beck, B. J.; Paulusse, J. M. J.; Hawker, C. J.; Kim, S. Y., Polymeric nanoparticles via noncovalent cross-linking of linear chains. *Macromolecules* **2008,** *41* (17), 6413-6418.

3.   Ryu, J. H.; Chacko, R. T.; Jiwpanich, S.; Bickerton, S.; Babu, R. P.; Thayumanavan, S., Self-Cross-Linked Polymer Nanogels: A Versatile Nanoscopic Drug Delivery Platform. *Journal of the American Chemical Society* **2010,** *132* (48), 17227-17235.

4.   Ryu, J. H.; Jiwpanich, S.; Chacko, R.; Bickerton, S.; Thayumanavan, S., Surface-Functionalizable Polymer Nanogels with Facile Hydrophobic Guest Encapsulation Capabilities. *Journal of the American Chemical Society* **2010,** *132* (24), 8246-+.

5.   van der Ende, A. E.; Kravitz, E. J.; Harth, E., Approach to formation of multifunctional polyester particles in controlled nanoscopic dimensions. *Journal of the American Chemical Society* **2008,** *130* (27), 8706-8713.

6.   van der Ende, A.; Croce, T.; Hamilton, S.; Sathiyakumar, V.; Harth, E., Tailored polyester nanoparticles: post-modification with dendritic transporter and targeting units via reductive amination and thiol-ene chemistry. *Soft Matter* **2009,** *5* (7), 1417-1425.

7.   van der Ende, A. E.; Harrell, J.; Sathiyakumar, V.; Meschievitz, M.; Katz, J.; Adcock, K.; Harth, E., "Click" Reactions: Novel Chemistries for Forming Well-defined Polyester Nanoparticles. *Macromolecules* **2010,** *43* (13), 5665-5671.

8.   van der Ende, A. E.; Sathiyakumar, V.; Diaz, R.; Hallahan, D. E.; Harth, E., Linear release nanoparticle devices for advanced targeted cancer therapies with increased efficacy. *Polymer Chemistry* **2010,** *1* (1), 93-96.

9.   Passarella, R. J.; Spratt, D. E.; van der Ende, A. E.; Phillips, J. G.; Wu, H. M.; Sathiyakumar, V.; Zhou, L.; Hallahan, D. E.; Harth, E.; Diaz, R., Targeted Nanoparticles That Deliver a Sustained, Specific Release of Paclitaxel to Irradiated Tumors. *Cancer Research* **2010,** *70* (11), 4550-4559.

10.   Drumright, R. E.; Gruber, P. R.; Henton, D. E., Polylactic acid technology. *Advanced Materials* **2000,** *12* (23), 1841-1846.

11.   Martina, M.; Hutmacher, D. W., Biodegradable polymers applied in tissue engineering research: a review. *Polymer International* **2007,** *56* (2), 145-157.

12.   Uhrich, K. E.; Cannizzaro, S. M.; Langer, R. S.; Shakesheff, K. M., Polymeric systems for controlled drug release. *Chemical Reviews* **1999,** *99* (11), 3181-3198.

13.   Albertsson, A. C.; Varma, I. K., Recent developments in ring opening polymerization of lactones for biomedical applications. *Biomacromolecules* **2003,** *4* (6), 1466-1486.

14.   Rokicki, G., Aliphatic cyclic carbonates and spiroorthocarbonates as monomers. *Prog Polym Sci* **2000,** *25* (2), 259-342.

15.   Kamber, N. E.; Jeong, W.; Waymouth, R. M.; Pratt, R. C.; Lohmeijer, B. G. G.; Hedrick, J. L., Organocatalytic ring-opening polymerization. *Chemical Reviews* **2007,** *107* (12), 5813-5840.

16.   Bourissou, D.; Moebs-Sanchez, S.; Martin-Vaca, B., Recent advances in the controlled preparation of poly(alpha-hydroxy acids): Metal-free catalysts and new monomers. *Comptes Rendus Chimie* **2007,** *10* (9), 775-794.

17.   Dove, A. P.; Pratt, R. C.; Lohmeijer, B. G. G.; Culkin, D. A.; Hagberg, E. C.; Nyce, G. W.; Waymouth, R. M.; Hedrick, J. L., N-Heterocyclic carbenes: Effective organic catalysts for living polymerization. *Polymer* **2006,** *47* (11), 4018-4025.

18.   Sanders, D. P.; Fukushima, K.; Coady, D. J.; Nelson, A.; Fujiwara, M.; Yasumoto, M.; Hedrick, J. L., A Simple and Efficient Synthesis of Functionalized Cyclic Carbonate Monomers Using a Versatile Pentafluorophenyl Ester Intermediate. *Journal of the American Chemical Society* **2010,** *132* (42), 14724-14726.

19.   Wang, R.; Chen, W.; Meng, F. H.; Cheng, R.; Deng, C.; Feijen, J.; Zhong, Z. Y., Unprecedented Access to Functional Biodegradable Polymers and Coatings. *Macromolecules* **2011,** *44* (15), 6009-6016.

20.   Xu, J. W.; Prifti, F.; Song, J., A Versatile Monomer for Preparing Well-Defined Functional Polycarbonates and Poly(ester-carbonates). *Macromolecules* **2011,** *44* (8), 2660-2667.

21.   Tempelaar, S.; Mespouille, L.; Dubois, P.; Dove, A. P., Organocatalytic Synthesis and Postpolymerization Functionalization of Allyl-Functional Poly(carbonate)s. *Macromolecules* **2011,** *44* (7), 2084-2091.

22.   Mullen, B. D.; Tang, C. N.; Storey, R. F., New aliphatic poly(ester-carbonates) based on 5-methyl-5-allyloxycarbonyl-1,3-dioxan-2-one. *J Polym Sci Pol Chem* **2003,** *41* (13), 1978-1991.

23.   Hu, X. L.; Chen, X. S.; Xie, Z. G.; Liu, S.; Jing, X. B., Synthesis and characterization of amphiphilic block copolymers with allyl side-groups. *Journal of Polymer Science Part a-Polymer Chemistry* **2007,** *45* (23), 5518-5528.

24.   Fukushima, K.; Pratt, R. C.; Nederberg, F.; Tan, J. P. K.; Yang, Y. Y.; Waymouth, R. M.; Hedrick, J. L., Organocatalytic Approach to Amphiphilic Comb-Block Copolymers Capable of Stereocomplexation and Self-Assembly. *Biomacromolecules* **2008,** *9* (11), 3051-3056.

25.   Pratt, R.; Lohmeijer, B.; Long, D.; Lundberg, P.; Dove, A.; Li, H.; Wade, C.; Waymouth, R.; Hedrick, J., Exploration, optimization, and application of supramolecular thiourea-amine catalysts for the synthesis of lactide (co)polymers. *Macromolecules* **2006,** *39* (23), 7863-7871.

CHAPTER III

TIN TRIFLATE CATALYZED RING-OPENING POLYMERIZATION OF

FUNCTIONALIZED LACTONES AND CARBONATES

Introduction

Functional polyester and polycarbonate materials are two of the most important classes of degradable polymers used in biomedical applications.[1, 2, 3, 4] To further advance the field and design specialized delivery materials, a practical and well-controlled synthesis of functionalized linear polyesters and polycarbonates is paramount. These building blocks enable the preparation of more complex systems such as nanoparticles for drug release[5] with the goal to overcome limitations of traditional polyester materials such as crystallinity. These building blocks are also valuable for the development of other advanced biomedical materials such as hydrogels.[6] Here, the integrated functionalities along the polymer backbone allow reactions with hydrophilic crosslinking units to obtain nanoparticles with decreased crystallinity[7] and tailored release rates as observed in developed nanosponges.[8]

Sn(Oct)$_2$ has been the most applied metal catalyst to prepare polyester homo and copolymers in ring-opening polymerization (ROP) techniques.[5, 9] Numerous approaches have also demonstrated its versatility through the incorporation of functional groups such as allyls, ketones, and propargyls and have been utilized in the formation of specialized nanomaterials such as drug release particles[10] and layered coatings[11]. Nevertheless, reaction temperatures of over 100 °C and high polydispersities (PDIs) have been reported, and polymers require dialysis to achieve narrower polydispersities. However, there are only a few reports investigating ring-opening polymerization procedures for the preparation of polyester homo and copolymers with

Sn(OTf)$_2$ as catalyst. Sn(OTf)$_2$ has not been intensively investigated yet due to its reported high reactivity and formation of bimodal polymers that can only be purified by column chromatography.[12] Moreover, the polymerization of functionalized cyclic carbonate monomers derived of the 5-methyl-2-oxo-1,3-dioxane-5-carboxylate family have not been studied with this particular catalyst.[13] Previous reports have focused on aluminum, alkaline earth-based catalysts, rare earth metal-based catalysts, and transition metal-based catalytic systems, but many of these systems yielded polymers with typical PDI's of 1.30 and 2.50.[14, 15, 16]

The development of organic catalysts has led to polyesters and polycarbonates with narrow polydispersities and good incorporation of functional groups.[17, 18, 19] However, the primary disadvantage of organic catalysts is the strict inert atmosphere conditions that are required to prepare well-defined polymers. This leads to extensive preparation times in addition to the actual synthesis and typically must be completed inside a glovebox. Although organocatalysts are preferred for recyclable plastics and microelectronics, polyester materials prepared via metal catalysis are widely used for biomedical applications.[20]

Therefore, we sought to revisit metal-catalyzed polymerization techniques but investigate more active catalysts that work at room temperature and produce well defined polyesters and polycarbonates.[21, 12] Methods were developed by investigating ideal temperatures, reaction times, reaction conditions, catalyst and monomer concentrations, and initiator selection. In this work, we present the controlled living ring-opening polymerization of functionalized polyesters and polycarbonates with Sn(OTf)$_2$ that does not require the use of a glovebox and gives, in simple and practical approaches, well-defined polyesters and polycarbonates with narrow polydispersities.

Results and Discussion

We report the synthesis of functionalized polycarbonates and polyesters employing stannous (II) trifluoromethane sulfonate [Sn(OTf)$_2$] in homo and copolymerizations with monomers of the valerolactone family such as valerolactone and δ -allyl-valerolactone using ring-opening polymerization (ROP) techniques and cyclic carbonate monomers such as 5-methyl-5-allyloxycarbonyl-1,3-dioxane-2-one (MAC) and 5-methyl-5-ethyloxycarbonyl-1,3-dioxane-2-one (MEC). Practical reaction methodologies and work up conditions were established which circumvented the typically high polydispersities associated with Sn catalysts.
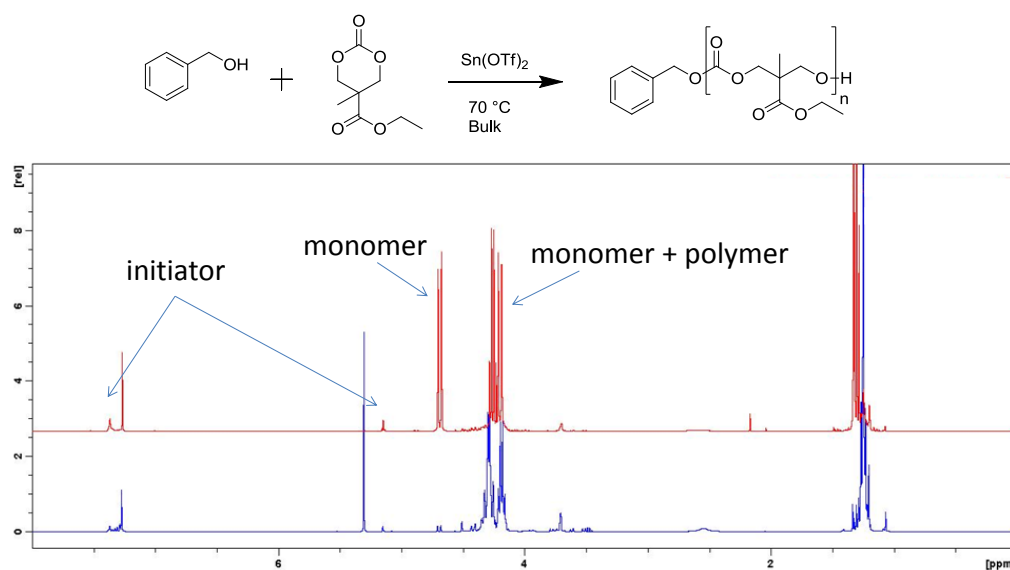
Figure III-1. ^{1}H NMR spectra of MEC homopolymer at the beginning of a reaction (top) and towards the end of a reaction (bottom) using benzyl alcohol as initiator.

Development of reaction conditions for polycarbonate homopolymers and allyl-containing copolymers

While metal catalyzed ring opening polymerizations of polyesters are well studied, the polymerization of polycarbonates with Sn(OTf)$_2$ has not been investigated yet. In general, the

incorporation of functionalized monomers has been easier since the ring opening polymerization reaction is not impaired by the position of the functional group in the monomer. In the past, one of the limitations to study polymerization methods and conditions has been the rather low-yielding syntheses of functionalized carbonate monomers, but recent improvements made these monomers more accessible.[22] The homopolymerization of 5-methyl-5-ethyloxycarbonyl-1,3-dioxane-2-one (MEC) was first conducted in solution either in THF or DMF at room temperature. However, polymerization times extended over a week, and therefore faster reaction
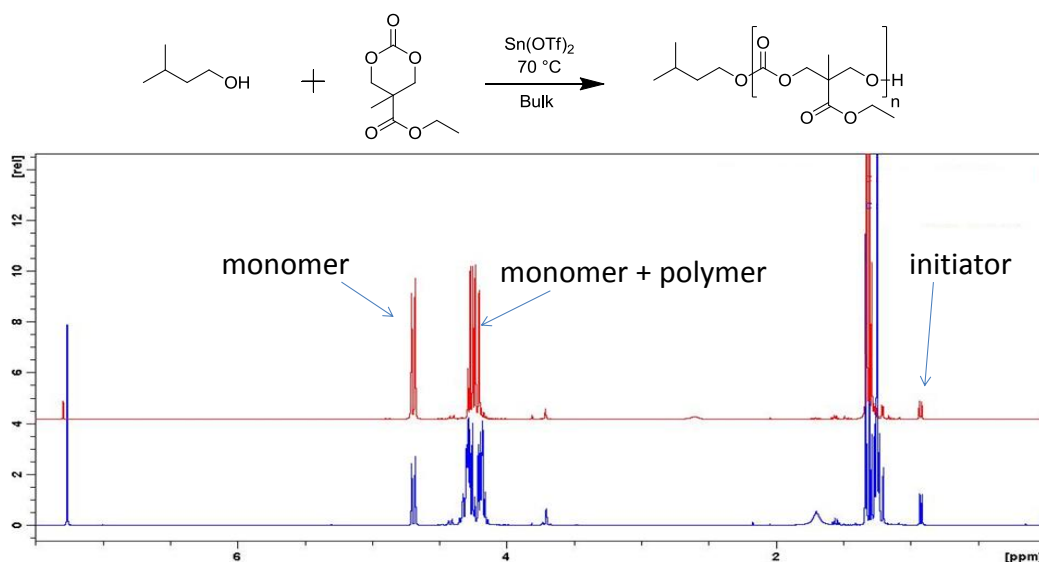
Figure III-2. ^{1}H NMR spectra of MEC homopolymer at the beginning of a reaction (top) and towards the end of a reaction (bottom) using 3-methyl-1-butanol as initiator.

times were sought. Although tin(II) triflate is active at room temperature, elevated temperatures were employed for bulk polymerizations. Consequently, homopolymerizations performed at 70 °C in bulk were complete after 3 days and yielded polymers with excellent molecular weight control and narrow polydispersities. Initially, benzyl alcohol was utilized as the polymer

initiator, but the compound eventually showed signs of degradation at higher polymerization temperatures as indicated by multiplet formation and reduction of the benzyl protons as seen in the ^{1}H NMR (Figure III-1). In contrast, 3-methyl-1-butanol is less sensitive towards various polymerization conditions and the characteristic NMR peaks can be more reliably analyzed in the presented polymerization studies (Figure III-2). The controlled nature of the polymerization was also verified in the linear relationship of the monomer conversion and the number average molecular weight (Mn) (Figure III-3).

Figure III-3. Number-average molecular weight (Mn) against % monomer conversion for the homopolymerization of MEC as determined by ^{1}H NMR.

The copolymerization with 5-methyl-5-allyloxycarbonyl-1,3-dioxane-2-one (MAC) showed, as expected, a well-controlled incorporation of MAC at a 20% monomer feed ratio as summarized in Figure III-4. As pointed out, functionalities on carbonate monomers do not

interfere with the catalyst during the ring-opening polymerization process, and the incorporation is not as challenging as experienced with α-functionalizations on the valerolactone ring.

Figure III-4. Top: Gel permeation chromatography traces of copolymerization of MEC and MAC. Bottom: [a]All polymerizations were completed at 70°C in bulk conditions. [b]Mn at full conversion. [c,e]Determined by NMR. [d]Determined by GPC.
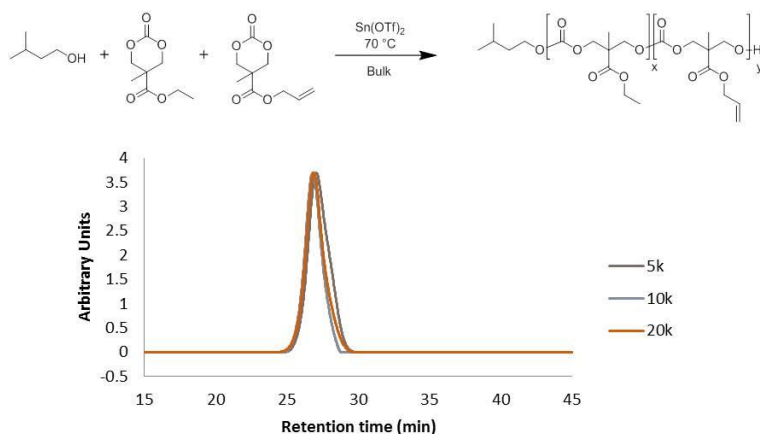
Polymer Feed Ratio (MEC: MAC)[a]	Mn predicted (Da)[b]	Mn (NMR)[c]	PDI[d]	Polymer Composition (MEC-MAC)[e]	Time (hours)
100:0	4,700	5,000	1.16	100	70
100:0	18,800	18,400	1.11	100	87
80:20	4,800	6,500	1.11	81:19	71
80:20	9,500	11,200	1.10	80:20	63
80:20	19,000	20,800	1.08	78:22	74

Synthesis of polyester homopolymers and allyl-containing copolymers

The initial conditions of the homopolymerization of δ-valerolactone included a monomer concentration of 8.7M in dichloromethane with 3.2×10^{-3} molar equivalents of tin(II) triflate as catalyst. The polymerization was living and controlled over a broad molecular weight range with narrow polydispersities of 1.08 as illustrated in Figure III-5. Therefore, the same conditions were chosen to test the polymerization of copolymers of δ-valerolactone (vl) with α-allyl-δ-

valerolactone (avl). Copolymers yielded slightly higher polydispersities, but interestingly the incorporation of α-allyl-valerolactone monomer was poor. For example, a calculated 10% incorporation of avl yielded 3% incorporation, and an attempted incorporation of 5% yielded 1% (Figure III-6). The reactions were typically run for one hour until the polymerization stopped stirring. However, a 20% feed ratio of the allyl monomer resulted in the polymerization becoming viscous but would not solidify. Nevertheless, the viscous mixture could be precipitated and yielded a white powder like the other homo and copolymers. Therefore, the polymerization
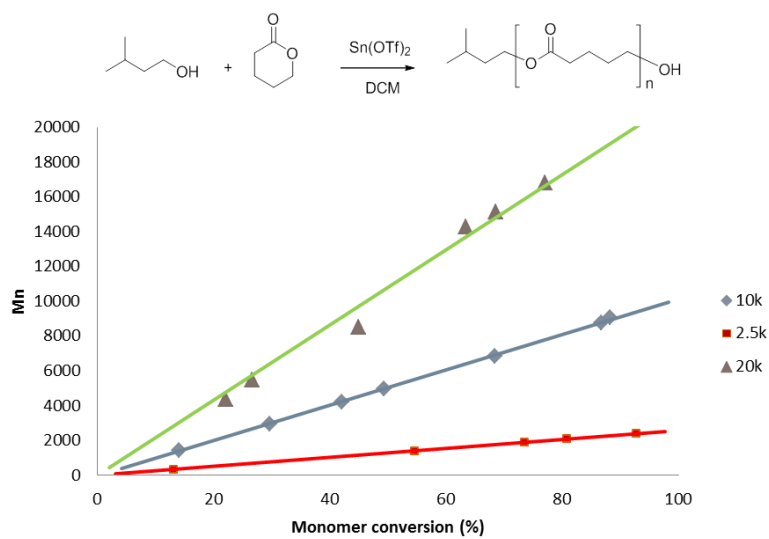
Polymer Feed Ratio (vl:avl) [a]	Mn predicted (Da) [b]	Mn NMR (Da) [c]	PDI [d]	Polymer Composition (vl:avl) [e]	Time (hours)
100:0	2,500	2,900	1.21	100:0	1
100:0	5,000	4,800	1.28	100:0	1.3
100:0	10,000	9,900	1.08	100:0	1.5
100:0	20,000	20,000	1.09	100:0	15

Figure III-5. Top: Number-average molecular weight (Mn) against % monomer conversion for the homopolymerization of valerolactone. Bottom: [a]Polymerizations were completed in dichloromethane at 25°C, [monomer] = 8.7 M. [b]Mn at full conversion. [c]Reactions were precipitated and immediately subjected to NMR analysis. [d]GPC against poly(styrene) standards in THF at 1 mL min^{-1}. [e]Determined by NMR analysis.

was allowed to run overnight to determine if the increased reaction time would lead to higher avl incorporation. When the reaction time was increased to 15 hours, avl incorporation increased up to 80% of the desired incorporation (Figure III-6).

Polymer Feed Ratio (vl:avl)[a]	Mn Predicated (Da)[b]	Mn NMR (da)[c]	PDI[d]	Polymer Composition (vl:avl)[e]	Time (hours)
90:10	2,000	2,000	1.25	97:3	1
95:5	3,000	3,300	1.21	99:1	1
80:20	3,000	2,600	1.14	91:9	1
80:20	4,000	5,000	1.13	84:16	15
80:20	20,000	16,300	1.15	86:14	15
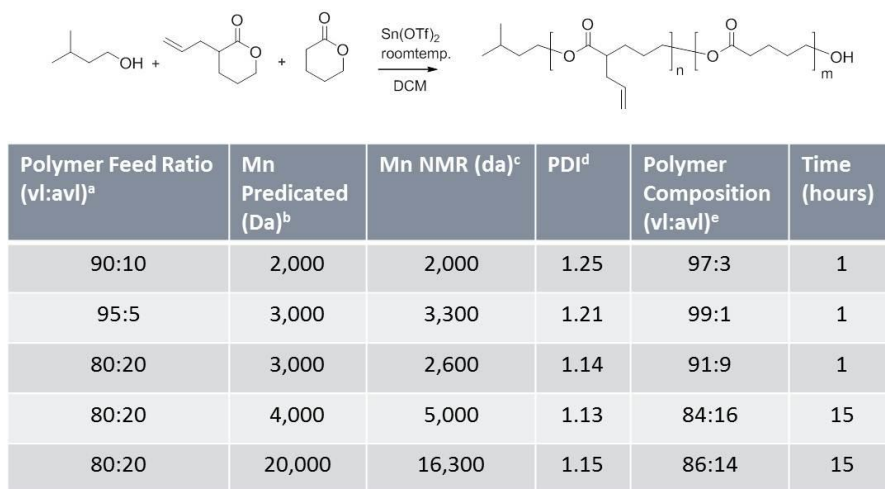
Figure III-6. Copolymerization of δ-valerolactone and α-allyl-δ-valerolactone. [a]Polymerizations were completed in dichloromethane at 25°C, [monomer] = 8.7 M. [b]Mn at full conversion. [c,e]Determined by NMR. [d]Determined by GPC.

It is known that α-allyl-valerolactone is a challenging monomer to copolymerize and incorporate because of the substitution in α- position that can influence the insertion ring opening polymerization mechanism of the ester group. To improve avl incorporation, a more dilute reaction concentration was investigated (6.6 M). Consequently, the reaction times increased, but the avl incorporation into the polymers increased while polydisperisities remained low. As shown in Figure III-7, the polymerization has a molecular weight control over low and high molecular weight polymers of 2.5k, 5k, and 20k and yielded narrow polydispersities of 1.14 to 1.19. Additionally, we conducted the homopolymerization of valerolactone to determine the effect of the dilution. The control of polymerization remained the same with a slight

improvement of the polydispersity to 1.15. The living polymers were precipitated twice in methanol to remove any unreacted monomers but also to remove the reactive Sn endgroup.[23] The methanol exchanges with the Sn catalyst at the chain end of the polymer thereby successfully removing the reactive catalyst from the terminal end of the polymer.[24] However, since residual tin was detected using elemental analysis (88 ppm), efforts were sought to decrease the amount of catalyst used. As a result, it was determined that similar polyester copolymers with excellent avl incorporation and low polydispersities could be formed using 10-fold less $Sn(OTf)_2$ catalyst. Therefore, an exact amount of catalyst isn't required to form excellent polymers; rather, any amount of catalyst within this range will suffice.
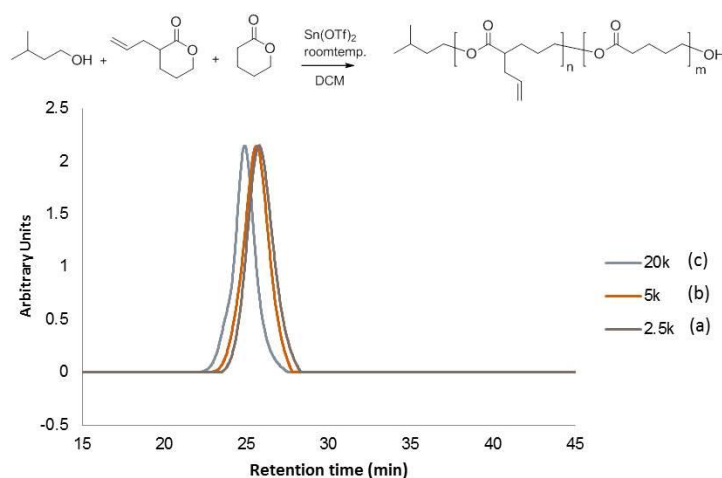
Polymer Feed Ratio (vl:avl)[a]	Mn Predicted(Da)[b]	Mn NMR (Da)[c]	PDI[d]	Polymer Composition (vl:avl)[e]	Time (hours)
100:0	2,500	2,400	1.19	-	5
100:0	5,000	4,600	1.15	-	5
90:10 (a)	2,500	2,800	1.19	91:9	21
90:10 (b)	5,000	5,300	1.19	91:9	21
90:10 (c)	20,000	17,300	1.14	90:10	21

Figure III-7. Top: Gel permeation chromatography traces of copolymerization of δ-valerolactone and α-allyl-δ-valerolactone. Bottom: [a]Polymerizations were completed in dichloromethane at 25°C, [monomer] = 6.6 M. [b]Mn at full conversion. [c,e]Determined by NMR. [d]Determined by GPC.

Conclusion

In this work, we have developed a new, practical methodology to prepare functionalized polyester and polycarbonate homo and copolymers using $Sn(OTf)_2$ as catalyst and 3-methyl-1-butanol as initiator with excellent control over the molecular weight and narrow polydisperisties. Reaction concentration was found to be critical to incorporate challenging monomers such as δ-allyl-valerolactone in the desired monomer ratios. Poly(valerolactone, α-allyl δ-valerolactone) copolymers could be prepared with excellent incorporation of the α-allyl-valerolactone monomer using a monomer concentration of 6.6 M in dichloromethane. Interestingly, bulk conditions for the polycarbonate polymerization were found to be preferential compared to traditional solution conditions. Bulk polymerizations of polycarbonates showed excellent control over molecular weight, narrow polydispersities, and predictable incorporation of functional groups such as 5-methyl-5-allyloxycarbonyl-1,3-dioxane-2-one (MAC) at 70 °C. The purification of polymer in methanol removes the reactive metal catalyst chain end from the living chain end via an exchange reaction.
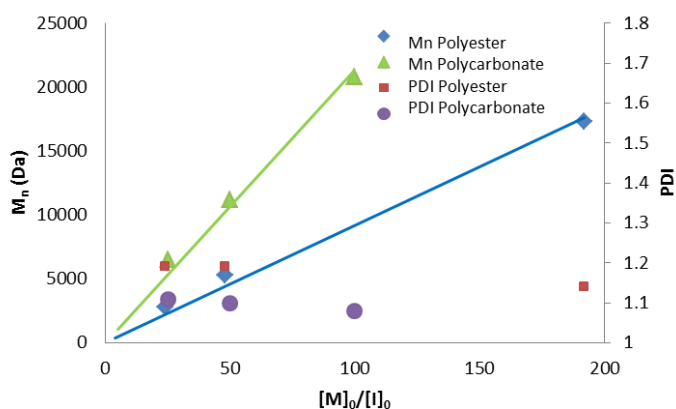
Figure III-8. Number-average molecular weight (Mn) and polydispersity against initial monomer-to-initiator ratio ($[M]_0/[I]_0$) for the copolymerization of MEC/MAC (20%) and δ-valerolactone/α-allyl valerolactone (10%).

The linear correlation between number-average molecular weight (Mn) of copolymers MEC with 20% MAC and δ-valerolactone with 10% α-allyl valerolactone against $[M]_0/[I]_0$ while maintaining low PDI's demonstrates that both polymerizations are well controlled (Figure III-8). The advantage of these methods is their practicality and accurate preparation of polymers to build refined biomaterials and nanostructures. Since the allyl functionality was successfully incorporated into the polymer, we believe other functionalized carbonate and ester monomers can be successfully introduced into similarly controlled polymers using the polymerization methods described such as alkyne and chloro groups. Although polycarbonates have been used for decades, the ability to synthesize these materials with practical methods allows them to become a critical part of very sophisticated materials such as hydrogels for drug delivery applications.

Experimental

Materials

Tin(II) trifluoromethanesulfonate was obtained from Strem Chemicals Inc. and used as received. 5-methyl-5-ethyloxycarbonyl-1,3-dioxane-2-one (MEC) and 5-methyl-5-allyloxycarbonyl-1,3-dioxane-2-one (MAC) were synthesized as reported previously and recrystallized several times before use.[25, 26] δ-valerolactone (vl) was obtained from Sigma Aldrich and vacuum distilled before use. α-allyl-δ-valerolactone (avl) was synthesized as reported previously[5] and vacuum distilled before use. Dichloromethane (anhydrous), 3-methyl-1-butanol (anhydrous), and CDCl$_3$/TMS were obtained from Sigma Aldrich and used as received. Spectra/Por® Dialysis membrane was purchased from Spectrum Laboratories Inc.

Characterization

^{1}H NMR and ^{13}C NMR spectra were obtained from a Bruker AC400 Fourier Transform Spectrometer, with CDCl$_3$/TMS as the solvent. Gel permeation chromatography (GPC) was carried out with a Waters chromatograph system equipped with a Waters 2414 refractive index detector, a Waters 2481 dual λ absorbance detector, a Waters 1525 binary HPLC pump, and four 5 mm Waters columns (300 mm x 7.7 mm), connected in series with increasing pore size (100, 1000, 100,000 and 1,000,000 Å respectively). All runs were performed with dimethylformamide (DMF) or tetrahydrofuran (THF) as the eluent at a flow rate of 1 mL/min.

General MEC Homopolymer Synthesis

A 25-mL round bottom flask was equipped with stir bar, capped with rubber septum, flame dried and nitrogen purged. Sn(OTf)$_2$ (7.0 mg, 0.0168 mmol) was added to the flask, and the flask was nitrogen purged once more. 3-methyl-1-butanol (5.8 uL, 0.0531 mmol) was added to the reaction flask via microsyringe, and the catalyst/initiator mixture was allowed to stir at room temperature for 30 minutes. MEC (0.500 g, 2.657 mmol) was added to the flask and allowed to stir in 70 °C oil bath for 87 hours. Polymer was purified by precipitation into methanol or by using Spectra/Por dialysis membrane (MWCO = 1,000 Da) against dichloromethane/methanol to yield colorless polymer (Theoretical Mn = 18,800 Da, NMR Mn = 18,400 Da, PDI = 1.11, yield = 0.460 g). ^{1}H NMR (400MHz, CDCl$_3$/TMS, ppm) δ: 4.40-4.15 (m, -OC(O)OCH_2), 1.30-1.22 (m, CH_3, -OCH$_2$CH_3), 0.93-0.91 (d, 3-methyl-1-butanol, -OCH$_2$CH$_2$CH(CH_3)$_2$).

General MEC, MAC Copolymer Synthesis

A 1-dram vial was equipped with stir bar, capped with rubber septum, flame dried and nitrogen

purged. $Sn(OTf)_2$ (3.5 mg, 0.0084 mmol) was added to the vial, and the vial was nitrogen purged once more. 3-methyl-1-butanol (11.4 uL, 0.105 mmol) was added to the reaction vial by microsyringe, and the catalyst/initiator solution was allowed to stir at room temperature for 30 minutes. MEC (0.395 g, 2.099 mmol) and MAC (0.105 g, 0.5245 mmol) were added to the vial, melted at 70 °C, and allowed to stir in 70 °C oil bath for 71 hours when stirring became greatly impeded. The resulting polymer was purified by precipitation into methanol or by dialysis using Spectra/Por dialysis membrane (MWCO = 1,000 Da) against methanol/dichloromethane to yield colorless polymer (Calculated Mn = 4,800 Da, NMR Mn = 6,500 Da, PDI = 1.11, yield = 0.359 g) theoretical allyl incorporation = 20.0%, actual allyl incorporation = 19.0%). ^{1}H NMR (400MHz, $CDCl_3$/TMS, ppm) δ: 5.91-5.85 (m, -OCH$_2$CHCH$_2$), 5.34-5.23 (m, -OCH$_2$CHCH_2), 4.64-4.62 (m, -OCH_2CHCH$_2$), 4.40-4.15 (m, MAC & MEC, -OC(O)OCH_2), 1.30-1.22 (m, MAC & MEC, CH$_3$; MEC, -OCH$_2$CH_3), 0.93-0.91 (d, 3-methyl-1-butanol, OCH$_2$CH$_2$CH(CH_3)$_2$). ^{13}C NMR (400 MHz, $CDCl_3$/TMS, ppm) δ: 174.1, 172.1, 154.9, 154.4, 131.7, 118.5, 68.6, 65.9, 64.7, 61.2, 50.8, 48.2, 46.5, 24.8, 22.4, 17.5, 14.1.

General Valerolactone Homopolymer Synthesis (6.6 M)

A 25-ml round bottom flask was equipped with a stir bar, capped with a rubber septum, nitrogen purged and flame dried. $Sn(OTf)_2$ (6.7 mg, 0.016 mmol) was weighed directly into the flask. The flask was sealed with rubber septum and nitrogen purged. 3-methyl-1-butanol (21.8 uL, 0.200 mmol) and 0.272 mL anhydrous dichloromethane was added to the flask via syringe, and the catalyst/initiator solution was allowed to stir at room temperature for 30 minutes. Delta-valerolactone (0.500 g, 4.994 mmol) was added to the solution and stirred 5 hours. Polymer was purified by precipitating into cold methanol to yield white product (Theoretical Mn = 2,500 Da,

NMR Mn = 2,400 Da, PDI = 1.19, yield = 0.451 g). ^{1}H NMR (400MHz, CDCl$_3$/TMS, ppm) δ: 4.08 (m, -OCH_2), 2.34 (m, -O(O)CH_2CH$_2$), 1.68 (m, -CHCH_2CH_2-), 0.93-0.91 (d, 3-methyl-1-butanol, -OCH$_2$CH$_2$CH(CH_3)$_2$).

General Valerolactone, allyl-Valerolactone Copolymer Synthesis

A 25-ml round bottom flask was equipped with a stir bar, capped with a rubber septum, nitrogen purged and flame dried. Sn(OTf)$_2$ (6.4 mg, 0.015 mmol) was weighed directly into the flask. The flask was sealed with rubber septum and nitrogen purged. 3-methyl-1-butanol (21.8 uL, 0.200 mmol) and 0.243 mL anhydrous dichloromethane was added to the flask via syringe, and the catalyst/initiator solution was allowed to stir at room temperature for 30 minutes. δ-valerolactone (0.433 g, 4.322 mmol, vl) and δ -allyl-δ-valerolactone (0.067 g, 0.477 mmol, avl) were added to the solution, and reaction was allowed to stir for 21 hours. Polymer was purified by precipitating into cold methanol to yield white product (Theoretical Mn = 2,500 Da, NMR Mn = 2,800 Da, PDI = 1.19, yield = 0.381 g, theoretical avl incorporation = 10.0%, actual avl incorporation = 9.3%). ^{1}H NMR (400MHz, CDCl$_3$/TMS, ppm) δ: 5.75-5.70 (m, -CH=CH$_2$), 5.10-5.01 (t, J = 18.2 Hz, J = 11.5 Hz, 2H, -CH=CH_2), 4.08 (m, -OCH_2), 2.34 (m, vl, -O(O)CH_2CH$_2$; avl, -O(O)CHCH$_2$CH=CH$_2$, -CHCH_2CH=CH$_2$), 1.68 (m, avl & vl, -CHCH_2CH_2), 0.93-0.91 (d, 3-methyl-1-butanol, -OCH$_2$CH$_2$CH(CH_3)$_2$). ^{13}C NMR (400 MHz, CDCl$_3$/TMS, ppm) δ: 175.2, 173.4, 135.2, 117.1, 64.1, 44.9, 37.4, 33.8, 28.1, 26.5, 25.1, 22.5, 21.3.

Number average molecular weight (Mn) – monomer conversion experiment

Valerolactone and MEC homopolymers were prepared as mentioned previously, but CDCl$_3$ was used as solvent for the valerolactone polymerization in order to be used for immediate NMR

analysis. At predetermined time points depending on the polymer reaction, a small amount of the polymerization was removed and analyzed immediately by ^{1}H NMR.

Termination of Polymerization

Polymerizations were terminated by precipitating twice in cold methanol, effectively removing the catalyst from the terminal end of the polymer. Polymers were analyzed by ICP atomic emission techniques (Applied Technical Services, Inc.) Elemental analysis: 88 ppm Sn.

References

1.   Tang, Z. Y.; Wang, Y.; Podsiadlo, P.; Kotov, N. A., Biomedical applications of layer-by-layer assembly: From biomimetics to tissue engineering. *Advanced Materials* **2006,** *18* (24), 3203-3224.

2.   Watanabe, J.; Kotera, H.; Akashi, M., Reflexive interfaces of poly(trimethylene carbonate)-based polymers: Enzymatic degradation and selective adsorption. *Macromolecules* **2007,** *40* (24), 8731-8736.

3.   Vandermeulen, G.; Rouxhet, L.; Arien, A.; Brewster, M. E.; Preat, V., Encapsulation of amphotericin B in poly(ethylene glycol)-block-poly(epsilon-caprolactone-co-trimethylenecarbonate) polymeric micelles. *International Journal of Pharmaceutics* **2006,** *309* (1-2), 234-240.

4.   Matsuda, T.; Kwon, I. K.; Kidoaki, S., Photocurable biodegradable liquid copolymers: Synthesis of acrylate-end-capped trimethylene carbonate-based prepolymers, photocuring, and hydrolysis. *Biomacromolecules* **2004,** *5* (2), 295-305.

5.   van der Ende, A. E.; Kravitz, E. J.; Harth, E., Approach to formation of multifunctional polyester particles in controlled nanoscopic dimensions. *J Am Chem Soc* **2008,** *130* (27), 8706-8713.

6.   Truong, V.; Barker, I.; Tan, M.; Mespouille, L.; Dubois, P.; Dove, A., Preparation of in situ-forming poly(5-methyl-5-allyloxycarbonyl-1,3-dioxan-2-one)-poly(ethylene glycol) hydrogels with tuneable swelling, mechanical strength and degradability. *Journal of Materials Chemistry B* **2013,** *1* (2), 221-229.

7.   van der Ende, A. E.; Kravitz, E. J.; Sathiyakumar, V.; Harth, E., One-pot synthesis of well-defined polyester nanoparticles and their postmodification. *Abstr Pap Am Chem S* **2009,** *237*.

8.   van der Ende, A.; Croce, T.; Hamilton, S.; Sathiyakumar, V.; Harth, E., Tailored polyester nanoparticles: post-modification with dendritic transporter and targeting units via reductive amination and thiol-ene chemistry. *Soft Matter* **2009,** *5* (7), 1417-1425.

9.   Majerska, K.; Duda, A.; Penczek, S., Kinetics and mechanism of cyclic esters polymerisation initiated with tin(II) octoate, 4 - Influence of proton trapping agents on the kinetics of epsilon-caprolactone and L,L-dilactide polymerisation. *Macromol Rapid Comm* **2000,** *21* (18), 1327-1332.

10.   Passarella, R. J.; Spratt, D. E.; van der Ende, A. E.; Phillips, J. G.; Wu, H. M.; Sathiyakumar, V.; Zhou, L.; Hallahan, D. E.; Harth, E.; Diaz, R., Targeted Nanoparticles That Deliver a Sustained, Specific Release of Paclitaxel to Irradiated Tumors. *Cancer Res* **2010,** *70* (11), 4550-4559.

11.   Amir, E.; Antoni, P.; Campos, L. M.; Damiron, D.; Gupta, N.; Amir, R. J.; Pesika, N.; Drockenmuller, E.; Hawker, C. J., Biodegradable, multi-layered coatings for controlled release of small molecules. *Chem Commun* **2012,** *48* (40), 4833-4835.

12.   Parrish, B.; Quansah, J. K.; Emrick, T., Functional polyesters prepared by polymerization of alpha-allyl(valerolactone) and its copolymerization with epsilon-caprolactone and delta-valerolactone. *J Polym Sci Pol Chem* **2002,** *40* (12), 1983-1990.

13.   Albertsson, A. C.; Varma, I. K., Recent developments in ring opening polymerization of lactones for biomedical applications. *Biomacromolecules* **2003,** *4* (6), 1466-1486.

14.   Labet, M.; Thielemans, W., Synthesis of polycaprolactone: a review. *Chem Soc Rev* **2009,** *38* (12), 3484-3504.

15.   Ajellal, N.; Carpentier, J. F.; Guillaume, C.; Guillaume, S. M.; Helou, M.; Poirier, V.; Sarazin, Y.; Trifonov, A., Metal-catalyzed immortal ring-opening polymerization of lactones, lactides and cyclic carbonates. *Dalton Transactions* **2010,** *39* (36), 8363-8376.

16.   Weiser, J. R.; Zawaneh, P. N.; Putnam, D., Poly(carbonate-ester)s of Dihydroxyacetone and Lactic Acid as Potential Biomaterials. *Biomacromolecules* **2011,** *12* (4), 977-986.

17.   Coulembier, O.; Degee, P.; Hedrick, J. L.; Dubois, P., From controlled ring-opening polymerization to biodegradable aliphatic polyester: Especially poly(beta-malic acid) derivatives. *Progress in Polymer Science* **2006,** *31* (8), 723-747.

18.   Coulembier, O.; Mespouille, L.; Hedrick, J. L.; Waymouth, R. M.; Dubois, P., Metal-free catalyzed ring-opening polymerization of, beta-lactones: Synthesis of amphiphilic triblock copolymers based on poly(dimethylmalic acid). *Macromolecules* **2006,** *39* (12), 4001-4008.

19.   Suriano, F.; Pratt, R.; Tan, J. P. K.; Wiradharma, N.; Nelson, A.; Yang, Y. Y.; Dubois, P.; Hedrick, J. L., Synthesis of a family of amphiphilic glycopolymers via controlled ring-opening

polymerization of functionalized cyclic carbonates and their application in drug delivery. *Biomaterials* **2010,** *31* (9), 2637-2645.

20.   Seyednejad, H.; Ghassemi, A. H.; van Nostrum, C. F.; Vermonden, T.; Hennink, W. E., Functional aliphatic polyesters for biomedical and pharmaceutical applications. *J Control Release* **2011,** *152* (1), 168-176.

21.   Moller, M.; Kange, R.; Hedrick, J. L., Sn(OTf)(2) and Sc(OTf)(3): Efficient and versatile catalysts for the controlled polymerization of lactones. *J Polym Sci Pol Chem* **2000,** *38* (11), 2067-2074.

22.   Stevens, D. M.; Tempelaar, S.; Dove, A. P.; Harth, E., Nanosponge Formation from Organocatalytically Synthesized Poly(carbonate) Copolymers. *Acs Macro Lett* **2012,** *1* (7), 915-918.

23.   Koo, D.; Du, A.; Palmese, G. R.; Cairncross, R. A., Synthesis and water sorption of standard and end-capped polylactides: the effect of morphology. *Polym Chem-Uk* **2012,** *3* (3), 718-726.

24.   Du, A.; Koo, D.; Ziegler, M.; Cairncross, R. A., The Effect of Heat Treatment on Water Sorption in Polylactide and Polylactide Composites via Changes in Glass-Transition Temperature and Crystallization Kinetics. *J Polym Sci Pol Phys* **2011,** *49* (12), 873-881.

25.   Fukushima, K.; Pratt, R. C.; Nederberg, F.; Tan, J. P. K.; Yang, Y. Y.; Waymouth, R. M.; Hedrick, J. L., Organocatalytic Approach to Amphiphilic Comb-Block Copolymers Capable of Stereocomplexation and Self-Assembly. *Biomacromolecules* **2008,** *9* (11), 3051-3056.

26.   Hu, X. L.; Chen, X. S.; Xie, Z. G.; Liu, S.; Jing, X. B., Synthesis and characterization of amphiphilic block copolymers with allyl side-groups. *Journal of Polymer Science Part a-Polymer Chemistry* **2007,** *45* (23), 5518-5528.

CHAPTER IV

POLYESTER NANOSPONGE FORMATION FOR PACLITAXEL NANOSOLUBILIZATION

AND TAILORED DRUG RELASE

Introduction

In general, solubility is the primary clinical limitation for most drugs, and strategies to improve drug solubility are paramount for the continued improvement of therapeutics. Biodegradable polymeric nanoparticles utilized as a controlled release formulation of drugs is an effective strategy for the improvement of numerous therapeutic applications.[1, 2, 3] Nanoparticles are excellent drug delivery vehicles due to their modular synthesis that allows for complete customization of the vehicles to meet various applications in which the therapeutic could otherwise be limited by size or solubility. For example, chemotherapeutics such as paclitaxel belong to class IV of the biopharmaceutics classification system (BCS) because they have low solubility and low permeability, which leads to poor bioavailability.[4] Ideally, a single therapeutic dose would allow for a high dissolution of the drug and an exact amount of drug to release in a specific amount of time to meet the individual needs of any patient.

Currently, many approaches synthesize a single type of vehicle that allows for a single, or slightly adjustable, drug release rate and then identify suitable biomedical applications. Also, drug release is often rapid, especially within the first 48 hours. For example, multilayered nanoparticles from block copolymers or nanoparticles mixed with surfactant result in rapid release profiles, and release rates can only be controlled by copolymer makeup and type of surfactant used, respectively.[5, 6, 7] Likewise, micelles offer quick and easy preparation, but often

lead to rapid release of drug.[8, 9, 2] One strategy has been to design prodrugs with stimuli-responsive covalent bonds to attach the drug to the carrier with a programmed release.[10] Although this strategy is very successful for selected drugs, the high specification prevents a broader application for a range of established and newly developed drugs which imposes a major limitation.[11, 12]

Alternatively, the next generation of drug delivery will allow complete customization of a single platform vehicle that can be easily tuned to meet any therapeutic need. Therefore, we investigated the synthesis of biodegradable, polyester nanoparticles, the ability to encapsulate and nanosolubilize paclitaxel encapsulation, and for the first time, demonstrate the ability to control the release of paclitaxel by adjusting the single parameter of the particles' crosslinking density. Additionally, particles with different densities can be mixed to yield various rates of release that can be fast or slow depending on the specific application. The ability of these particles to withstand simulated gastric fluid allows for the possibility of an oral drug delivery route.

Results and Discussion

Polyester nanosponges were prepared with varied degrees of crosslinking densities of 4%, 7% and 10% and an average nanoscopic size of 100 nm. The crosslinking density and the influence towards the release kinetics of paclitaxel, a BCS class IV drug, for individual particles and a mixture of particles from two different crosslinking densities are investigated in buffer and gastrointestinal fluid and employs fully adjustable release rates suitable for intravenous and oral delivery. Herein, we present the synthesis of biodegradable nanoparticles capable of paclitaxel entrapment, and we demonstrate the ability to control release of paclitaxel by adjusting the single

parameter of the crosslinking density of the particles. Additionally, particles with different densities can be mixed to yield various rates of release that can be fast or slow depending on the specific application. The ability of these particles to withstand simulated gastric fluid allows for the possibility of an oral drug delivery route while the therapeutic remains amorphous in the nanoparticle.

Synthesis of epoxide-functionalized polyesters – precursors to nanosponge formation

Figure IV-1. Epoxidation of the allyl group at full conversion (top) or partial conversion (bottom) based on equivalents of mCPBA.

Epoxide functionalized polyester precursors were prepared by first synthesizing allyl-valerolactone, valerolactone copolymers (poly(avl,vl)) described previously[13], and then converting the allyl group to an epoxide using meta-chloroperoxybenzoic acid (mCPBA) to yield poly(evl,vl). This reaction was performed using 1.2 equivalents mCPBA per alkene in dichloromethane at an alkene concentration of 0.065 M for 48 hours. It was determined that washing the resulting polymer in saturated sodium bicarbonate effectively removed the acid while still achieving good yields (greater than 70%). This was significantly more effective than

precipitating in diethyl ether which often required multiple precipitations in large volumes of ether resulting in yields between 50-70%. In this study, the conversion of allyl to epoxide was 100% as indicated by ^{1}H NMR analysis. However, partial epoxidation is possible by reducing the equivalents of the mCPBA or by reducing the overall reaction time. The ability to adjust this conversion allows a fine tuning of the polyester precursor that will be used to synthesize the resulting nanoparticle. This is especially important for applications that require further modifications of the resulting nanoparticles. For example, partial epoxidation of the polyester allows a quantifiable number of allyl groups remaining which can be used to attach targeting peptides to the surface of the nanoparticle using thiolene click chemistry. The ability to undergo partial epoxidiation can also be important to achieve a desired amount of epoxide which is responsible for the nanoparticles' crosslinking density.
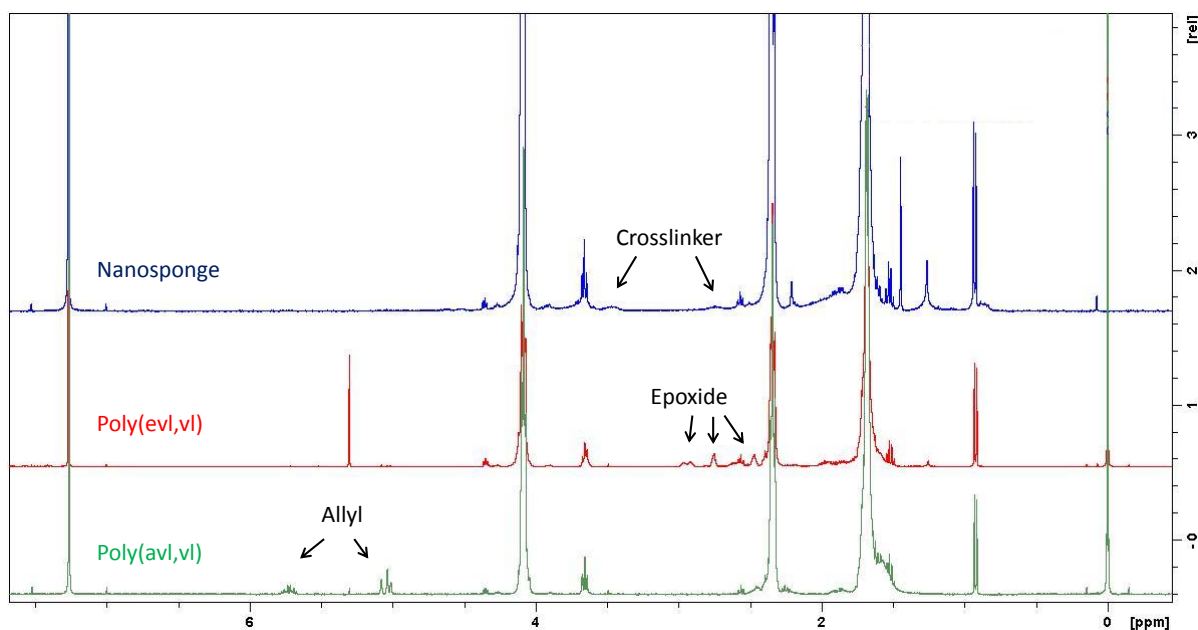
Figure IV-2. ^{1}H NMR spectra of poly(avl,vl) before (bottom) and after epoxide conversion (middle) and of nanosponge after amine-epoxide crosslinking (top).

53

Synthesis of polyester nanosponges via amine-epoxide chemistry

Nanoparticles were synthesized via intermolecular crosslinking between a bisamine crosslinker and epoxide functionalized polyesters at an epoxide concentration of 3.24 x 10^{-3} M for 12 hours at 45 °C (Figure IV-3). Epoxide functionality within the polyesters ranged from 4-10% while the equivalents of amine per epoxide used remained constant (1.5 amines per epoxide). The definition of crosslinking density is based on the amount of epoxide present in the polyester precursor.[14] In other words, the percentage of epoxide in the polyester precursor determined the crosslinking density of the subsequent nanoparticle. The slight excess of amine crosslinker is useful to ensure that free amines will remain within the nanonetwork after the nanoparticles are formed, and these amines can also be used for post-modification reactions such as attaching imaging dyes using NHS-ester chemistry.
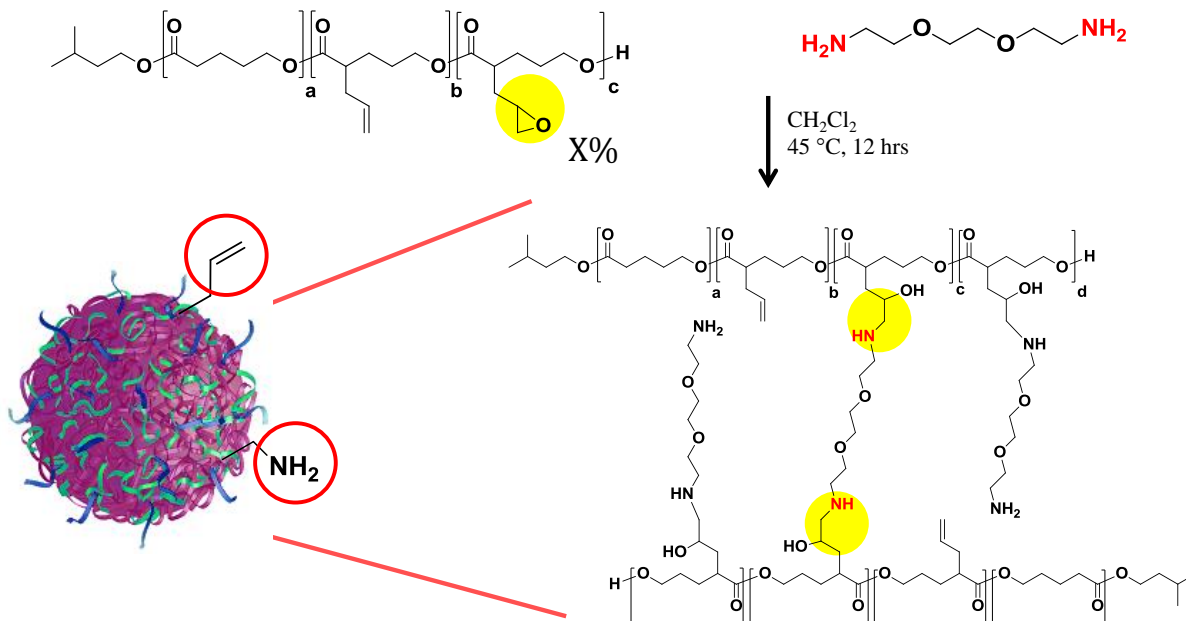
Figure IV-3. Intermolecular crosslinking reaction between epoxide functionalized polyesters and bis(amine) polyethylene glycol crosslinker to form functionalized nanosponges.

Although 10% crosslinking density was the highest crosslinking in this study, the average nanoparticle size remained similar compared to particles with less dense networks. For example, particles with 9.8% crosslinking density were 103 ± 21.5 nm and particles with 4.1% crosslinking density were 107 ± 16.4 nm (Figure IV-4). Previous studies[15] suggested particle size would increase with increased epoxide functionality; however, the variability within this range of epoxide functionality does not appear to exhibit a significant effect on particle size. In other words, polymers containing more than 10% epoxide may be necessary to synthesize particles of greater size using these conditions. This nanoparticle size was chosen as it considered the ideal size not only for intravenous injections to avoid accumulation in organs such as the liver, as often observed for larger particle sizes, but also the ideal size to cross the intestinal epithelial layer in oral drug delivery approaches.[16, 17, 18, 19]
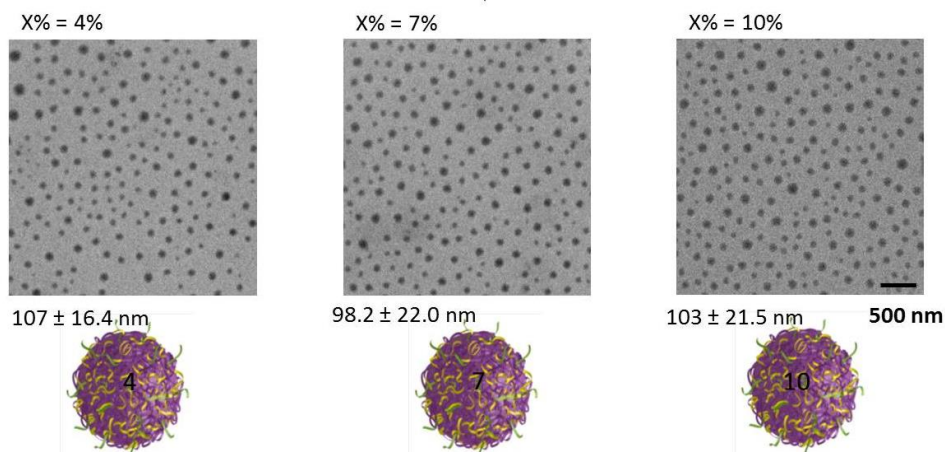
Figure IV-4. TEM analysis with representative images of nanosponges with three different crosslinking densities of 4.1%, 7.1% and 9.8%.

As therapeutics become increasingly hydrophobic, a smart formulation that a.) keeps the therapeutic from crystallizing and in an amorphous state, b.) maintains the maximum ability to

cross the intestinal barrier, c.) does not accumulate in organs once circulating in the bloodstream, and d.) has adjustable release profiles represents the ideal therapeutic carrier. Moreover, it has been reported that 100 nm particles are ideal for oral drug delivery and are also superior to 50 nm, 200 nm and 500 nm particle sizes.[17] With this, the 100 nm particle range can be prepared to meet the needs of therapeutic delivery in oral and IV administration.

Nanosolubilization of Paclitaxel
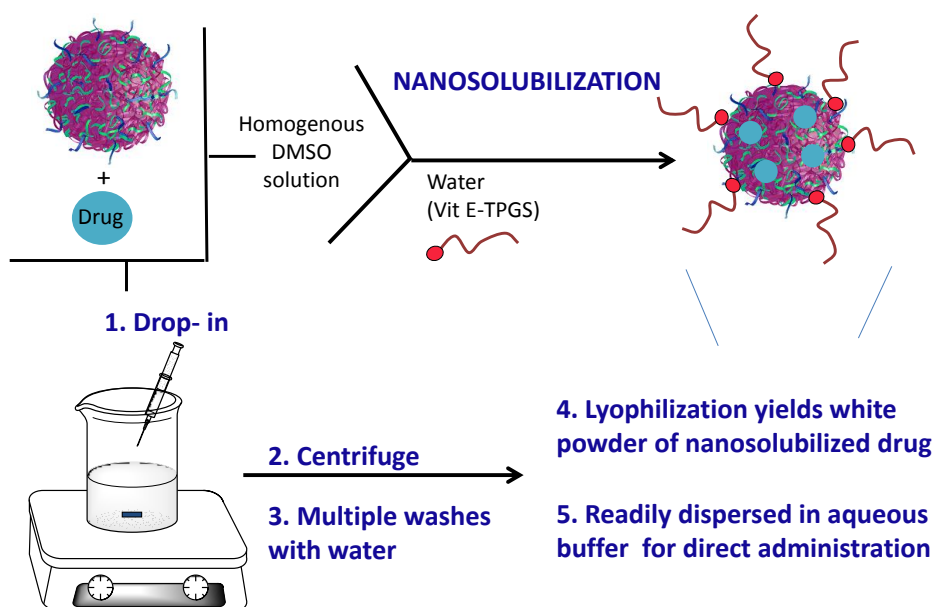
Figure IV-5. Nanosolubilization method for encapsulating drugs within the nanosponge.

The prepared particles were loaded with paclitaxel as a model drug after the nanoparticle was formed (post-loading) in a developed nanosolubilization method[20] which is demonstrated in Figure IV-5. Post-loading can be accomplished due to the full solubility of both the particle and drug in DMSO to form a homogenous solution. Once added to the aqueous environment,

precipitation occurs, and the drug incorporates into the polyester nanosponge via hydrophobic interactions. D-α tocopherol polyethyleneglycol(1000) succinate (Vit E-TPGS) was utilized to enhance the hydrophilicity of the nanoparticle surface and increase circulation half-life by preventing premature clearance and immune response during *in vivo* applications.[21, 22] The amount of the formulated paclitaxel into the particle was determined by HPLC analysis, and an average of 13% paclitaxel (wt/wt) in the final product could be achieved.

X-ray diffraction (XRD) and differential scanning calorimetry (DSC) analysis of nanosponge and encapsulated paclitaxel

To determine if the polymeric nanonetwork of the particle prevents the crystallization of the drug which allows for better dissolution in the biological environment, DSC and XRD measurements were undertaken (Figure IV-6 top). The XRD spectrum of paclitaxel shows numerous peaks, particularly in the 2θ range of 5-25 °C, which are in accord with published data of paclitaxel's unique crystallization pattern.[23] These peaks are also visible in a physical mixture of paclitaxel and polyester nanoparticle (13% ptx wt/wt), indicating the paclitaxel remains crystalline when physically mixed with the nanoparticle, as expected. However, these peaks are not visible in the encapsulated paclitaxel sample, indicating the drug is in an amorphous state once encapsulated, and is in agreement with other published studies.[24] The amorphous state of the encapsulated paclitaxel is also demonstrated using differential scanning calorimetry (Figure IV-6 bottom). The DSC curve of paclitaxel shows an endothermic melting point at 223 °C which matches previously published data.[23] However, this melting point is absent in the encapsulated paclitaxel due to the amorphous state of the drug in this formulation. These results suggest that confining the drug to the nanoscale through nanoparticle encapsulation decreases the drug crystallinity which allows for improved water solubility.
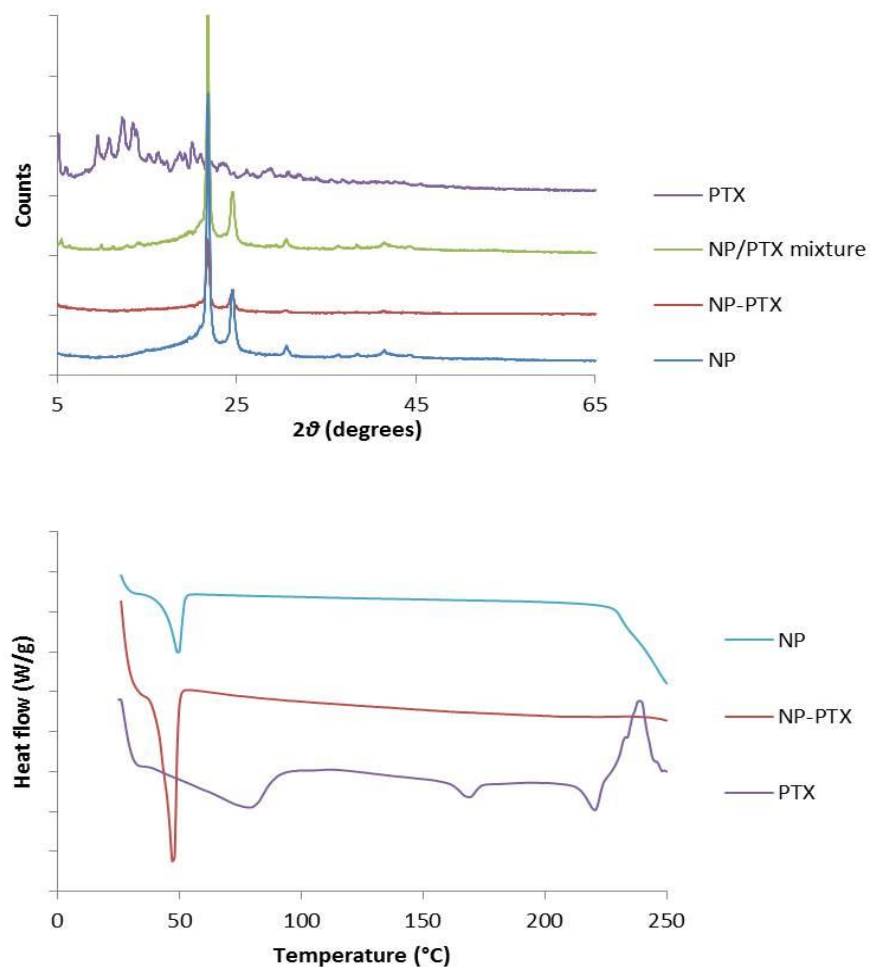
Figure IV-6. Top: XRD analysis of ptx, nanoparticle/ptx mixture, encapsulated ptx (NP-PTX), and nanoparticle alone (NP). Bottom: DSC analysis of ptx, encapsulated ptx, and nanoparticle alone. Endotherms are down.

Paclitaxel release from particles with 4, 7, and 10% crosslinking density in PBS

To investigate the influence of the varied crosslinking densities, which also varies the percentiles of ethylene oxide ratios present in the particle, drug release kinetics were first performed PBS employing the individual particles with 4%, 7% and 10% crosslinking density. Paclitaxel was chosen as a model drug since it is one representative of the BCS class IV and also is a powerful chemotherapeutic.[4] For BCS class II drugs, which have a low solubility but

typically are permeable, successful high saturation carriers such as cellulose esters and derivatives are sufficient to achieve a higher bioavailability.[25, 26] In contrast, BCS IV drugs require both high solvation and tailored carriers in the optimized size to permeabilize and release the drugs in controlled release mechanisms once in the blood, tissue or cell.

Crosslinking Density	Average [PTX] released per day
4%	6.3 μM
7%	2.9 μM
10%	2.0 μM
Mix(4%, 10%) 1:1	2.9 μM
Mix(4%, 10%) 4:1	4.4 μM
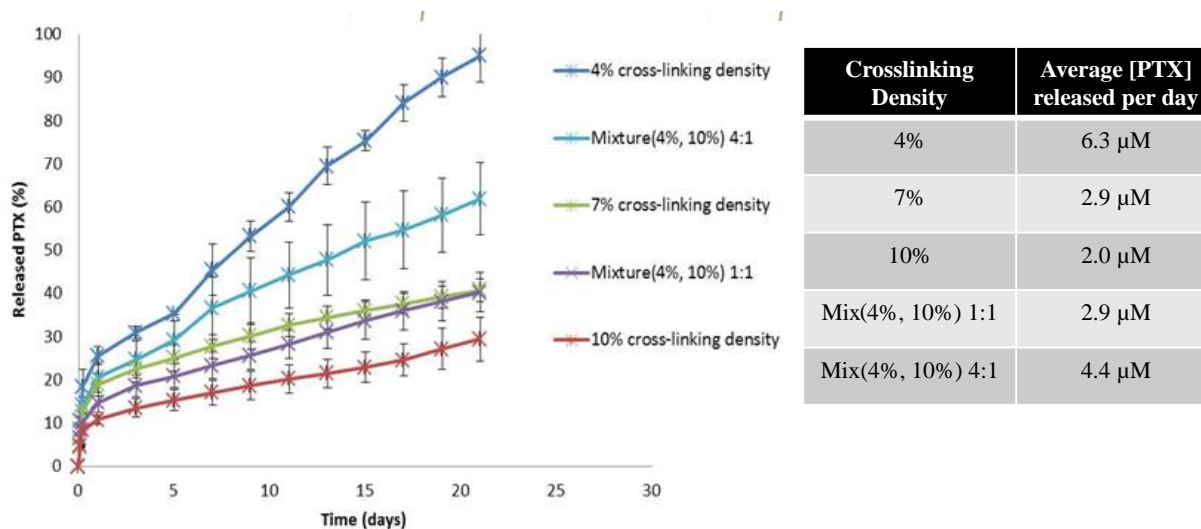
Figure IV-7. Left: Cumulative release of individual and a mixture of particles loaded with paclitaxel measured in PBS. Right: Average released paclitaxel concentration per day for each release profile.

Paclitaxel release from nanoparticles with 4, 7, or 10% crosslinking density in PBS (pH 7.4, 0.1% Tween-80 v/v) at 37 °C is shown in Figure IV-7. Tween-80 was utilized in the release buffer as it prevents binding of free drug to the vessel during the experiment.[27] Critically, different release rates were achieved by simply adjusting the crosslinking density of the particle, with the fastest release from a 4% and the slowest from a 10% crosslinked particle during the 21 day release period. Since the crosslinking density originates from the linear polyester precursor, a simple variation of the epoxide percentage allows the observed far reaching effect on drug release kinetics. For example, particles with the lowest crosslinking 4% crosslinking density

released 95% of the drug during the 21 days. On the other hand, a 10% crosslinked particle only released 29% total drug after 21 days. Interestingly, the least dense network 4% showed a higher amount of drug released after 5 hours (18%), compared to the relatively denser network (10% crosslinking) that showed only 8% paclitaxel release after 5 hours. This trend is also seen in the release curve of a 7% crosslinked particle that initially releases 13% paclitaxel after 5 hours, but the sustained release rate is very similar to that of the 10% crosslinked particle. The initial higher release can be clinically desirable to achieve high plasma concentrations similarly seen from an IV bolus injection or, in the case of cancer therapeutics, to allow local high drug concentrations at the tumor. However, the initial release rates are significantly lower than those for self-assembled poly(lactic-co-glycolic acid) (PLGA) particles in which an initial drug release can be over 40% in the first 48 hours.[28] Furthermore, a self-assembled system allows rather limited variation of release rates guided in part by the amount of surfactant used.[7] Overall, we conclude from these release studies that drug release rates can be controlled and adjusted by modulating the single parameter of the particle's crosslinking density to achieve faster or slower release rates *in vitro*.

In general, *in vitro* studies suggest that paclitaxel duration has a greater effect on cytotoxicity compared to paclitaxel concentration[29, 30]; therefore, a sustained release of low paclitaxel concentrations could potentially be investigated as an alternative to the currently established regimens. For patients with non-small cell lung carcinoma, the recommended dose of paclitaxel is 135 mg/m^2 through a 24 hour infusion every three weeks, and steady-state plasma concentrations typically range between 0.12-2.17 μM.[31] It has also been reported that myelosuppresion becomes more severe when plasma concentrations exceed 0.05-0.1 μM for long periods of time.[32, 33, 34] In this study, the average concentration of released paclitaxel per 24

hours ranged from 6.3 µM (using the 4% crosslinked particles) to 2.0 µM (using the 10% crosslinked particles). However, it must be noted that these concentrations are dependent on the volume of PBS used which is based on the initial concentration of 0.15 mM paclitaxel that was chosen. Therefore, these concentrations of released paclitaxel are obviously not an indication of what plasma concentrations would be *in vivo* and should not be viewed as such. For *in vivo* purposes, the encapsulated paclitaxel dose can be scaled up or down to achieve the desired plasma concentrations.

Paclitaxel release from combined particles with different densities

Drug release rates could also be adjusted by combining particles that contained different crosslinking densities. For example, when particles with 4% crosslinking were mixed in a 1:1 ratio with particles with 10% crosslinking density, the overall release rate, as expected, was neither as fast as 4% crosslinked particles nor as slow as 10% crosslinked particles. Rather, this mixture allowed two simultaneous release rates that resembled an overall rate similar to particles with 7% crosslinking density. This was confirmed by repeating the experiment but using a 4:1 ratio of 4% to 10% crosslinked particles. As expected, the overall release rate was faster compared to 7% crosslinked particles, but not as fast as 4% crosslinked particles. Although paclitaxel was chosen as our model drug, we believe similar results can be achieved with any hydrophobic, small molecule drug. These results suggest that by mixing particles of different densities in adjusted ratios, the nanosponge intermolecular crosslinking methodology is a platform technology in which drug release kinetics can be adjusted to ratios that will serve the needs of an individual patient or disease.

Paclitaxel release from particles in simulated gastric fluid

Early studies have shown the potential of the nanosponge for the treatment of various cancer types in mouse tumor models as demonstrated by a single type of nanosponge delivered intravenously.[35, 36] Since we synthesized particles with the ideal size for an oral drug delivery system, we sought to test the release rate in simulated gastric fluid to determine the potential of this vehicle to survive the acidic conditions of the stomach from an oral drug delivery administration since orally available drugs are the most patient compliant. Although the normal stomach emptying time ($T_{1/2}$) ranges from minutes to several hours[37], paclitaxel release was measured up to 12 hours in simulated gastric fluid (Figure IV-6). Surprisingly, a slow and
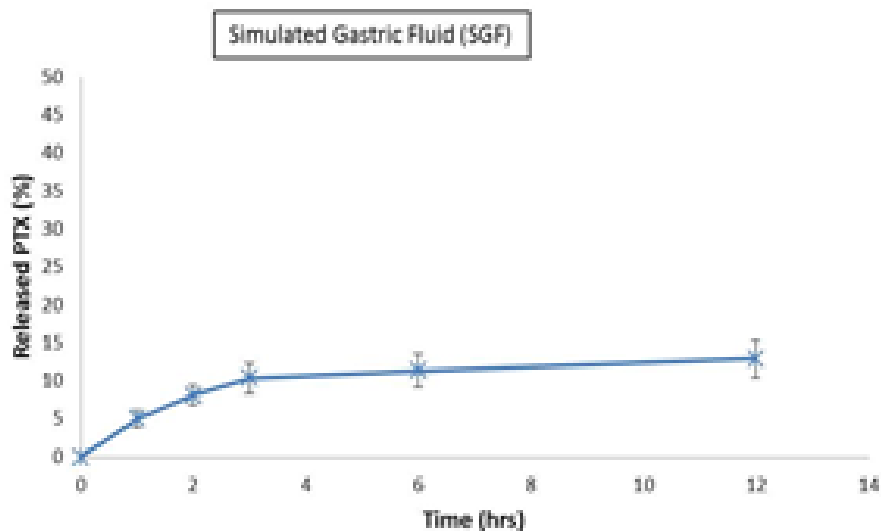

Figure IV-6. Cumulative release of a 4% crosslinked particle loaded with paclitaxel measured in simulated gastric fluid (SGF).

sustained release of paclitaxel was achieved despite the acidic conditions. Only 8% of the drug was released after 2 hours and only 13% was released after 12 hours using a particle with 4%

crosslinking density. This suggests these nanoparticles will not release a significant amount of its therapeutic cargo despite the acidic conditions of the stomach. With the ability to maintain therapeutic cargo in the stomach while being able to transport across the intestines, the use of polyester nanosponges could have a major impact on improving the bioavailability of poorly absorbed drugs.

Conclusion

The presented research assessed the ability of the nanosponges prepared from intermolecular chain crosslinking reactions with resulting crosslinking densities of 4%, 7%, and 10% to serve as platform technology for complete customization of release profiles to meet the need of a patient through IV or oral administration. We have demonstrated with paclitaxel, one representative of the BCS IV class which is one of the most challenging drug classes that includes drugs with low solubility and permeability, can be solvated and formulated without crystallization of the drug. Furthermore, drug release kinetics measured in buffer could not only confirm that the crosslinking density of the particle is responsible for the variation in release rates but also more importantly a fine tuning and customization of unprecedented levels can be achieved by mixing particles of different crosslinking densities in varied ratios, as demonstrated in two examples. All particles were prepared in a 100 nm size range which is ideal for both IV administration and oral delivery of drugs, particularly BCS IV drugs. Investigations of release kinetics in simulated gastrointestinal fluid showed a slow release profile that supports the use of nanosponges for oral administration of BSC IV class drugs to afford high solubilization, high permeability, and a fully adjustable release profile of the therapeutic.

Experimental

Materials

Meta-chloroperoxybenzoic acid was purchased from Sigma Aldrich and recrystallized in methanol before use. Paclitaxel was obtained from LC Laboratories. Phosphate buffered saline was obtained from Gibco by Life Technologies and pH was adjusted to 7.4 and supplemented with Tween-80 (0.1% v/v). Simulated gastric fluid was prepared by dissolving 2.0 grams sodium chloride in 7.0 mL concentrated HCl, diluting to 1.0 L with water, adjusting pH to 1.2, and supplemented with Tween-80 (0.1% v/v). Spectra/Por® Dialysis membrane was purchased from Spectrum Laboratories Inc. All other materials were obtained from Sigma Aldrich and used as received.
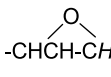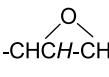
Characterization

Samples for transmission electron microscopy (TEM) imaging were prepared by dissolving 0.5 mg nanoparticles in 1 mL filtered, deionized water. The samples were sonicated for 30 min and stained with 6 drops of 3% phosphotungstic acid. The carbon grids were prepared by slowly dipping an Ultrathin Carbon Type-A 400 Mesh Copper Grid (Ted Pella, Inc., Redding, CA) into the particle solution three times and air drying the grid at room temperature. A Philips CM20T transmission electron microscope operating at 200 kV in bright-field mode was used to obtain TEM micrographs of the polymeric nanoparticles. ^{1}H NMR spectra were obtained from a Bruker AC400 Fourier Transform Spectrometer with $CDCl_3$/TMS as solvent. High-performance liquid chromatography (HPLC) was carried out using a Waters chromatograph equipped with a Waters 2996 variable wavelength photodiode array detector, a Waters 1525 binary HPLC pump, and a reverse phase column (100 x 4.6 mm i.d., pore size 5 μm, Thermo Scientific). All runs were

performed using an isocratic gradient of water and acetonitrile (1:1 v/v) at a flow rate of 1 mL/min. X-ray diffraction analysis was performed using a Scintag X1 θ/θ automated powder X-ray diffractometer with a Cu target, a Peltier cooled solid-state detector, and a zero-background Si(510) sample support. Scans were collected at a rate of 1°/min in the 2θ range from 5 to 65°. Differential scanning calorimetry was conducted using a TA Instruments Differential Scanning Calorimeter (DSC) Model 2920. Samples were added to aluminum pans and non-hermetically sealed. All samples scanned between 25 and 250°C at a rate of 10°C/min after equilibrating at 25 °C.

Polyester nanoparticle synthesis (NP)

Poly(α-allyl-valerolactone, valerolactone)[13] containing 4, 7, or 10% allyl functionality was epoxidized by stirring meta-chloroperoxybenzoic acid (mcpba, 1.2 eq per alkene) in CH_2Cl_2 (0.065 M alkene) for 48 hours and washing with saturated sodium bicarbonate. Resulting polymer was dried under reduced pressure to yield poly(evl-vl) (yield = 75%). ^{1}H NMR (400 MHz, $CDCl_3$/TMS, ppm) δ: 4.08 (m, $-OCH_2$), 2.96-2.91 (m, -CHCH-CH_2 epoxide), 2.75, (m, -CHCH-CH$_2$ epoxide), 2.47 (m, -CHCH-CH_2 epoxide), 2.34 (m, evl and vl, $-O(O)CH_2CH_2$), 1.68 (m, evl and vl, $-CHCH_2CH_2$; evl -CHCH-CH$_2$ epoxide), 0.93–0.91 (d, 3-methyl-1-butanol, $-OCH_2CH_2CH(CH_3)_2$). Nanoparticles were formed by refluxing 2,2'-ethylenedioxy-bis(ethylamine) (1.5 amines per epoxide) with poly(evl-vl) in CH_2Cl_2 (3.24 x 10^{-3} M epoxide) at 46 °C for 12 hours. For example, a 4% crosslinked nanoparticle was formed by adding 2,2'-ethylenedioxy-bis(ethylamine) (7.5 μL, 0.51 mmol) to a stirring solution of poly(evl-vl) (0.173 g, M_n = 3,644 Da, 6.83 x 10^{-2} mmol epoxide) containing 4% epoxide dissolved in CH_2Cl_2 (21.1 mL). The refluxing mixture stirred for 12 hours at 46 °C.

Residual bisamine was removed by dialyzing with Snakeskin Pleated Dialysis Tubing (MWCO = 10,000 Da) against CH_2Cl_2 to yield nanoparticles (NP, 123.8 mg). ^{1}H NMR (400 MHz, CDCl$_3$/TMS, ppm) δ: The significant change is the disappearance of the epoxide ring protons at 2.96, 2.76, and 2.47 ppm and the emergence of small, broad peaks at 3.50-3.45 ppm from the methylene protons adjacent to the oxygens in the crosslinker and 2.75-2.68 ppm from the methylene protons adjacent to the secondary amine after crosslinking. Particles with 7% and 10% crosslinking densities were synthesized in a similar manner with poly(evl-vl) containing 7% and 10% epoxide functionality, respectively, and reacting with 2,2'-ethylenedioxy-bis(ethylamine) (1.5 amines per epoxide) in CH_2Cl_2 (3.24 x 10^{-3} M epoxide) for 12 hours at 46 °C.

Paclitaxel encapsulation into nanoparticles (NP-PTX)

A solution of nanoparticle (70.0 mg) and paclitaxel (15.4 mg) in DMSO (0.150 mL) was added drop-wise to a vortexing solution of aqueous 1% d-α-tocopherol polyethyleneglycol (1000) succinate (Vit E-TPGS, 35.0 mL). The resulting precipitation was centrifuged to remove the free drug from the encapsulated drug. The precipitation underwent three cycles of centrifugation at 7830 rpm for 20 minutes and replacing the supernatant each time with fresh deionized water. The precipitation was freeze-dried to yield a white powder (13.0% paclitaxel wt/wt determined by HPLC detecting at 227 nm).

In vitro drug release

The release of paclitaxel from the nanoparticles was measured in PBS (pH 7.4) or simulated gastric fluid (pH 1.2) containing Tween-80 (0.1% v/v) at 37 °C at a paclitaxel concentration of

0.15 mM. For example, a 4% crosslinked nanoparticle containing 13.0% paclitaxel wt/wt (4.8 mg) was suspended in 5.0 mL PBS (pH 7.4, 0.1% Tween-80 v/v). At each time point, the suspension was centrifuged at 7830 rpm for 15 minutes and the supernatant was collected and replaced with 5.0 mL fresh buffer. For release studies in PBS, the supernatant at each time point was analyzed by HPLC as described in the characterization section. For release studies in simulated gastric fluid, the supernatant was neutralized with sodium bicarbonate to pH 7 and extracted three times with 5 mL CH_2Cl_2. The CH_2Cl_2 was evaporated and the resulting solid was dissolved in acetonitrile/water (1:1 v/v) and analyzed by HPLC.   All experiments were performed in triplicate.

References

1.   Davis, M.; Zuckerman, J.; Choi, C.; Seligson, D.; Tolcher, A.; Alabi, C.; Yen, Y.; Heidel, J.; Ribas, A., Evidence of RNAi in humans from systemically administered siRNA via targeted nanoparticles. *Nature* **2010,** *464* (7291), 1067-U140.

2.   McCarley, R.; Forsythe, J.; Loew, M.; Mendoza, M.; Hollabaugh, N.; Winter, J., Release Rates of Liposomal Contents Are Controlled by Kosmotropes and Chaotropes. *Langmuir* **2013,** *29* (46), 13991−13995.

3.   Parveen, S.; Sahoo, S., Long circulating chitosan/PEG blended PLGA nanoparticle for tumor drug delivery. *European Journal of Pharmacology* **2011,** *670* (2-3), 372-383.

4.   Reddy, B. B. K.; Karunakar, A., Biopharmaceutics Classification System: A Regulatory Approach. *Dissolut Technol* **2011,** *18* (1), 31-37.

5.   Potineni, A.; Lynn, D.; Langer, R.; Amiji, M., Poly(ethylene oxide)-modified poly(beta-amino ester) nanoparticles as a pH-sensitive biodegradable system for paclitaxel delivery. *Journal of Controlled Release* **2003,** *86* (2-3), 223-234.

6.   Tyrrell, Z.; Shen, Y.; Radosz, M., Multilayered Nanoparticles for Controlled Release of Paclitaxel Formed by Near-Critical Micellization of Triblock Copolymers. *Macromolecules* **2012,** *45* (11), 4809-4817.

7.   Mu, L.; Feng, S., A novel controlled release formulation for the anticancer drug paclitaxel (Taxol (R)): PLGA nanoparticles containing vitamin E TPGS. *Journal of Controlled Release* **2003,** *86* (1), 33-48.

8.   Gong, C.; Xie, Y.; Wu, Q.; Wang, Y.; Deng, S.; Xiong, D.; Liu, L.; Xiang, M.; Qian, Z.; Wei, Y., Improving anti-tumor activity with polymeric micelles entrapping paclitaxel in pulmonary carcinoma. *Nanoscale* **2012,** *4* (19), 6004-6017.

9.   Wang, H.; Tang, L.; Tu, C.; Song, Z.; Yin, Q.; Yin, L.; Zhang, Z.; Cheng, J., Redox-Responsive, Core-Cross-Linked Micelles Capable of On-Demand, Concurrent Drug Release and Structure Disassembly. *Biomacromolecules* **2013,** *14* (10), 3706-3712.

10.   Kryger, M. B. L.; Wohl, B. M.; Smith, A. A. A.; Zelikin, A. N., Macromolecular prodrugs of ribavirin combat side effects and toxicity with no loss of activity of the drug. *Chem Commun* **2013,** *49* (26), 2643-2645.

11.   Mura, S.; Nicolas, J.; Couvreur, P., Stimuli-responsive nanocarriers for drug delivery. *Nature Materials* **2013,** *12* (11), 991-1003.

12.   Ihre, H. R.; De Jesus, O. L. P.; Szoka, F. C.; Frechet, J. M. J., Polyester dendritic systems for drug delivery applications: Design, synthesis, and characterization. *Bioconjugate Chemistry* **2002,** *13* (3), 443-452.

13.   Stevens, D.; Watson, H.; LeBlanc, M.; Wang, R.; Chou, J.; Bauer, W.; Harth, E., Practical polymerization of functionalized lactones and carbonates with Sn(OTf)(2) in metal catalysed ring-opening polymerization methods. *Polymer Chemistry* **2013,** *4* (8), 2470-2474.

14.   van der Ende, A. E.; Kravitz, E. J.; Harth, E., Approach to formation of multifunctional polyester particles in controlled nanoscopic dimensions. *J Am Chem Soc* **2008,** *130* (27), 8706-8713.

15.   van der Ende, A.; Kravitz, E.; Harth, E., Approach to formation of multifunctional polyester particles in controlled nanoscopic dimensions. *Journal of the American Chemical Society* **2008,** *130* (27), 8706-8713.

16.   Zhang, Z.; Feng, S., The drug encapsulation efficiency, in vitro drug release, cellular uptake and cytotoxicity of paclitaxel-loaded poly(lactide)-tocopheryl polyethylene glycol succinate nanoparticles. *Biomaterials* **2006,** *27* (21), 4025-4033.

17.   McClean, S.; Prosser, E.; Meehan, E.; O'Malley, D.; Clarke, N.; Ramtoola, Z.; Brayden, D., Binding and uptake of biodegradable poly-DL-lactide micro- and nanoparticles in intestinal epithelia. *European Journal of Pharmaceutical Sciences* **1998,** *6* (2), 153-163.

18.   Win, K.; Feng, S., Effects of particle size and surface coating on cellular uptake of polymeric nanoparticles for oral delivery of anticancer drugs. *Biomaterials* **2005,** *26* (15), 2713-2722.

19.   Win, K. Y.; Feng, S. S., Effects of particle size and surface coating on cellular uptake of polymeric nanoparticles for oral delivery of anticancer drugs. *Biomaterials* **2005,** *26* (15), 2713-2722.

20.	van der Ende, A. E.; Sathiyakumar, V.; Diaz, R.; Hallahan, D. E.; Harth, E., Linear release nanoparticle devices for advanced targeted cancer therapies with increased efficacy. *Polym Chem-Uk* **2010,** *1* (1), 93-96.

21.	Niidome, T.; Yamagata, M.; Okamoto, Y.; Akiyama, Y.; Takahashi, H.; Kawano, T.; Katayama, Y.; Niidome, Y., PEG-modified gold nanorods with a stealth character for in vivo applications. *Journal of Controlled Release* **2006,** *114* (3), 343-347.

22.	Peracchia, M.; Fattal, E.; Desmaele, D.; Besnard, M.; Noel, J.; Gomis, J.; Appel, M.; d'Angelo, J.; Couvreur, P., Stealth (R) PEGylated polycyanoacrylate nanoparticles for intravenous administration and splenic targeting. *Journal of Controlled Release* **1999,** *60* (1), 121-128.

23.	Liggins, R.; Hunter, W.; Burt, H., Solid-state characterization of paclitaxel. *Journal of Pharmaceutical Sciences* **1997,** *86* (12), 1458-1463.

24.	Hamoudeh, M.; Diab, R.; Fessi, H.; Dumontet, C.; Cuchet, D., Paclitaxel-loaded microparticles for intratumoral administration via the TMT technique: Preparation, characterization, and preliminary antitumoral evaluation. *Drug Development and Industrial Pharmacy* **2008,** *34* (7), 698-707.

25.	Yin, L. G.; Hillmyer, M. A., Preparation and Performance of Hydroxypropyl Methylcellulose Esters of Substituted Succinates for in Vitro Supersaturation of a Crystalline Hydrophobic Drug. *Molecular Pharmaceutics* **2014,** *11* (1), 175-185.

26.	Li, B.; Harich, K.; Wegiel, L.; Taylor, L. S.; Edgar, K. J., Stability and solubility enhancement of ellagic acid in cellulose ester solid dispersions. *Carbohydrate Polymers* **2013,** *92* (2), 1443-1450.

27.   Nsereko, S.; Amiji, M., Localized delivery of paclitaxel in solid tumors from biodegradable chitin microparticle formulations. *Biomaterials* **2002,** *23* (13), 2723-2731.

28.   Vicari, L.; Musumeci, T.; Giannone, I.; Adamo, L.; Conticello, C.; De Maria, R.; Pignatello, R.; Puglisi, G.; Gulisano, M., Paclitaxel loading in PLGA nanospheres affected the in vitro drug cell accumulation and antiproliferative activity. *Bmc Cancer* **2008,** *8*.

29.   Lopes, N.; Adams, E.; Pitts, T.; Bhuyan, B., Cell kill kinetics and cell-cycle effects of taxol on human and hamster ovarian cell-lines. *Cancer Chemotherapy and Pharmacology* **1993,** *32* (3), 235-242.

30.   Georgiadis, M.; Russell, E.; Gazdar, A.; Johnson, B., Paclitaxel cytotoxicity against human lung cancer cell lines increases with prolonged exposure durations. *Clinical Cancer Research* **1997,** *3* (3), 449-454.

31.   Rowinsky, E.; Jiroutek, M.; Bonomi, P.; Johnson, D.; Baker, S., Paclitaxel steady-state plasma concentration as a determinant of disease outcome and toxicity in lung cancer patients treated with paclitaxel and cisplatin. *Clinical Cancer Research* **1999,** *5* (4), 767-774.

32.   Ohtsu, T.; Sasaki, Y.; Tamura, T.; Miyata, Y.; Nakanomyo, H.; Nishiwaki, Y.; Saijo, N., Clinical pharmacokinetics and pharmacodynamics of paclitaxel: A 3-hour infusion versus a 24-hour infusion. *Clinical Cancer Research* **1995,** *1* (6), 599-606.

33.   Gianni, L.; Kearns, C.; Giani, A.; Capri, G.; Vigano, L.; Locatelli, A.; Bonadonna, G.; Egorin, M., Nonlinear pharmacokinetics and metabolism of paclitaxel and its pharmacokinetic/pharmacodynamic relationships in humans. *Journal of Clinical Oncology* **1995,** *13* (1), 180-190.

34.   Rowinsky, E.; Wright, M.; Monsarrat, B.; Lesser, G.; Donehower, R., Taxol - pharmacology, metabolism and clinical implications. *Cancer Surveys* **1993,** *17*, 283-304.

35.   Hariri, G.; Edwards, A. D.; Merrill, T. B.; Greenbaum, J. M.; van der Ende, A. E.; Harth, E., Sequential Targeted Delivery of Paclitaxel and Camptothecin Using a Cross-Linked "Nanosponge" Network for Lung Cancer Chemotherapy. *Molecular Pharmaceutics* **2014,** *11* (1), 265-275.

36.   Passarella, R. J.; Spratt, D. E.; van der Ende, A. E.; Phillips, J. G.; Wu, H. M.; Sathiyakumar, V.; Zhou, L.; Hallahan, D. E.; Harth, E.; Diaz, R., Targeted Nanoparticles That Deliver a Sustained, Specific Release of Paclitaxel to Irradiated Tumors. *Cancer Research* **2010,** *70* (11), 4550-4559.

37.   Hellmig, S.; Von Schoning, F.; Gadow, C.; Katsoulis, S.; Hedderich, J.; Folsch, U.; Stuber, E., Gastric emptying time of fluids and solids in healthy subjects determined by C-13 breath tests: influence of age, sex and body mass index. *Journal of Gastroenterology and Hepatology* **2006,** *21* (12), 1832-1838.

CHAPTER V

NANOSPONGE/POLYGLYCIDOL DUAL DRUG DELIVERY OF MEK INHIBITOR AND

BONE MORPHOGENETIC PROTEIN 2 FOR IMPROVED BONE HEALING

Introduction

Neurofibromatosis 1 (NF1) is an autosomal dominant disease caused by mutations of the tumor-suppressor gene *NF1*[1, 2], a gene encoding the RAS GTP-ase activating protein neurofibromin[3, 4], and patients with NF1 frequently suffer from skeletal defects including decreased bone mineral density, tibia bowing, and impaired bone healing following fracture (pseudoarthrosis).[5, 6] The focal nature of the dysplastic skeletal lesions in NF1 and the identified second hit mutations in *NF1* detected in biopsies from NF1 pseudarthroses[7] suggest that a restricted population of bone mesenchymal progenitors characterized by *NF1* loss of function triggers the focal skeletal dysplasia associated with NF1. In support of this hypothesis, neurofibromin is expressed in bone-forming cells and its loss of function leads to chronic and uncontrolled RAS-ERK activity in multiple cell lineages, including chondrocytes and osteoblasts.[8, 9, 10]

Since the etiology of the skeletal disorder is not fully known, treatment is often limited to surgical correction or amputation.[11] Additionally, the development of novel therapeutics remains difficult due to the lack of animal models that can recapitulate the complex bone disorder associated with NF1. Engineering such a mouse model remains its own challenge since Nf1^{-/-} mice are embryonic lethal.[12, 13, 14] However, Elefteriou and coworkers generated a new mouse model that lack *Nf1* in post-natal *Osterix* (*Osx*)-positive osteoprogenitors ($Nf1_{osx}^{-/-}$ mice). This

model was generated by crossing mice with *Nf1* floxed alleles[15] and mice expressing the cre-recombinase under the control of the Osterix (*Osx*) promoter and Tet[off] system[16]. These mutant mice exhibit reduced stature due to *Osx*-cre activity in chondrocytes during development[17, 18], but are born with a normal size and do not show any short stature phenotype in adults when given doxycycline from conception to 2 weeks of age to repress cre-recombinase activity. This mouse model can be used to determine if loss of *Nf1* function in osteoblast progenitors impairs their differentiation *in vivo*, independent of developmental growth plate factors.

Constitutive activation of RAS and ERK are a consequence of *Nf1* deficiency, and this is believed to play a major role in osteoclastogenesis and improper healing in response to fracture. Recently, studies showed that combination treatment of bone morphogenetic protein 2 (BMP2) and bisphosphonates could improve bone production in Nf1^{+/-} mice, but did not rescue the impaired signaling pathway.[19] BMP2 can promote cell differentiation through either the RAS/ERK or SMAD signaling pathways; however, the constitutive ERK activity caused by *Nf1* deficiency blunts the response to the osteogenic property of BMP2 since ERK negatively regulates the SMAD signaling pathway. Therefore, a MEK inhibitor would allow some control or negative regulation of the constitutively active ERK. *In vitro* results indicated neither therapeutic alone could rescue the signaling defects, but rather both BMP2 and a MEK inhibitor were required simultaneously.

BMP2 is commercially available and is a current therapeutic option for numerous bone healing applications.[20, 21] However, BMP2 is cleared within hours upon administration and a sustained release technology is desired to circumvent frequent dosing. Trametinib, a MEK inhibitor (GSK), is completely insoluble in water and therefore is difficult to administer systemically. A sustained release of MEK inhibitor is also desired in order to continuously act on

the healing bone tissue in conjunction with BMP2. Therefore, a dual drug delivery system is required that would allow the release of two different classes of therapeutics simultaneously. The polyester nanosponge is an excellent vehicle to nanosolubilize the MEK inhibitor to decrease its crystallinity and increase its water solubility. Also, the nanosponge allows for a tailored release of the MEK inhibitor. However, an alternative material is required for the sustained release of a protein growth factor. For example, polyglycidol is a semi-branched, PEG-like polymer that can act as a matrix for larger biologically active structures. In this way, BMP2 can slowly diffuse out of the polyglycidol matrix, and at the same time, MEK inhibitor will be released from the nanosponge. The success of this system is not only a significant achievement from a drug delivery and nanotechnology standpoint but also for the development of new technologies for bone healing applications and novel treatments for diseases that are otherwise difficult to treat such as NF1.

Results and Discussion

Encapsulation of MEK inhibitor in polyester nanosponge

Nanoparticles containing 4% crosslinking density were synthesized as previously described.[22] A lower crosslinking density was chosen since maximum release of the drug was desired within the first three weeks. MEK inhibitor was encapsulated into the particles using the nanosolubilization process described earlier. Although the MEK inhibitor is hydrophobic, its solubility in DMSO is not as high compared to paclitaxel and thus additional DMSO was required to fully solubilize for encapsulation. Because of this, precipitation was more challenging, and the final product only contained 6.4% wt/wt drug after an 18% drug loading

ratio. Nevertheless, the drug was successfully encapsulated and could be incorporated into the final formulation at a therapeutically relevant concentration.
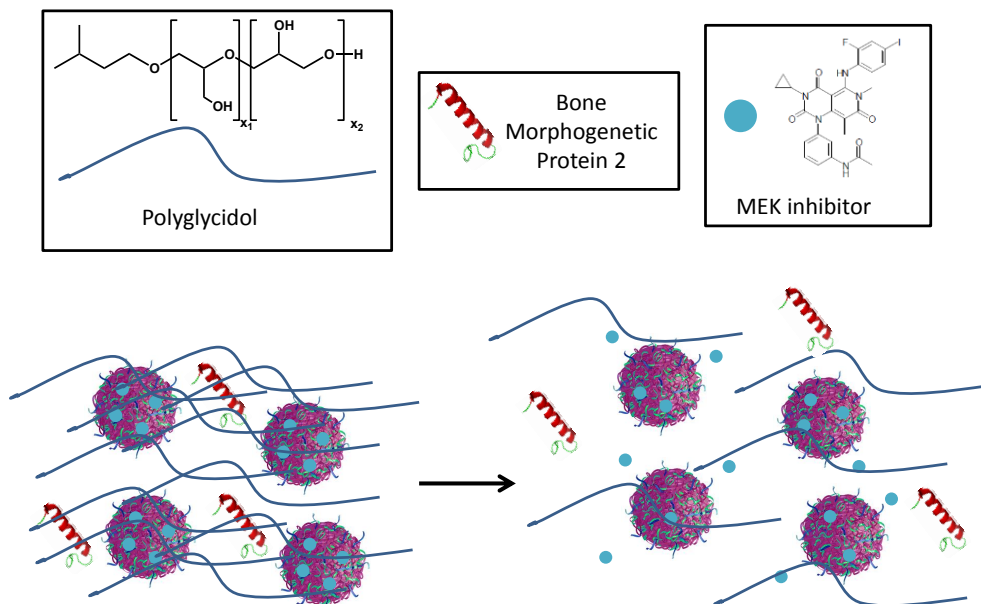
Figure V-1. Illustration of encapsulated MEK inhibitor with BMP2 in polyglycidol matrix. Over time, BMP2 and MEK inhibitor is released simultaneously.

BMP2 formulation in polyglycidol and dual drug delivery formulation

Polyglycidol is a semi-branched, water-soluble, and anti-fouling polymer. Because of its polyethyleneglycol-like characteristics, biocompatibility, viscosity, and semi-branched nature, polyglycidol was chosen to act as a matrix for the incorporation of biologically active peptides and proteins, in this case BMP2. Polyglycidol was synthesized by Benjamin Spears of the Harth Laboratory (Vanderbilt University) as previously reported.[23] Since vacuum-dried polyglycidol is very viscous, phosphate buffered saline (PBS) was added to reduce its viscosity in order to load into an insulin syringe. A defined volume of PBS was added until the mixture could successfully be taken up by an insulin needle, and this exact ratio of PBS to polyglycidol served as a measure

for all formulations. It was determined that a polyglycidol concentration of 0.46 g/mL in PBS served as the maximum concentration that could be taken up into the insulin needle for injection. With this viscosity, it is believed the injected material will remain at the injection site and slowly dissolve over time while the drugs are released.

The purpose of the dual drug delivery formulation is to locally release both the BMP2 and the MEK inhibitor at the fracture site to allow synergistic therapeutic effects for up to a week (Figure V-1). Each injection contained 10 µg BMP2 and 3.76 µg MEK inhibitor, as previous studies suggested these doses would be within the therapeutic range. The encapsulated MEK inhibitor was suspended in PBS and ultrasonicated before being transferred to the polyglycidol/BMP2 mixture and diluted with PBS to achieve the 0.46 g/mL polyglycidol concentration. Once injected, the polyglycidol should protect and mediate the release of the BMP2 and at the same time, MEK inhibitor will be released due to diffusion and degradation of the nanoparticle.

In vivo analysis of bone healing following fractures and treatment

Mid-tibia fractures were performed on $Nf1_{osx}^{-/-}$ mice hours before injection of treatment group, and a second treatment injection was performed 7 days later. After 21 days, the mice were sacrificed, and the bones were collected for analysis. Wild-type mice were used as a control group, and treatment groups included vehicle (unloaded nanoparticle in the polyglycidol matrix), BMP2 (mixed with polyglycidol), GSK (MEK inhibitor encapsulated within nanoparticle and mixed in polyglycidol matrix), and BMP2+GSK (encapsulated MEK inhibitor mixed with polyglycidol matrix and BMP2). 20 µL injections were used as this was the maximum injection volume at the fracture site without spillage. Wild-type mice were expected to develop significant

and strong callus formation after 21 days of fracture compared to the Nf1 lacking mice that were expected to develop very little callus without successful treatment.
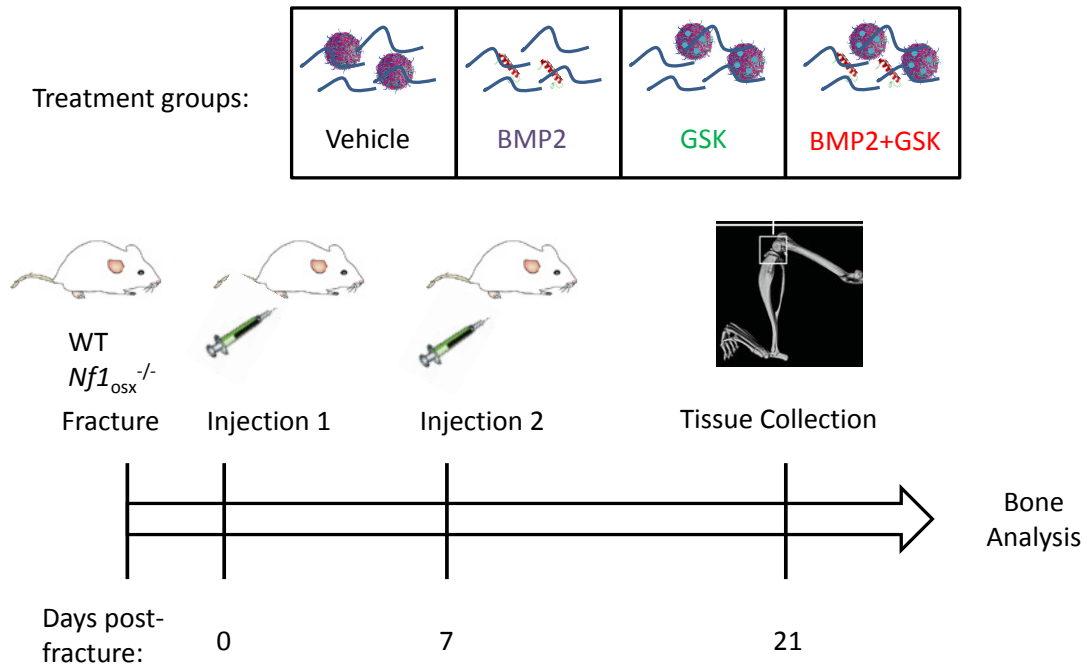
Figure V-2. Experimental design for treating fractures *in vivo*.

X-ray analysis of the fracture at day 0 and day 21 for each treatment group is shown in Figure V-3. In all cases, a fracture can be seen at day 0 with no callus formation. However, the wild-type control has a significant callus formation at the fracture site after 21 days which is indicative of normal, healthy bone healing process. This effect is absent in the $Nf1_{osx}^{-/-}$ mice with vehicle treatment, and little to no callus formation is seen in either one of the single treatment groups (BMP2 or GSK). Rather, only the dual drug delivery treatment group achieved significant callus formation indicating an enhanced bone healing response to fractures, comparable to what is seen in healthy wild-type mice.
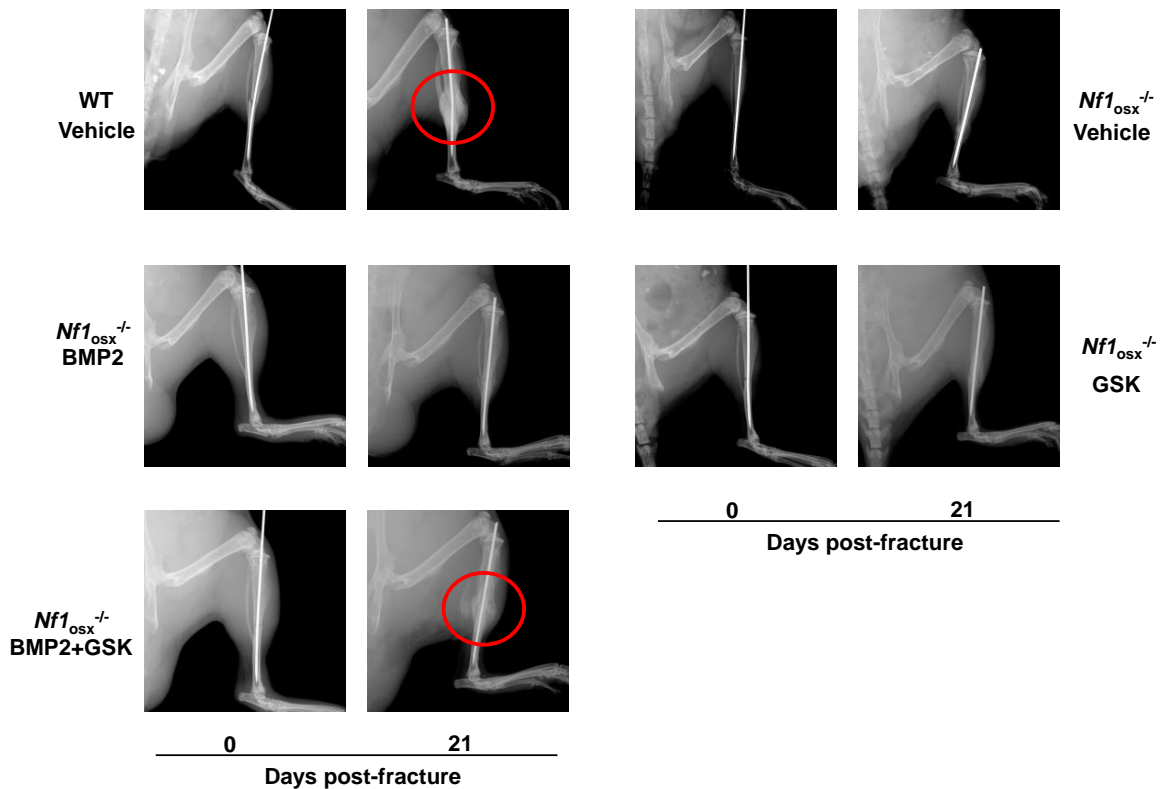
Figure V-3. X-ray analysis of fracture at days 0 and 21 for all treatment groups. Red circles indicate noticeable callus formation. Analysis and figure provided by Dr. Jean of Elefteriou Lab, Vanderbilt University.

These results were further validated via microCT scanning of the callus and performing quantitative analyses. MicroCT scan of the callus of each treatment group after 21 days is shown in Figure V-4A. The WT vehicle treatment group responded as expected, resulting in dense, healthy callus formation. Comparably, the vehicle and single treatment groups of the $Nf1_{osx}^{-/-}$ mice formed callus that appears much less dense. Rather, only the combination treatment group achieved healthy and dense callus formation similarly seen in the wild type control. Mineral density (such as calcium) is a quantitative measurement that represents an estimate of bone strength. The vehicle and single treatment groups of $Nf1_{osx}^{-/-}$ mice had lower mineral density

compared to wild-type, but the combination treatment group had significantly greater mineral density compared to the single treatment groups, indicating enhanced bone strength. Callus total volume was measured to provide a volume of the callus formed after 21 days, and total callus bone volume was measured as well to indicate how much of the callus volume consisted of actual bone. In both cases, only the dual drug delivery treatment group had significantly greater response compared to BMP2 or GSK alone and was comparable to the wild-type response.
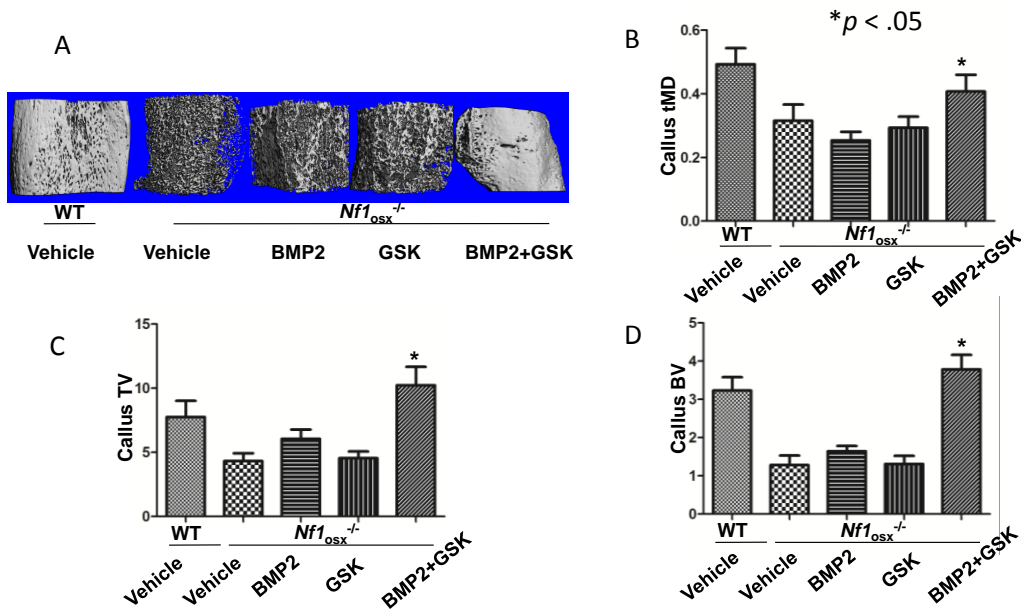
Figure V-4. A: microCT analysis of callus after 21 days of treatment. B: total mineral density of callus after 21 days of treatment. C: total callus volume. D: total callus bone volume Analysis and figure provided by Dr. Jean Ndong of Elefteriou Lab, Vanderbilt University.

Although callus and bone formation are necessary for the healing process following a fracture, bone strength is equally as important as bone volume. Figure V-5 shows the callus peak force and callus stiffness analysis, both of which are used to indicate bone strength. In both analyses, only the BMP2+GSK treatment group achieved significant bone strength during the

experiment and is comparable to the wild-type response. In contrast, neither BMP2 nor GSK alone achieved significant bone strength during the 21 day experiment.
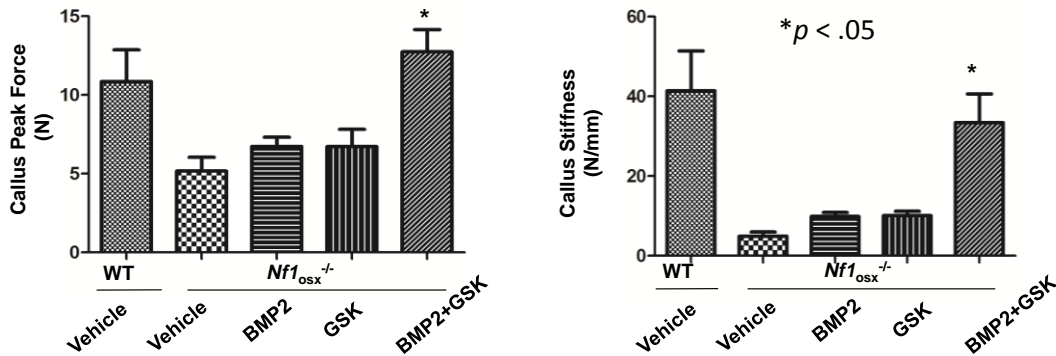
Figure V-5. Left: Callus peak force analysis of tibia after 21 days of treatment. Right: Callus stiffness analysis of tibia. Analysis and figure provided by Dr. Jean Ndong of Elefteriou Lab, Vanderbilt University.

Conclusion

In summary, this study confirmed the early differentiation defect typical of *Nf1*-deficient osteoprogenitors revealed a block in BMP2 response as a cause of their impaired differentiation and led to preclinical data supporting the efficacy of a novel targeted approach to promote bone healing in individuals with NF1 pseudoarthrosis, based on the use of MEK inhibition and an osteogenic stimulus in the form of BMP2. We can conclude from these analyses that neither BMP2 nor GSK can act alone to lead to successful bone healing following a fracture in $Nf1_{Osx}^{-/-}$ mice. Instead, the administration of both drugs simultaneously allowed by the unique dual drug delivery formulation resulted in not only for a high volume of callus and bone but also strong, healthy bone tissue. The MEK inhibitor used (Trametinib) is already FDA-approved for the treatment of patients with unresectable or metastatic melanoma with $BRAF^{V600E}$ or $BRAF^{V600K}$

mutations. Hence, transition for use in the NF1 setting could be accelerated compared to other drugs.[24, 25] This drug delivery formulation potentially could be used for various other combination therapy approaches that involve protein or peptide therapeutics.

Experimental

Polyester nanoparticle synthesis (NP)

Poly(α-allyl-valerolactone, valerolactone)[26] containing 4% allyl functionality was epoxidized with meta-chloroperoxybenzoic acid (mcpba, 1.2 eq per alkene, Sigma) in CH_2Cl_2 (0.065 M alkene) for 48 hours and washed with saturated sodium bicarbonate. Resulting polymer was dried under reduced pressure. 2,2'-ethylenedioxy-bis(ethylamine) (7.5 µL, 0.51 mmol, Sigma) was added to a solution of poly(epoxide-valerolactone, valerolactone) (0.173 g, M_n = 3,644 Da) dissolved in CH_2Cl_2 (21.1 mL). The reaction mixture refluxed at 12 hours at 46° C. Residual bisamine was removed by dialyzing with Snakeskin Pleated Dialysis Tubing (MWCO = 10,000) against CH_2Cl_2 to yield nanoparticles (NP).

MEK inhibitor encapsulation into nanoparticles (NP-MEK)

A solution of nanoparticle (23.0 mg) and MEK inhibitor (5.0 mg, GlaxoSmithKline) in DMSO (1.00 mL) was added drop-wise to a vortexing solution of aqueous 1% d-α-tocopherol polyethyleneglycol (1000) succinate (Vit E-TPGS (Sigma), 14.0 mL). The resulting precipitation was washed by three cycles of centrifugation at 7830 rpm for 20 minutes and replacing the supernatant each time with fresh deionized water. The precipitation was freeze-dried to yield a white powder (6.4% MEK inhibitor wt/wt determined by NanoDrop UV-Vis at 258 nm, NP-MEK).

Polyglycidol-NP-MEK dual drug delivery system for MEK inhibitor and BMP2

Polyglycidol homopolymer[23] was synthesized by first stirring 3-methyl-1-butanol (0.98 mL, 1.7 M in anhydrous THF) with Sn(OTf)$_2$ (1.28 mL, 0.037 M in anhydrous THF) in a nitrogen-purged flask. Glycidol monomer (10.0g, 135 mmol, Sigma) was added drop-wise to the cooled reaction mixture. After the monomer addition was complete, the reaction vessel was allowed to warm up to room temperature. Once stirring was completely impeded, the crude viscous polymer product was dissolved in a minimal amount of methanol and precipitated into vigorously stirring acetone, which was then decanted to afford the pure glycidol homopolymer product as a translucent, viscous material. BMP2 (Creative BioMart) suspended in 20 mM acetic acid (10 mg/mL) and was added to polyglycidol and diluted with PBS for a BMP2 concentration of 0.50 µg/µL and polyglycidol concentration of 0.46 g/mL. For MEK inhibitor injections and combo injections, encapsulated MEK inhibitor was first sonicated in PBS and transferred to the polyglycidol mix to yield a MEK inhibitor concentration of 0.188 µg/µL. Vehicle was prepared using unloaded nanoparticles and formulated similarly as described above.

Animals

All procedures were approved by the Institutional Animal Care and Use Committee (IACUC) at Vanderbilt University Medical Center. WT and $Nf1_{osx}^{-/-}$ were generated by crossing $Nf1^{flox/flox}$ mice and $Nf1^{flox/flox}$; Osx-tTA,*tetO*-cre mice ($Nf1_{osx}^{-/-}$). To repress transactivation of Cre by the *Osx* promoter during development, 200µg/ml doxycycline was given to pregnant mothers and pups in drinking water and refreshed every 2-3 days, as indicated in the text. All experimental mice were originated from the same colony to increase genetic homogeneity. Closed mid-diaphyseal fracture of the tibia was created by three-point bending with an Einhorn device in 2

months-old mice, as previously described [25]. To produce stabilized fractures, an intramedullary fixation was used by inserting a 0.25 mm metal insect pin in the tibial tuberosity through the patellar tendon, prior to the creation of the fracture. Buprenorphine was administered subcutaneously for pain control. Males and females were used. X-rays were taken following fracture to exclude any mice with unsatisfactory fractures. All mice handling, bone analyses, and statistical analysis were performed by Dr. Jean Ndong of the Elefteriou Laboratory at Vanderbilt University.

X-ray and μCT analyses.

Radiographs were obtained using a digital cabinet X-ray system (LX-60, Faxitron X-Ray, USA). μCT analyses were performed using a Scanco μCT 40 system (Scanco Medical, Bassersdorf, Switzerland). Tomographic images were acquired at 55 kVp and 145 mA with an isotropic voxel size of 12 μm and at an integration time of 250ms with 500 projections collected per 180° rotation.

Biomechanical testing

The fractured tibia from WT and $Nf1_{Osx}^{-/-}$ mice was cleaned of soft tissue and stored frozen in PBS until thawed for testing. Three-point-bending was accomplished in displacement control on an Instron Dynamight 4481 servo-hydraulic material testing apparatus (Instron, Norwood, MA). Hydrated samples were tested with span of 6mm at a rate of 3mm/min.[27] Force was measured using a 100N load cell, and displacement was measured by a linear variable differential transformer. Structural properties were extracted from force-displacement curves by custom

Matlab algorithms (Mathworks, Natick, MA). Material properties were calculated by accounting for structure by utilizing cross-sectional area and moment of inertia as measured by μCT.

Statistical analysis.

A one-way analysis of variance (ANOVA) was used to determine whether differences existed in μCT -, Raman-, and biomechanical-derived properties among experimental groups. In the event that standard deviations were significantly different, the ANOVA was done by the non-parametirc Kruskal-Wallis test. When differences existed at $p<0.05$, post-hoc, pair-wise comparisons were tested for significance in which the p-value was adjusted ($p_{adj}<0.05$) by Holm-Sidak's method or Dunn's method (non-parametric). Statistical analysis was performed using GraphPad PRISM (v6.0a, La Jolla, CA). Data are provided as mean +/- SD.

References

1.   Stevenson, D.; Birch, P.; Friedman, J.; Viskochil, D.; Carey, J.; Group, N.-P. W., Descriptive analysis of tibial pseudarthrosis in patients with neurofibromatosis 1. *American Journal of Human Genetics* **1997,** *61* (4), A35-A35.

2.   Viskochil, D.; Buchberg, A.; Xu, G.; Cawthon, R.; Stevens, J.; Wolff, R.; Culver, M.; Carey, J.; Copeland, N.; Jenkins, N.; White, R.; OConnell, P., Deletions and a translocation interrupt a cloned gene at the neurofibromatosis type-1 locus. *Cell* **1990,** *62* (1), 187-192.

3.   Cawthon, R.; Weiss, R.; Xu, G.; Viskochil, D.; Culver, M.; Stevens, J.; Robertson, M.; Dunn, D.; Gesteland, R.; OConnell, P.; White, R., A major segment of the neurofibromatosis type-1 gene - CDNA sequence, genomic structure, and point mutations. *Cell* **1990,** *62* (1), 193-201.

4.   Marchuk, D.; Saulino, A.; Tavakkol, R.; Swaroop, M.; Wallace, M.; Andersen, L.; Mitchell, A.; Gutmann, D.; Boguski, M.; Collins, F., CDNA cloning of the type-1 neurofibromatosis gene - complete sequence of the NF1 gene-product. *Genomics* **1991,** *11* (4), 931-940.

5.   Alwan, S.; Armstrong, L.; Joe, H.; Birch, P.; Szudek, J.; Friedman, J., Associations of osseous abnormalities in neurofibromatosis 1. *American Journal of Medical Genetics Part a* **2007,** *143A* (12), 1326-1333.

6.   Crawford, A.; Parikh, S.; Schorry, E.; Von Stein, D., The immature spine in type-1 neurofibromatosis. *Journal of Bone and Joint Surgery-American Volume* **2007,** *89A*, 123-142.

7.   Stevenson, D. A.; Zhou, H.; Ashrafi, S.; Messiaen, L. M.; Carey, J. C.; D'Astous, J. L.; Santora, S. D.; Viskochil, D. H., Double inactivation of NF1 in tibial pseudarthrosis. *American journal of human genetics* **2006,** *79* (1), 143-8.

8.   Ono, K.; Karolak, M. R.; Ndong, J. D.; Wang, W.; Yang, X.; Elefteriou, F., The Ras-GTPase activity of neurofibromin restrains ERK-dependent FGFR signaling during endochondral bone formation. *Hum Mol Genet* **2013**.

9.   Sharma, R.; Wu, X.; Rhodes, S. D.; Chen, S.; He, Y.; Yuan, J.; Li, J.; Yang, X.; Li, X.; Jiang, L.; Kim, E. T.; Stevenson, D. A.; Viskochil, D.; Xu, M.; Yang, F. C., Hyperactive Ras/MAPK signaling is critical for tibial nonunion fracture in neurofibromin-deficient mice. *Hum Mol Genet* **2013**.

10.   Wang, W.; Nyman, J. S.; Ono, K.; Stevenson, D. A.; Yang, X.; Elefteriou, F., Mice lacking Nf1 in osteochondroprogenitor cells display skeletal dysplasia similar to patients with neurofibromatosis type I. *Hum Mol Genet* **2011,** *20* (20), 3910-24.

11.	Traub, J.; O'Connor, W.; Masso, P., Congenital pseudarthrosis of the tibia: A retrospective review. *Journal of Pediatric Orthopaedics* **1999,** *19* (6), 735-738.

12.	Lakkis, M.; Epstein, J., Neurofibromin modulation of ras activity is required for normal endocardial-mesenchymal transformation in the developing heart. *Development* **1998,** *125* (22), 4359-4367.

13.	Brannan, C.; Perkins, A.; Vogel, K.; Ratner, N.; Nordlund, M.; Reid, S.; Buchberg, A.; Jenkins, N.; Parada, L.; Copeland, N., Targeted disruption of the neurofibromatosis type-1 gene leads to developmental abnormalities of the heart and various neural crest-derived tissues. *Genes & Development* **1994,** *8* (22), 2792-2792.

14.	Jacks, T.; Shih, T.; Schmitt, E.; Bronson, R.; Bernards, A.; Weinberg, R., Tumor predisposition in mice heterozygous for a targeted mutation in NF1. *Nature Genetics* **1994,** *7* (3), 353-361.

15.	Zhu, Y.; Romero, M. I.; Ghosh, P.; Ye, Z.; Charnay, P.; Rushing, E. J.; Marth, J. D.; Parada, L. F., Ablation of NF1 function in neurons induces abnormal development of cerebral cortex and reactive gliosis in the brain. *Genes & development* **2001,** *15* (7), 859-76.

16.	Rodda, S. J.; McMahon, A. P., Distinct roles for Hedgehog and canonical Wnt signaling in specification, differentiation and maintenance of osteoblast progenitors. *Development* **2006,** *133* (16), 3231-44.

17.	Chen, J.; Shi, Y.; Regan, J.; Karuppaiah, K.; Ornitz, D. M.; Long, F., Osx-Cre targets multiple cell types besides osteoblast lineage in postnatal mice. *PLoS One* **2014,** *9* (1), e85161.

18.	Maes, C.; Kobayashi, T.; Selig, M. K.; Torrekens, S.; Roth, S. I.; Mackem, S.; Carmeliet, G.; Kronenberg, H. M., Osteoblast precursors, but not mature osteoblasts, move into developing and fractured bones along with invading blood vessels. *Dev Cell* **2010,** *19* (2), 329-44.

19.   Schindeler, A.; Ramachandran, M.; Godfrey, C.; Morse, A.; McDonald, M.; Mikulec, K.; Little, D., Modeling bone morphogenetic protein and bisphosphonate combination therapy in wild-type and Nf1 haploinsufficient mice. *Journal of Orthopaedic Research* **2008,** *26* (1), 65-74.

20.   Schlegel, K.; Thorwarth, M.; Plesinac, A.; Wiltfang, J.; Rupprecht, S., Expression of bone matrix proteins during the osseus healing of topical conditioned implants: an experimental study. *Clinical Oral Implants Research* **2006,** *17* (6), 666-672.

21.   Schliephake, H.; Aref, A.; Scharnweber, D.; Bierbaum, S.; Roessler, S.; Sewing, A., Effect of immobilized bone morphogenic protein 2 coating of titanium implants on peri-implant bone formation. *Clinical Oral Implants Research* **2005,** *16* (5), 563-569.

22.   Stevens, D. M.; Gilmore, K. A.; Harth, E. M., An assessment of nanosponges for intravenous and oral drug delivery of BCS class IV drugs: Drug delivery kinetics and solubilization. *Polymer Chemistry* **2014**.

23.   Spears, B.; Waksal, J.; McQuade, C.; Lanier, L.; Harth, E., Controlled branching of polyglycidol and formation of protein-glycidol bioconjugates via a graft-from approach with "PEG-like" arms. *Chemical Communications* **2013,** *49* (24), 2394-2396.

24.   Kolanczyk, M.; Kuhnisch, J.; Kossler, N.; Osswald, M.; Stumpp, S.; Thurisch, B.; Kornak, U.; Mundlos, S., Modelling neurofibromatosis type 1 tibial dysplasia and its treatment with lovastatin. *Bmc Med* **2008,** *6*, 21.

25.   Wang, W.; Nyman, J. S.; Moss, H. E.; Gutierrez, G.; Mundy, G. R.; Yang, X.; Elefteriou, F., Local low-dose lovastatin delivery improves the bone-healing defect caused by Nf1 loss of function in osteoblasts. *Journal of bone and mineral research : the official journal of the American Society for Bone and Mineral Research* **2010,** *25* (7), 1658-67.

26.   van der Ende, A. E.; Kravitz, E. J.; Harth, E., Approach to formation of multifunctional polyester particles in controlled nanoscopic dimensions. *Journal of the American Chemical Society* **2008,** *130* (27), 8706-8713.

27.   Tan, A. M.; Tan, C. L.; Phua, K. B.; Joseph, V. T., Chemotherapy for hepatoblastoma in children. *Annals of the Academy of Medicine, Singapore* **1990,** *19* (2), 286-9.

CHAPTER VI

POST-MODIFICATION REACTIONS: ASSESSMENT OF NANOSPONGES FOR

TARGETED DRUG DELIVERY

Introduction

Despite significant advancements in drug discovery and the development of many promising therapeutics, numerous diseases such as cancer remain difficult to treat. The discovery of siRNA and the burgeoning field of gene therapy potentially marked the end of even the most severe and rare diseases. Although these promising therapies work well *in vitro*, significant obstacles arose when translating to animal models and humans. One of the biggest obstacles is delivering the therapeutics to a specific site of action. For example, cancer therapeutics affect healthy cells as well as cancerous cells which results in side effects such as neutropenia and myelosuppression.[1] Ideally, the cancer drugs would attack only the tumor cells having no effect on healthy cells. Therefore, a need still exists to develop advanced targeted drug delivery technologies to overcome these obstacles.

In the case of cancer treatment, most drug delivery strategies target cell surface receptors that are commonly upregulated in numerous cell types.[2] Many common receptors have been targeted including transferrin[3, 4], EGFR[5], and folate[6]. Ligands with high specificity for these receptors have been identified and attached to nanoparticle surfaces to act as targeted drug delivery vehicles as well as diagnostic markers for cell progression.[7] Integrin receptors have also been identified to be highly upregulated in tumor cells[8, 9], and RGD containing peptide sequences have been used as targeting agents to help treat tumors since they bind with high

affinity for integrin receptors.[10] In this work, we investigated the potential of our developed, multifunctional nanosponges to attach targeting peptides and imaging dyes for cell surface targeting of cancer cells. The nanosponge is an excellent platform vehicle for this purpose due to the pendant functionalities that can undergo post-modification reactions. For example, accessible alkene groups from the nanoparticle surface can be utilized to undergo thiolene click reactions with thiol-containing targeting ligands to form covalent bonds.

The loss of pancreatic beta cells is a major hallmark of type 1 diabetes, and despite its worldwide prevalence, much is still unknown regarding its pathology. Therefore, the ability to noninvasively quantitate beta cell mass and directly target therapeutic cargo to these cells are paramount to enable a greater understanding of diabetes pathology, provide a diagnostic marker for both type 1 and type 2 diabetes, and help develop current and new therapeutic approaches. Pancreas transplants and islet cell transplantation are available medical options, but it is difficult to quantitatively measure the number of surviving islets after transplantation. Currently, radiolabels can be used to quantitate biomarkers of beta cells, but this only indirectly reflects beta cell mass and does not determine whether the beta cell mass is increasing or decreasing.[11] Other imaging agents have been investigated as well including glucose analogs[12] and antibodies[13] but have failed to provide an accurate quantitative measure of beta cells. Pancreatic islet cell mass can be measured histologically, but this requires surgical removal of the pancreas.[14] Therefore, a major medical goal is to develop a method to measure the increase and decrease of beta cell mass over time and indicate the appropriate time course to intervene if necessary. Currently, there is no way to successfully target islet cell receptors with high specificity that would allow accurate quantification of beta cells or allow a targeted drug delivery approach.

A targeted, dye-labeled nanoparticle could potentially act as a way to image and quantitate beta cells in the pancreas as well as allow the potential for drug delivery to these specific cells to treat type 1 or type 2 diabetes. An ideal vehicle to image or deliver therapeutic cargo directly to the beta cells in Islets of Langerhans would be non-toxic and biodegradable, allow flexible payloads for delivery of a wide range of drugs, possess targeting capabilities specifically to the islet surface, and have high-affinity to the islets with minimal off target effects. As previously demonstrated, the polyester nanosponge is a biodegradable platform delivery vehicle that is capable of encapsulating and releasing drugs and also possesses pendant functionalities on the particle surface for post-modification reactions such as attaching targeting moieties. The major advantages of the nanosponge include: tailored nanoscopic size, adjustable crosslinking density to control drug release at a defined release rate, conjugation of various targeting ligands via thiolene click reactions, and attachment of reporter dyes via NHS-ester chemistry or hydrazide-aldehyde orthogonal chemistry.

Exendin-4 (also known as exenatide) is an agonist for the glucagon-like peptide-1 receptor[15] and has been shown to be an effective treatment for diabetes patients.[16] Its high affinity for the GLP1 receptor makes it an attractive targeting ligand for beta cells in the Islets of Langerhans. Compared to antibodies, peptides are much easier to handle, less sensitive, and easier to analyze in regards to organic modification reactions such as conjugation to a nanoparticle surface. Exendin-4 is commercially available and can be synthesized with a cysteine amino acid on the N-terminus that would allow for thiolene click reactions with alkenes without affecting peptide activity. Therefore, a nanoparticle with pendant exendin-4 peptides and imaging dyes could potentially act as diagnostic tools to accurately measure beta cell mass within the pancreas. Additionally, targeted nanoparticles have the potential to be loaded with

various drugs for the direct treatment of cells in the pancreas. In this work, we investigated orthogonal chemistries to attach exendin-4 and imaging dyes to the surface of nanoparticles to act as targeted vehicles to cells expressing GLP1 receptor, particularly pancreatic islet cells.

Results and Conclusions

The introduced functionalities of the nanoparticles are utilized for post-modification reactions including targeting peptide attachments and dye attachments. Multi-step orthogonal chemistry approaches were developed in order to eliminate side reactions that could potentially interfere with the structure or activity of the biologically active targeting peptides. For cancer cell targeting strategies, a cRGD peptide was covalently linked to the nanoparticle surface followed by a dye attachment step which was then incubated with HeLa cells and imaged for cell-surface localization. For pancreatic islet cell targeting strategies, cysteine-modified exendin-4 was attached to the nanoparticle surface followed by dye attachment using orthogonal aldehyde-hydrazine chemistry.
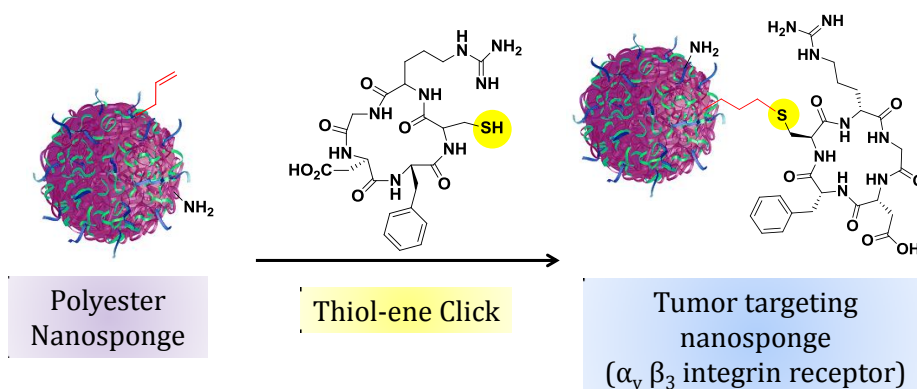

Figure VI-1. Attachment of cRGD peptide to nanoparticle surface via thiolene click.

Attachment of cRGD peptide and imaging dye to nanoparticle surface via thiolene click and NHS-ester chemistries

The pendant functionalities of the nanosponge and its solubility in organics allow for simple post-modification reactions. Polyester nanosponges can be synthesized to contain a defined number of alkene groups which can then be utilized for reactions such as thiolene click. In this study, 100 nm nanoparticles containing 4% avl and 7% crosslinking density were reacted with thiol-functionalized cRGD peptide using UV and 2,2-dimethoxy-2-phenylacetophenone as a photoinitiator. The success of the reaction can be analyzed with ^{1}H NMR by observing the slight reduction of the alkene peaks at 5.0 ppm and 5.7 ppm as well as the emergence of the peptide peaks at 4.4-4.7 ppm and 7.2 ppm of the purified product (Figure VI-2).
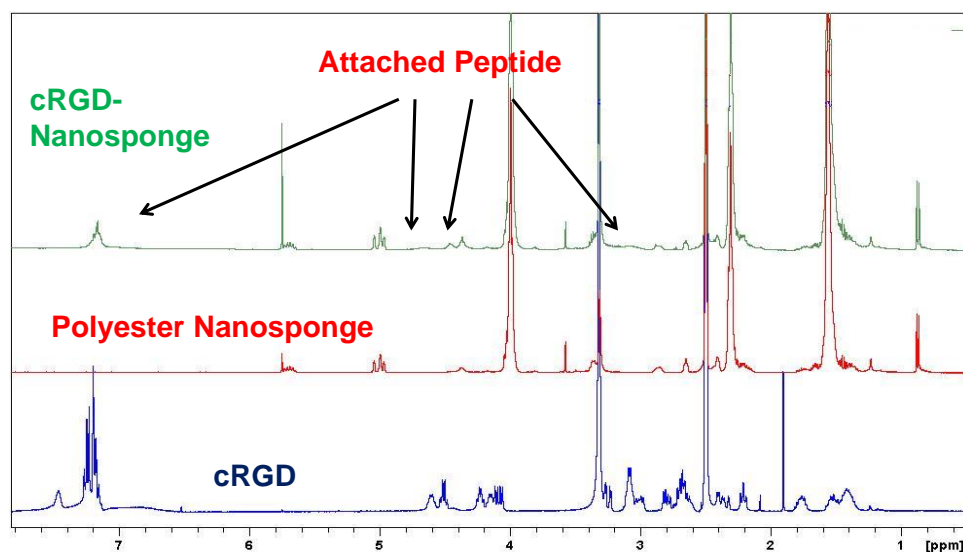

Figure VI-2. ^{1}H NMR spectra of cRGD peptide (bottom), polyester nanosponge (middle), and purified sample of nanoparticle with cRGD attached (top).

Since the nanoparticle synthesis uses an excess of bis(amine) crosslinker, free amines remain that can also be utilized for post-modification reactions. In order to determine targeting

capabilities of the cRGD-modified nanoparticle, an imaging dye attached to the nanoparticle is required. Simple and efficient NHS-ester chemistry was employed to react an NHS-ester AlexaFluor dye with the primary amines of the nanoparticle to form an amide.

In vitro imaging of fluorescent, targeted nanoparticles in HeLa cells

HeLa cells were chosen to test the targeting capabilities of the cRGD-nanoparticles due to their overexpression of integrin receptors.[17] Fluorescently-labeled, targeted nanoparticles were added to HeLa cells and imaged with confocal microscopy, and cell surface attachment was seen within two hours of incubation which is comparable to other nanovehicles using similar targeting strategies.[18, 19] No cell surface or cell uptake was seen in a non-targeted nanoparticle control group after 2 hours. This suggests that improved cancer cell targeting is due to the cRGD attachment to the nanoparticle surface as expected.
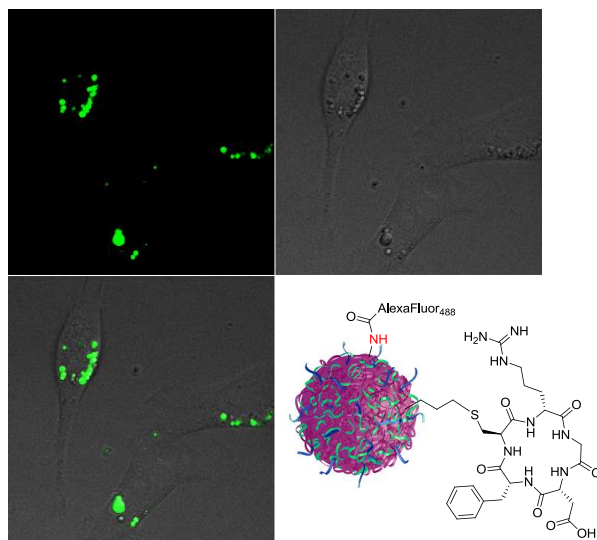

Figure VI-3. Confocal microscopy (63x magnification) of HeLa cells treated with AlexaFluor488 labeled, cRGD-nanosponges for two hours at a nanoparticle concentration of 70 µg/mL.

Orthogonal chemistries for sequential exendin-4 and dye attachment to nanoparticle surface

Biologically active targeting moieties are often sensitive to organic chemistry reactions and functionalized dye attachment is not always specific. For example, NHS-ester dyes can be used to attach dyes to particles that have pendant free amine groups; however, targeting peptides typically have at least one amine in the peptide structure which can potentially react with the dye. Therefore, orthogonal chemistry approaches must be carefully designed in order to successfully attach both targeting ligands and reporter dyes to the nanoparticle surface without side reactions. A combination of hydrazide-aldehyde and thiolene click reactions was employed to sequentially attach peptide and reporter dye to the surface of the nanoparticle (Figure VI-4).
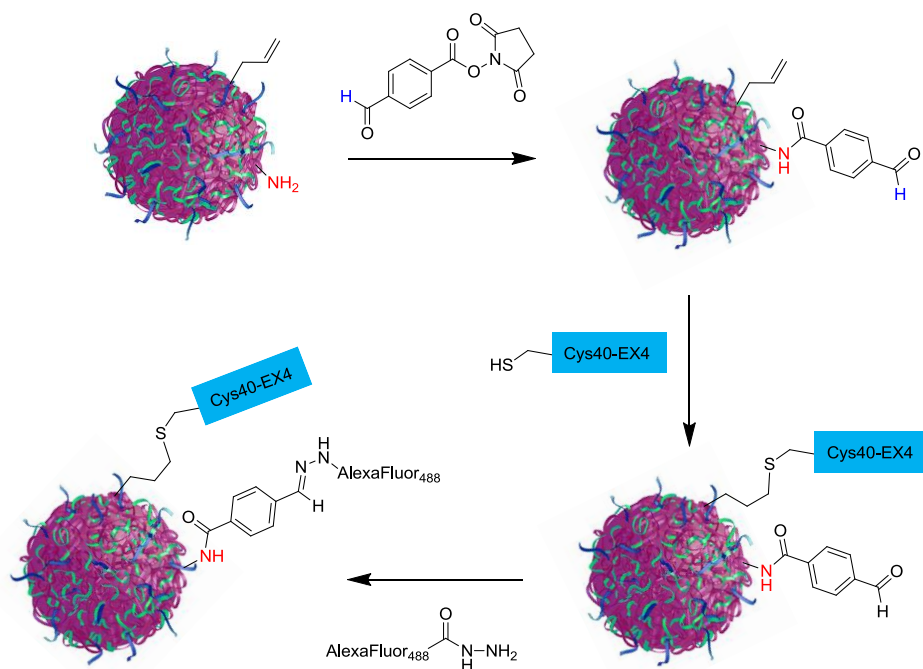

Figure VI-4. Reaction scheme to orthogonally attach Cys40-EX4 peptide and AlexaFluor dye to the nanoparticle.

In the first step, *N*-succinimidyl-p-formylbenzoate was reacted with a 100 nm nanoparticle containing 5% avl and 5% crosslinking density via NHS-ester chemistry overnight in DMSO and purified by dialysis. ^{1}H NMR showed the presence of aromatic peaks as well as aldehyde peaks from the aldehyde linker at 8.1-8.3 and 10.2 ppm, respectively. A cysteine-40 modified exendin-4 (Cys40-EX4) was added to this product along with 2,2-dimethoxy-2-phenylacetophenone to act as a photoinitiator, and this mixture was irradiated at 365 nm for 24 hours in deuterated DMSO. Deuterated solvent was used in order to easily analyze the reduction of alkenes via ^{1}H NMR without having to perform a purification step to remove the DMSO. The marked reduction of the allyl peaks as seen in Figure VI-5 indicates the success of the covalent attachment between the thiol and allyl group. Additionally, a significant retention time shift of the peptide was seen in the HPLC chromatograph after attachment to the nanoparticle surface which supports the success of the thiolene click reaction (Figure VI-6).
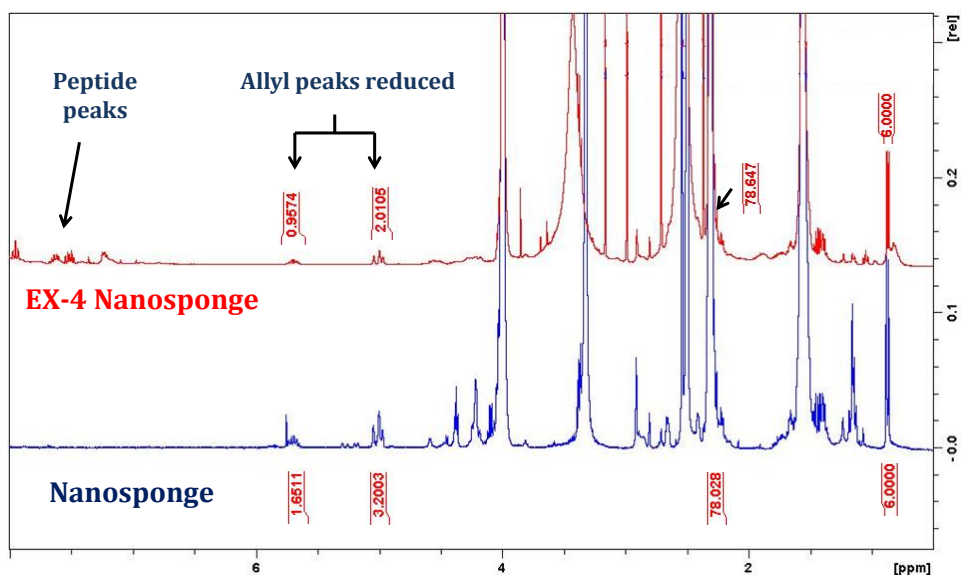
Figure VI-5. ^{1}H NMR spectra of nanosponge before and after exendin-4 peptide attachment.

In the final step, the hydrazide functionalized dye (iFluor750) as added to the EX-4 modified nanoparticles in DMSO and allowed to stir overnight. The hydrazide reacts directly with the aldehyde to form a hydrazone. This type of reaction is commonly found in protein conjugation kits that react well between pH 5 and pH 7. The final product was dialyzed to remove any potential free peptide as well as any unreacted dye.
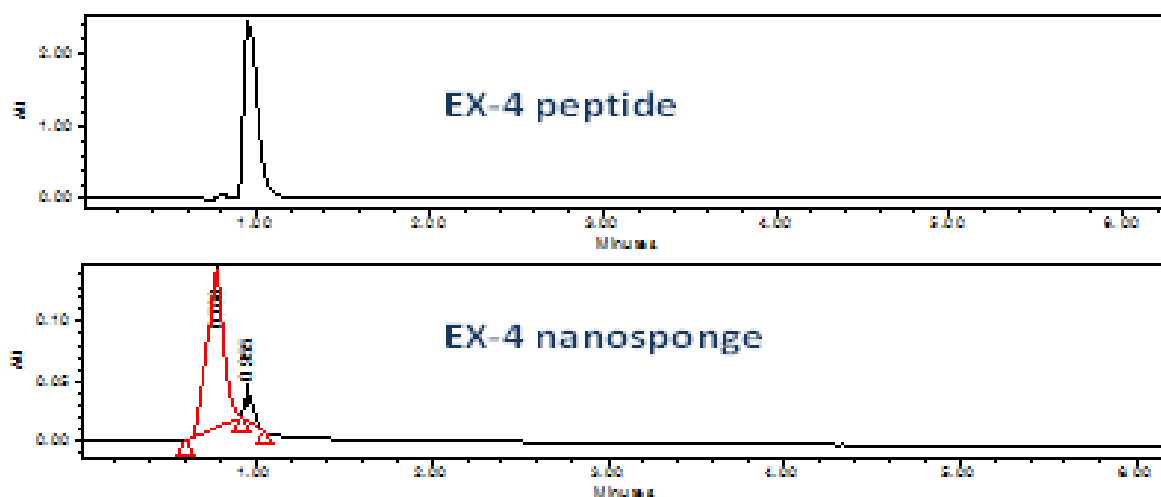
Figure VI-6. HPLC chromatograph of peptide (top) and nanoparticle after peptide attachment (bottom).

GLP1 receptor activation from EX-4 modified nanosponges

In order to confirm that exendin-4 activity was preserved after nanoparticle attachment, cAMP levels were measured in HEK 293 cells expressing GLP1R after treatment with the cys40-modified exendin-4 peptide, EX-4 modified nanoparticles (EX4-NP), and non-targeted nanoparticles (NP) and forskalin was used as a positive control (Figure VI-7). In this preliminary study, 1 μM of cys40-exendin-4 resulted in a 20-fold change of cAMP compared to basal levels as expected since exendin-4 activation of GLP1R increases cAMP. Similar cAMP levels were

achieved using the exendin-4 modified nanosponges (equivalent to 1 μM EX-4) indicating that exendin-4 activity is preserved even after attachment to the nanoparticle surface. Since 0.1 μM of EX4-NP also achieved a 20-fold change of cAMP levels, it's apparent that the cAMP response is not dose-dependent at these concentrations, and saturation has likely occurred. Therefore, lower concentrations should be utilized in future studies to achieve a dose-response curve that will better indicate if any exendin-4 activity is impacted due to nanoparticle attachment. Nevertheless, this preliminary experiment suggests that the exendin-4 modified nanosponges successfully bind and activate GLP1R and can be utilized as potential targeted drug delivery vehicles to cells expressing GLP1R, particularly the beta cells in the pancreatic islets.
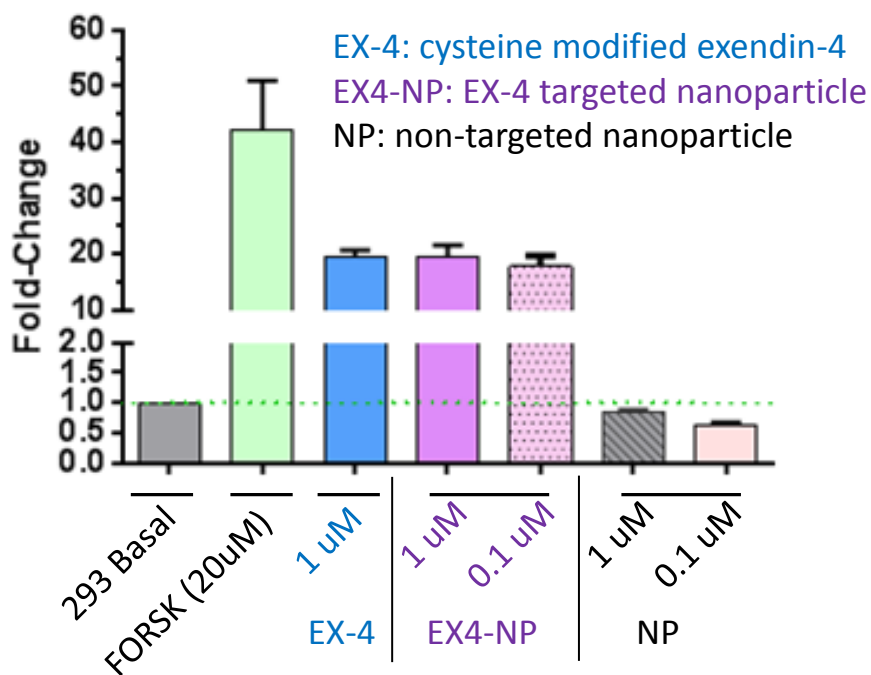

Figure VI-7. Measurement of cAMP levels in 293 cells after treatment with exendin-4, exendin-4 modified nanoparticles, and nanoparticle alone. Experiment and data were produced by Dr. Neil Phillips of the Al Powers Lab.

Biodistribution of EX-4 modified nanosponges *in vivo*

In order to test EX-4 modified nanosponges' ability to preferentially locate to GLP1R expressing cells, *in vivo* experiments must be undertaken. Although the ultimate goal is to specifically target the islet cells in the pancreas, an easier and more practical proof-of-concept experiment is to first target ectopic tumors from a cell line that over-expresses GLP1R. Tumors that over-express the GLP1 receptor will be grown in the hind legs of mice, and fluorescently labeled, targeted nanoparticles will be administered systemically. As a control, a separate set of mice will grow tumors from a similar cell line that does not express GLP1R.

The mice will undergo near infrared imaging at various time points. If successful, targeted nanosponges will preferentially locate to the GLP1R-expressing tumor over time whereas the nanosponges should be cleared from the mice containing the tumors that don't express GLP1R. The mice handling and imaging will be performed by Dr. Neil Phillips of the Al Powers Laboratory at Vanderbilt University.

Conclusion

Post-modification reactions were successfully utilized to attach targeting peptides and imaging dyes to the surface of nanoparticles for both cancer and diabetes applications. The attachment of cRGD peptides to the nanoparticle surface resulted in the cell surface localization of the nanoparticles in cancer cells. Therefore, this targeted drug delivery system could potentially act as a useful strategy to deliver chemotherapeutics directly to the tumor.

For the purpose of pancreatic islet cell targeting, a cysteine modified EX-4 was successfully attached to the nanoparticle using thiolene click chemistry. A unique aldehyde-hydrazide chemistry was employed to attach dyes to the surface of the nanosponge without

affecting the peptide. Preliminary experiments showed EX-4 activity was preserved despite nanosponge attachment and therefore can act as a targeting ligand for beta cells in pancreatic islets. The further development of this targeted delivery system could have major implications for the treatment of type 1 diabetes.

Experimental

Materials

Cyclic-RGD peptide was obtained from Peptides International and used as received. Cysteine-40 modified exendin-4 was obtained from Chem-Impex International and used as received. Alexafluor488 was received from Life Technologies and iFluor750 was acquired from AAT Bioquest. N-succinimidyl-p-formylbenzoate was purchased from Santa Cruz Biotechnology and used as received. Snakeskin pleated dialysis tubing was purchased from Thermo Scientific. DMEM was purchased from Gibco by Life Sciences and supplemented with 10% fetal bovine serum and 5% antibiotic-antimycotic. All other materials were obtained from Sigma Aldrich or Gibco by Life Technologies and used as received.

Characterization

^{1}H NMR spectra were obtained from a Bruker AC400 Fourier Transform Spectrometer with CDCl$_3$/TMS as solvent. High-performance liquid chromatography (HPLC) was carried out using a Waters chromatograph equipped with a Waters 2996 variable wavelength photodiode array detector, a Waters 1525 binary HPLC pump, and a reverse phase column (100 x 4.6 mm i.d., pore size 5 μm, Thermo Scientific). All runs were performed using an isocratic gradient of water and acetonitrile (1:1 v/v) at a flow rate of 1 mL/min. Confocal microscopy was performed using

a Zeiss Inverted LSM 510 Meta laser scanning confocal microscope, equipped with an argon laser, a 543 nm HeNe laser, a Plan-Neofluar 40x/1.3 oil lens and a Plan-Apochromat 63x/1.4 oil lens.

Synthesis of cRGD functionalized nanoparticle (cRGD-NP)

100 nm nanoparticles containing 7% epoxide and 4% allyl were synthesized as reported previously. In a nitrogen-purged 1-dram vial, nanoparticle (20 mg, Mw per alkene = 1408.5 g/mole, 1.42×10^{-5} moles alkene) was dissolved in a minimal amount of anhydrous, degassed DMSO (~0.100 mL). Cyclic RGD peptide (3.1 mg, Mw = 578.27 g/mole, 0.38 eq with respect to alkene, 5.33×10^{-6} moles) and 2,2-dimethoxy-2-phenylacetophenone (0.728 mg, 0.2 eq with respect to alkene, 2.84×10^{-6} moles) in minimal amount of DMSO were added to the nanoparticle solution and allowed to stir at 37 °C under UV lamp (365 nm) for 48 hours. Product was purified by dialyzing in Snakeskin Pleated Dialysis tubing (MWCO = 10,000 Da) against acetonitrile:methanol (50:50).

AlexaFluor488 dye attachment to cRGD-NP (cRGD-NP-488) and nontargeted nanoparticles (NP-488)

In a nitrogen-purged 1-dram vial, cRGD-NP (4.0 mg) was dissolved in DMSO (0.200 mL). AlexFluor488 (51.5 µL, 5 mg/mL stock in DMSO) was added to the vial using a microsyringe, the vial was covered in foil to protect from light, and the reaction was allowed to stir for 24 hours at room temperature. Product was purified by dialyzing in Snakeskin Pleated Dialysis tubing (MWCO = 10,000 Da) against acetonitrile: methanol (50:50). To form a non-targeted, fluorescent nanoparticle, the same reaction was performed except using nanoparticles without cRGD attached.

Confocal microscopy

HeLa cells were plated on uncoated 14 mm Microwell (MatTek) dishes at a density of 3×10^5 cells in medium. On the day of experiments, cells were washed three times with PBS and then incubated with phenol red free, high glucose DMEM containing 70 µg/mL of either cRGD-NP-488, NP-488, or unlabeled nanoparticle as a negative control for 2 hours at 37 °C in a 5% CO_2 environment. The cells were then washed four times with PBS to remove nanoparticles that did not undergo cell uptake or cell surface attachment, and 0.5 mL Opti-MEM was added for imaging.

Synthesis of aldehyde functionalized nanoparticle via NHS-ester chemistry

Nanoparticles (36.9 mg, 0.246 µmols) were added to a flame-dried, argon-purged 1-dram vial and dissolved in a minimal amount of anhydrous DMSO. *N*-succinimidyl-p-formylbenzoate (58 µL, 0.127 M in DMSO) was added and allowed to stir for 24 hours. The reaction was dialyzed with Snakeskin pleated dialysis tubing (MWCO = 10,000 g/mol) against dichloromethane. ^{1}H NMR confirmed presence of aromatic protons at 8.1-8.3 ppm and aldehyde protons at 10.2 ppm.

Sequential attachment of exendin-4 peptide via thiolene click chemistry and dye attachment via hydrazide chemistry

In a 1-dram vial, aldehyde-functionalized nanoparticle (15.0 mg, 5.67×10^{-6} moles alkene) was dissolved in a minimal amount of deuterated DMSO. Cys40-Exendin-4 peptide (3.9 mg, 9.00×10^{-7} moles) and 2,2-dimethoxy-2-phenylacetophenone (0.29 mg, 0.2 eq with respect to alkene, 1.13×10^{-6} moles) in minimal amount of deuterated DMSO were added to the nanoparticle solution and allowed to stir room temperature and exposed to UV (365 nm) for 24 hours. Crude ^{1}H NMR confirmed reduction of the allyl peaks and presence of peptide peaks. The crude

reaction mixture was used for next step to avoid product loss from an unnecessary purification step. EX-4 functionalized nanoparticle was already dissolved in DMSO from the previous reaction (15.0 mg, 1×10^{-7} mol). Alexafluor488 dye (0.57 mg from a 5 mg/mL stock solution in dmso, 1×10^{-6} mol) was added to the nanoparticles. Reaction stirred for 24 hours in darkness followed by dialysis against methanol/acetonitrile (50:50).

References

1.   Rowinsky, E.; Jiroutek, M.; Bonomi, P.; Johnson, D.; Baker, S., Paclitaxel steady-state plasma concentration as a determinant of disease outcome and toxicity in lung cancer patients treated with paclitaxel and cisplatin. *Clinical Cancer Research* **1999,** *5* (4), 767-774.

2.   Bielenberg, D.; Pettaway, C.; Takashima, S.; Klagsbrun, M., Neuropilins in neoplasms: Expression, regulation, and function. *Experimental Cell Research* **2006,** *312* (5), 584-593.

3.   Sahoo, S.; Ma, W.; Labhasetwar, V., Efficacy of transferrin-conjugated paclitaxel-loaded nanoparticles in a murine model of prostate cancer. *International Journal of Cancer* **2004,** *112* (2), 335-340.

4.   Davis, M.; Zuckerman, J.; Choi, C.; Seligson, D.; Tolcher, A.; Alabi, C.; Yen, Y.; Heidel, J.; Ribas, A., Evidence of RNAi in humans from systemically administered siRNA via targeted nanoparticles. *Nature* **2010,** *464* (7291), 1067-U140.

5.   Ciardiello, F.; Tortora, G., Epidermal growth factor receptor (EGFR) as a target in cancer therapy: understanding the role of receptor expression and other molecular determinants that could influence the response to anti-EGFR drugs. *European Journal of Cancer* **2003,** *39* (10), 1348-1354.

6.   Hattori, Y.; Maitani, Y., Folate-linked nanoparticle-mediated suicide gene therapy in human prostate cancer and nasopharyngeal cancer with herpes simplex virus thymidine kinase. *Cancer Gene Therapy* **2005,** *12* (10), 796-809.

7.   Benedetto, S.; Pulito, R.; Crich, S.; Tarone, G.; Aime, S.; Silengo, L.; Hamm, J., Quantification of the expression level of integrin receptor alpha(V)beta(3) in cell lines and MR imaging with antibody-coated iron oxide particles. *Magnetic Resonance in Medicine* **2006,** *56* (4), 711-716.

8.   Lossner, D.; Abou-Ajram, C.; Benge, A.; Reuning, U., Integrin alpha v beta 3 mediates upregulation of epidermal growth-factor receptor expression and activity in human ovarian cancer cells. *International Journal of Biochemistry & Cell Biology* **2008,** *40* (12), 2746-2761.

9.   Petricevic, B.; Vrbanec, D.; Jakic-Razumovic, J.; Brcic, I.; Rabic, D.; Badovinac, T.; Ozimec, E.; Bali, V., Expression of Toll-like receptor 4 and beta 1 integrin in breast cancer. *Medical Oncology* **2012,** *29* (2), 486-494.

10.   Lim, Y.; Kwon, O.; Lee, E.; Kim, P.; Yun, C.; Lee, M., A cyclic RGD-coated peptide nanoribbon as a selective intracellular nanocarrier. *Organic & Biomolecular Chemistry* **2008,** *6* (11), 1944-1948.

11.   Freeby, M.; Goland, R.; Ichise, M.; Maffei, A.; Leibel, R.; Harris, P., VMAT2 quantitation by PET as a biomarker for beta-cell mass in health and disease. *Diabetes Obesity & Metabolism* **2008,** *10*, 98-108.

12.   Nakamoto, Y.; Higashi, T.; Sakahara, H.; Tamaki, N.; Itoh, K.; Imamura, M.; Konishi, J., Evaluation of pancreatic islet cell tumors by fluorine-18 fluorodeoxyglucose positron emission tomography - Comparison with other modalities. *Clinical Nuclear Medicine* **2000,** *25* (2), 115-119.

13.   Moore, A.; Bonner-Weir, S.; Weissleder, R., Noninvasive in vivo measurement of beta-cell mass in mouse model of diabetes. *Diabetes* **2001,** *50* (10), 2231-2236.

14.   Signore, A.; Procaccini, E.; Toscano, A.; Ferretti, E.; Williams, A.; Beales, P.; Cugini, P.; Pozzilli, P., Histological study of pancreatic beta-cell loss in relation to the insulitis process in the nonobese diabetic mouse. *Histochemistry* **1994,** *101* (4), 263-269.

15.   Ding, X.; Saxena, N.; Lin, S.; Gupta, N.; Anania, F., Exendin-4, a glucagon-like protein-1 (GLP-1) receptor agonist, reverses hepatic steatosis in ob/ob mice. *Hepatology* **2006,** *43* (1), 173-181.

16.   Bunck, M.; Diamant, M.; Corner, A.; Eliasson, B.; Malloy, J.; Shaginian, R.; Deng, W.; Kendall, D.; Taskinen, M.; Smith, U.; Yki-Jarvinen, H.; Heine, R., One-year Treatment With Exenatide Improves beta-Cell Function, Compared With Insulin Glargine, in Metformin-Treated Type 2 Diabetic Patients A randomized, controlled trial. *Diabetes Care* **2009,** *32* (5), 762-768.

17.   Ryu, J.; Bickerton, S.; Zhuang, J.; Thayumanavan, S., Ligand-Decorated Nanogels: Fast One-Pot Synthesis and Cellular Targeting. *Biomacromolecules* **2012,** *13* (5), 1515-1522.

18.   Braun, K.; Wiessler, M.; Pipkorn, R.; Ehemann, V.; Bauerle, T.; Fleischhacker, H.; Muller, G.; Lorenz, P.; Waldeck, W., A cyclic-RGD-BioShuttle functionalized with TMZ by DAR(inv) "Click Chemistry" targeted to alpha(v)beta(3) integrin for therapy. *International Journal of Medical Sciences* **2010,** *7* (6), 326-339.

19.   Yin, P.; Wang, Y.; Qiu, Y.; Hou, L.; Liu, X.; Qin, J.; Duan, Y.; Liu, P.; Qiu, M.; Li, Q., Bufalin-loaded mPEG-PLGA-PLL-cRGD nanoparticles: preparation, cellular uptake, tissue distribution, and anticancer activity. *International Journal of Nanomedicine* **2012,** *7*, 3961-3969.

CHAPTER VII

POLYCARBONATE HYDROGELS WITH TUNABLE SWELLING AND DRUG RELEASE

Introduction

Polymeric networks continue to be essential in the development of hydrogel materials for advanced biomedical applications.[1, 2, 3] These polymer networks are versatile and increasingly important materials due to their tunable network composition that can be reconfigured in simultaneous network forming and deforming processes. Such materials have helped make significant improvements in the area of tissue engineering in segmenting biological and synthetic structures and in the area of re-shapeable glass like polymers called vitrimers. Much effort has been devoted towards acrylate based materials as they are biocompatible and hydrophilic with the ability to swell, protect, and release their cargo.[4, 5] One of the hallmarks of hydrogels is the ability to absorb large amounts of water and swell many times its own weight.[6] For years, researchers have developed smart, or stimuli-responsive, materials in which the chemical or mechanical properties of the hydrogel can change depending on temperature, pH, magnetic field, and solvent.[7, 8, 9, 10] However, degradability of these materials has been an obstacle since functionalized linear acrylates and multi-arm-PEG structures are the two main components that have pioneered the field on hydrogels to react under mild and fast reaction conditions such as thiolene click reactions.

Current research in the field is devoted to include degradable components and to investigate stimuli free reactions such as amine-oxime reactions in addition to other click reactions.[11] Although hydrogels have been demonstrated to act as useful vehicles for drug

delivery applications[12, 13, 14, 15, 16], one of the major limitations is the rapid release of the therapeutic.[6] Therefore, advanced hydrogel materials are required to overcome the limitation of rapid drug release in order to allow slower, adjustable drug release rates that can satisfy various medical needs. Although the hydrophobicity of degradable materials such as polyesters and polycarbonates offer some challenge if a high swellability of the material is anticipated, hydrophobic small molecules have a higher residence time in hydrophobic materials as opposed to hydrophilic materials in which a rapid release of therapeutics is a common problem.

To improve the rate of drug release and swellabilities in hydrogels, a balance between crosslinking density, hydrophilicity, and hydrophobic components must be accomplished. In this work, we sought to improve and further tune the swellabililty and hydrophilicity by introducing a three component system consisting of a linear polycarbonate, a linear dithiol ethylene oxide unit, and a novel semi-branched polyglycidol with a high number of reactive –OH groups, a branched PEG mimic. Recently discovered semi-branched polyglycidols maintain a lower branching compared to hyper-branched materials but resemble a shorter overall structure and more compatible version to higher molecular PEG units. This molecule is hydrophilic due to the large number of pendant hydroxyls which is thought to enhance the hydrophilicity of a gel when introduced within the gel network. Polycarbonates are one of the most well-known degradable polymers, and the improvement of synthetic procedures such as organo-catalyzed and metal catalyzed reactions enabled the integration of polycarbonates into complex materials. For example, intermolecular crosslinking with difunctionalized short PEG diamines and disulfides facilitated nanoparticles in a variety of selected sizes which consist of nanonetworks from hydrophilic and hydrophobic components.[17] This same concept of polymer crosslinking is translated to the development of three component hydrogels to form improved hydrogels that

include semibranched polyglycidol component. The polyglycidol does not participate the crosslinking reaction but rather acts as a "filler" in the network to influence the swelling and to control the drug release. However, the OH-functional groups of the polyglycidol can be made part of the hydrogel network through transesterification reactions in the presence of $Zn(OAc)_2$ to reconfigure the network. In this work, we synthesized and studied the influence of the width of the network maintained by the difunctional crosslinker and the introduction of the semibranched polyglycidol on swelling and drug release.

Results and Discussion

We report the synthesis polycarbonate based hydrogels that contain semi-branched polyglycidols entrapped into the polycarbonate-diethylene oxide matrix. The primary OH groups of the polyglycidol can react in a transesterification reaction to form reconfigurable crosslinked materials. We first synthesized allyl functionalized linear polycarbonates with $Sn(OTf)_2$ as catalyst and isoamyl alcohol as initiator. In a reaction with dithiol ethylene oxides, a crosslinked network was formed via thiolene click reactions in the presence or absence of semi-branched polyglycidols. The resulting two hydrogel materials were characterized via water swelling capabilities and degradation in phosphate buffered saline. Additionally, these gels could be formed in the presence of drugs thereby entrapping the drug within the network in a non-covalent manner. Paclitaxel was chosen as a model drug to study the drug release from these two carriers and was incorporated during the crosslinking reaction. The presence of the polyglycidol as well as the length of the dithiol crosslinker influenced the swelling capabilities and were responsible for a varied drug release behavior. Additionally, the present polyglycidol can be covalently attached to the network in a transesterification reaction with $Zn(OAc)_2$. The

reconfigurable nature of the transesterification reactions leads to novel materials which are tougher than the comparable hydrogels which only carry the entrapped semi-branched polyglycidols. The present work introduces and compares the effects of polyglycidols as components into polycarbonate crosslinked materials that are either present or absent in order to shape the physicochemical properties of hydrogels used as drug delivery materials.

Thiolene click model reaction

Allyl-functionalized polycarbonate was synthesized as previously reported.[18] To demonstrate the efficacy of the click reaction, dithiol crosslinker was added to a solution of poly(MAC, MEC) (1 thiol per alkene) and DMPA (0.2 equivalents per alkene) in DMSO-d6 at a concentration of 0.21 M and irradiated with UV light for 5 minutes. The sample was then immediately analyzed by ^{1}H NMR which indicated greater than 95% conversion based on the reduction of the alkene shifts at 5.87 ppm and 5.20 ppm. Therefore, the thiolene click reaction is rapid and successful, even at dilute concentrations. The model reaction was completed using dilute conditions since concentrated conditions result in the formation of hydrogel materials which are insoluble in solvent and cannot be analyzed by NMR.

Hydrogel Synthesis

Hydrogels were formed via thiolene click crosslinking of allyl-functionalized carbonate copolymers and a dithiol crosslinker. The polycarbonate copolymer was synthesized as reported previously.[18] The PC and PC-1.5k hydrogels were prepared by reacting the allyl with the short or long (1.5k) dithiol crosslinker in DMF with DMPA (0.2 eq per alkene) under UV light (365 nm) for 5 minutes. Gels readily formed within minutes and were rinsed with methanol and water to

remove unreacted material and residual DMF. Yields were determined by measuring the dried mass of the gel compared to the total mass of the precursor reactants, and typical yields were greater than 90%.
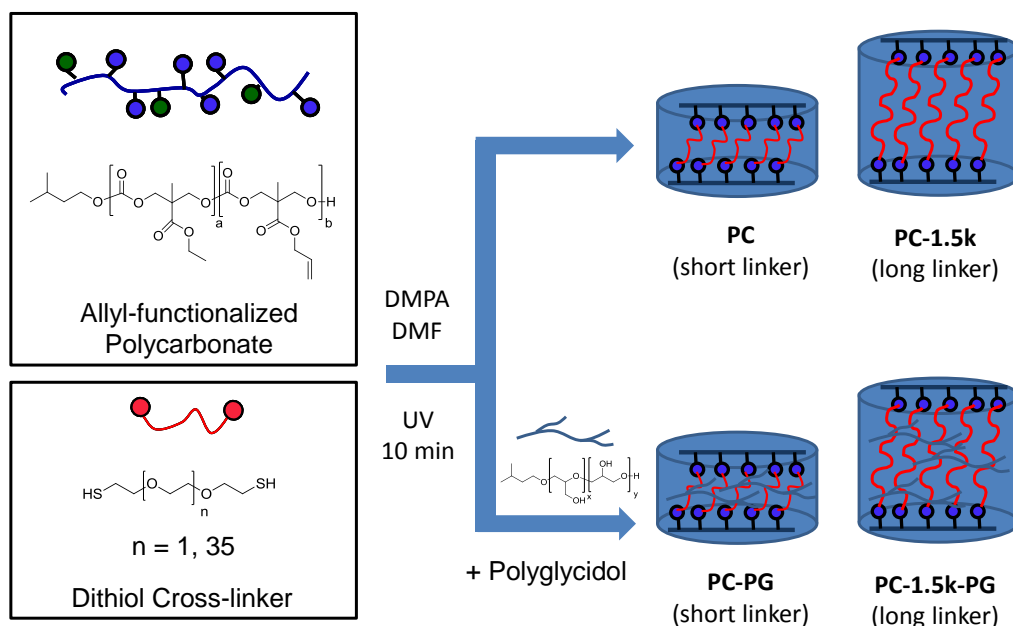

Figure VII-1. Synthesis of polycarbonate gels with short or long dithiol crosslinker in the presence or absence of polyglycidol.

In a separate series of gels, water-soluble polyglycidol was added to the precursor mix to investigate the change of gel properties due to introducing a hydrophilic component to the hydrogel matrix. Additionally, the entrapped polyglycidol can be used for post-modification reactions such as transesterification. These gels (PC-PG and PC-1.5k-PG) contained a 1:1 ratio of polycarbonate to polyglycidol by mass and were synthesized by reacting the allyl of the polycarbonate with the short or long (1.5k) dithiol crosslinker as described previously. The polyglycidol did not impede the thiolene reaction and was successfully incorporated into the

crosslinking network as indicated by the yields (greater than 75%) after soaking and rinsing with water and methanol sequentially. To ensure free polyglycidol was effectively washed away, these gels were soaked in water before rinsing several times with water and methanol.

Zinc acetate mediated transesterification reaction for gel network reconfiguration

Zinc acetate has been shown to promote transesterification rearrangements at high temperatures.[19] Thus, zinc acetate was mixed into the polymer precursor solution before gel formation to demonstrate reconfiguration capabilities. After gel formation, the gel was added to a 120 °C oil bath overnight, yielding a physically tougher gel due to the polyglycidol becoming covalently attached to the ester side groups of the polycarbonate. Thermogravimetric analysis (TGA) was used to characterize the materials before and after the transesterification step. As seen in the top TGA curve in Figure VII-2, the polymer materials began to degrade at 270 °C. Looking at the first-derivative curve (%/°C), two inflection points were seen at around 300 °C and 400 °C which indicate the points of greatest rate of weight change. The two inflection points are typical of a mixture which makes sense considering the polycarbonate gel and polyglycidol are non-covalently attached. However, a significant change in the TGA curve was seen after transesterification. As seen in the bottom TGA curve in Figure VII-2, the change in weight curve is more representative of a single-component material. Although two inflection points were still seen in the first-derivative curve (%/°C), the greatest rate of weight change occurred at 360 °C. These findings suggest the material underwent chemical modification during the transesterification step. Since transesterification is reversible, it's likely that not all polyglycidol became covalently linked within the network which would account for the first inflection point seen at 240 °C.
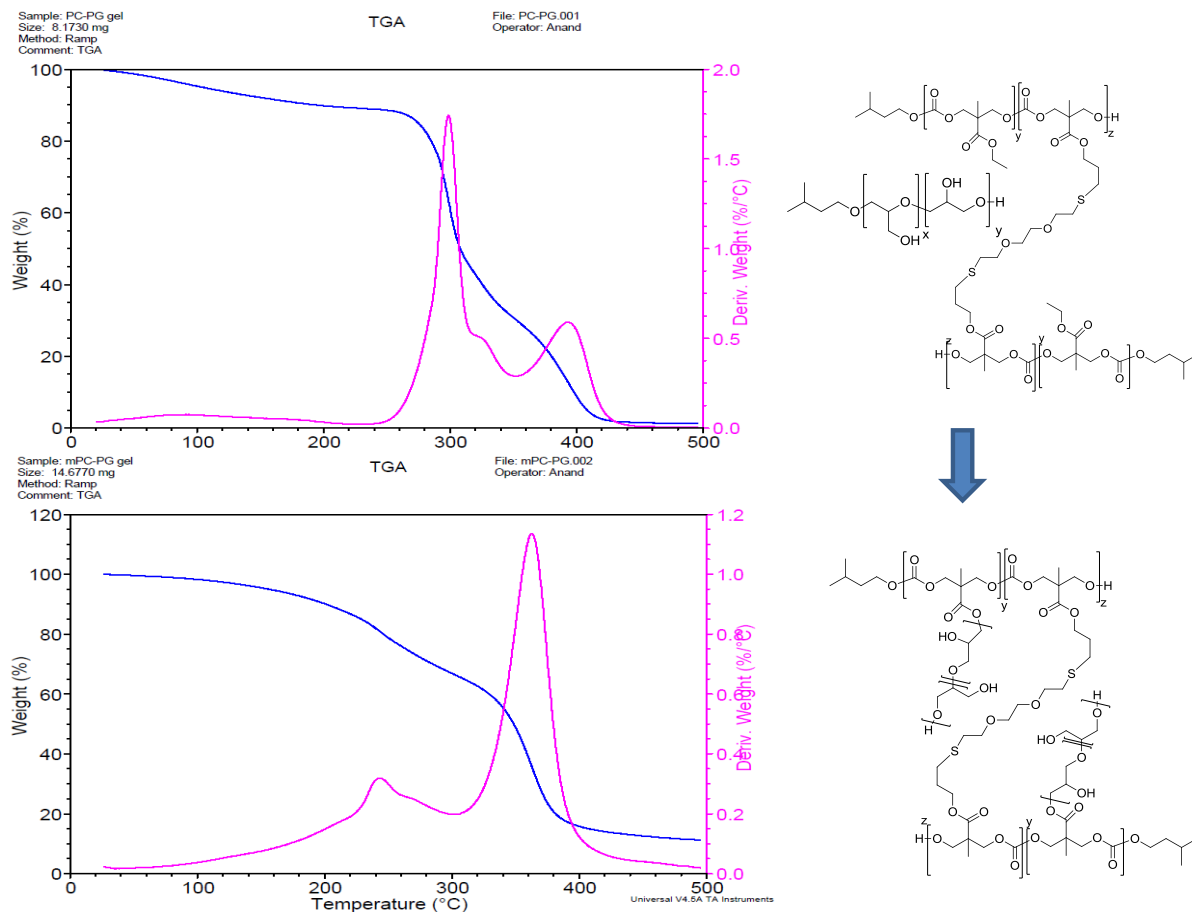
Figure VII-2. Thermogravimetric analysis of polycarbonate-polyglycidol hydrogel before (top) and after zinc acetate catalyzed transesterification (bottom). Analysis and data provided by Anand Rahalkar of the Muthukumar laboratory, University of Massachusetts Amherst.

Tunable swelling ability of hydrogels

Although gels made from hydrophilic polymers typically exhibit excellent water sorption capabilities[20], the hydrogels prepared in this study had low to moderate water sorption ability. As expected, water swelling increased with increasing hydrophilicity within the gel network. Equilibrium water content at room temperature averaged 20.0% for PC gels, 85.5% for PC-PG gels, 179% for PC-1.5k gels, and 211% for PC-1.5k-PG gels, and the swelling ability was not

sensitive to temperature or pH (Figure VII-3). The low water absorption for PC is expected due to the very hydrophobic nature of the polycarbonate backbone. Although the presence of the ethylene oxide crosslinker allows for a more hydrophilic environment, it is not enough to overcome the hydrophobicity of the polycarbonate unless the PEG crosslinker has a significantly greater molecular weight such as with the PC-1.5k gels, which had 9-fold greater swelling values compared to the PC gels. Also, the presence of polyglycidol in the network improved water swelling significantly, likely due to its hydrophilic nature. By simply adding this hydrophilic "filler" to the short crosslinker gels, swelling values increased over 4-fold. It is important to note that the recorded dried mass of the gels before and after swelling in water were generally consistent with each other, indicating insignificant degradation and loss of material during the duration of these swelling experiments. However, PC-PG and PC-1.5k gels lost mass after swelling in simulated gastric fluid (SGF), likely due to degradation but also because the gels broke into smaller pieces which made it difficult to measure the mass.
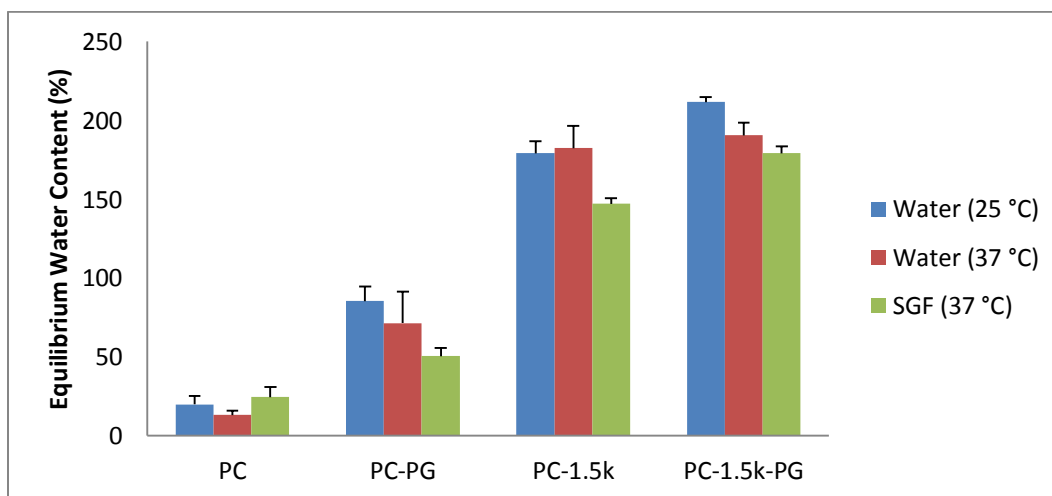

Figure VII-3. Swelling ability of each type of gel in water (25 and 37 °C) and simulated gastric fluid (pH 1.2).

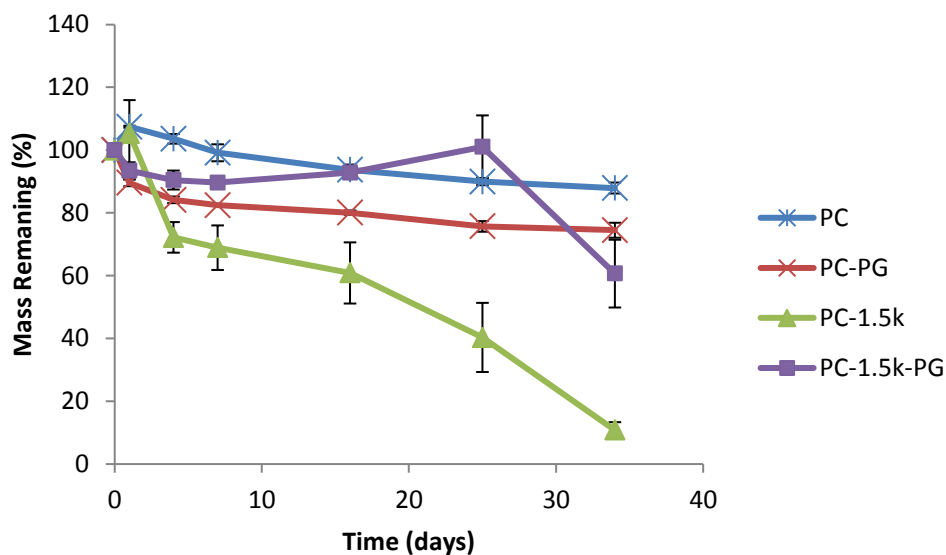**Hydrolytic degradation profiles of hydrogels**

Figure VII-4. Degradation profiles of each gel in PBS at 37 °C.

Polycarbonate materials typically degrade hydrolytically at very slow rates[21], and previous studies indicate the primary method of degradation of these gels is from hydrolysis of the ester side-group.[22] For *in vivo* applications, predictable gel degradation is imperative, and a tunable degradation would be ideal to meet specific needs of individual biomedical applications. Degradation experiments of the prepared gels were conducted under simulated physiological conditions (PBS pH 7.4 at 37 °C) and monitored by measuring the swelled mass over time. In all cases, the gels degraded slowly (Figure VII-4). Interestingly, gels containing the short crosslinker had significantly slower degradation rates with PC at 88% and PC-PG at 74% remaining mass after 34 days. This is likely due to the overwhelming hydrophobicity of these gels which are less likely to attract water for hydrolysis. PC-1.5k-PG gained mass up to day 25 before a loss of mass was recorded at day 34. The increase of mass over time can be attributed to the enhanced

swelling ability of the gel as the hydrophilic network of this gel is more exposed to water as the ester bonds degrade over time, and this agrees with what is reported with similar gels using long PEG-crossinkers.[22] Surprisingly, this trend was not seen for the PC-1.5k gel which had almost completed degraded by day 34.

Paclitaxel encapsulation and drug release

Gel	Average [PTX] released per day
PC-1.5k-PG	6.4 μM
PC-1.5k	4.2 μM
PC-PG	2.6 μM
PC	1.5 μM
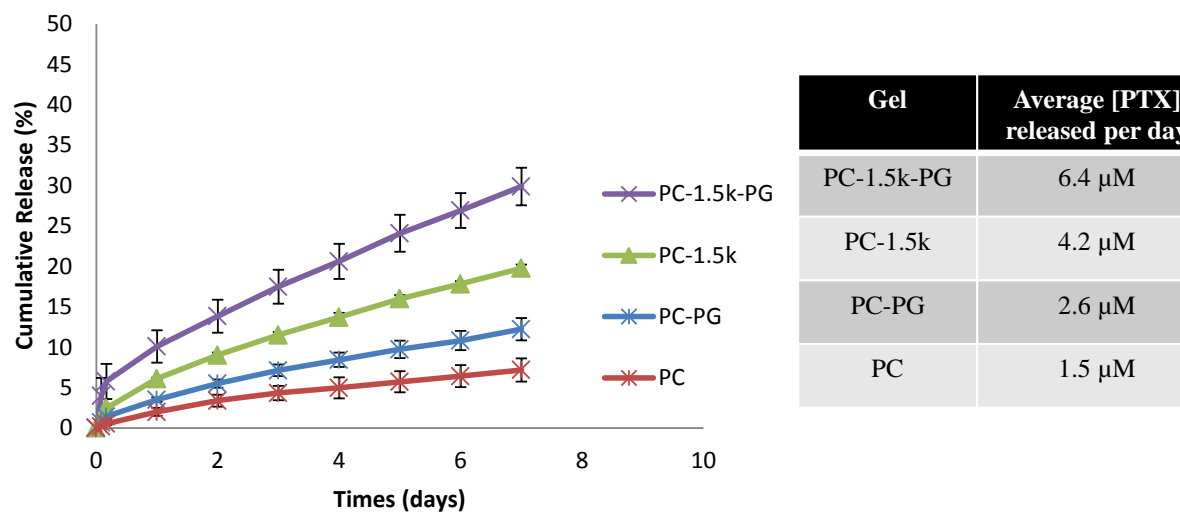
Figure VII-5. Left: Cumulative release of paclitaxel in PBS at 37 °C. Right: Average released paclitaxel concentration per day for each gel.

In order to encapsulate paclitaxel into the gel, the drug was mixed with the polymer precursors prior to gel formation, and these gels were purified as described previously. The solvent rinses were collected and analyzed for non-encapsulated paclitaxel by HPLC. Loading efficiency was determined by comparing the amount of non-encapsulated drug with the amount initially added to the polymer mix, and in all cases, loading efficiency was very high (> 98%).

PTX-loaded gels were placed in PBS (pH 7.4) at 37 °C to monitor the *in vitro* release rate of paclitaxel. In all cases, paclitaxel was released at controlled rates with PC achieving as low as 7.2% drug release and PC-1.5k-PG achieving as high as 29.9% drug release after 7 days. The rate of release is somewhat proportional to the gel's water swellability as the gels with greater swelling ability released paclitaxel at faster rates. This makes sense as more swelling would potentially allow faster rates of diffusion of paclitaxel from the gel. The differences in release rates may also be attributed to greater pore size within the gel networks. For example, PC-1.5k achieved 19.8% drug release after 7 days compared to 7.2% achieved by PC. The use of the significantly longer linker (1.5k) greatly enhances the hydrophilicity within the gel network, but it also potentially increases pore size within the network as crosslinks will not be as closely-knit as seen with the shorter crosslinker in PC. Additionally, polyglycidol played a significant role in drug release as seen in the 12.2% drug release after 7 days with the PC-PG gel which is 1.7-fold faster than PC. Again, this is attributable to polyglycidol's ability to enhance hydrophilicity within the network, but since polyglycidol acts as an additive, it can potentially affect pore size and drug release kinetics as well.[23]

PC and PC-PG gels containing paclitaxel were also used to measure drug release in simulated gastric fluid (pH 1.2) to determine if these gels could retain their therapeutic cargo in acidic conditions for an oral drug delivery route. In both cases, very little paclitaxel (less than 3%) was released even after 12 hours in the simulated gastric fluid. This suggests that these types of gels could potentially be investigated as an oral drug formulation. Also, the ability to withstand the acidic conditions of the stomach allows these gel materials to potentially act as enteric coating for other drug formulations.
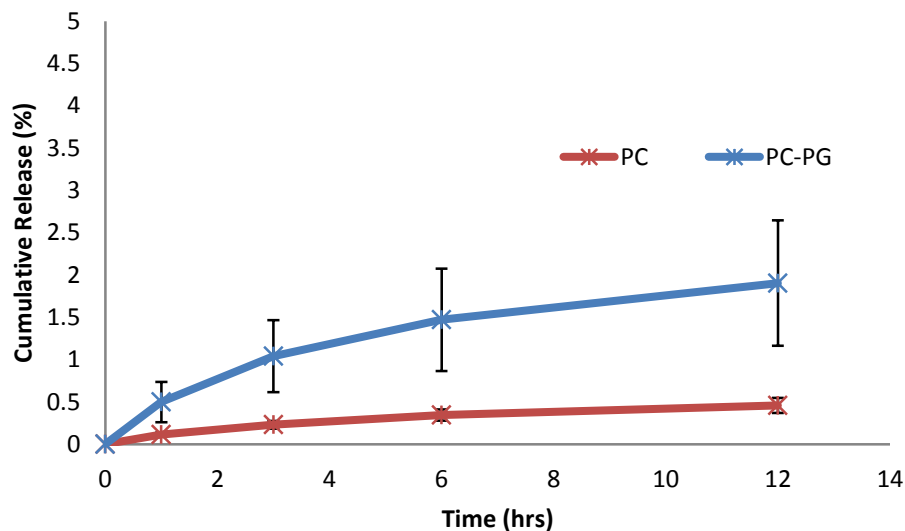
Figure VII-6. Cumulative release of paclitaxel in simulated gastric fluid at 37 °C.

Conclusion

A series of hydrogels were synthesized and characterized by their water swelling ability, degradation profile, and drug release profile. Indeed, allyl-functionalized polycarbonates undergo thiolene click reactions with dithiol crosslinkers to form insoluble, gel materials when conditions are concentrated. Hydrogels were formed with different sized crosslinkers in the presence or absence of a hydrophilic component, polyglycidol. The insertion of a hydrophilic component within the gel network caused significant effects on water swelling ability as well as rate of drug release. Additionally, increasing the size of the dithiol-PEG crosslinker resulted in similar effects. All gels degraded hydrolytically at slow rates and therefore could be used for various drug delivery routes including oral and implants. The ability to form a gel in the presence of a drug allows the possibility to create novel drug delivery formulations of a therapeutic that requires sustained release, and the overall drug release rate can be adjusted by manipulating the

118

hydrophilicity within the gel network. Therefore, this novel hydrogel material can act as a platform delivery formulation to meet the needs of various sustained release applications.

Experimental

Materials

Poly(MAC, MEC) and polyglycidols were synthesized as reported previously.[18, 24] Spectra/Por® Dialysis membrane was purchased from Spectrum Laboratories Inc. Phosphate Buffered Saline (PBS) was obtained from Gibco by Life Technologies and pH was adjusted to 7.4. Simulated gastric fluid (SGF) was prepared by mixing 2.0 g NaCl with 7.0 mL concentrated HCL, diluting with water to 1.0 L, and adjusting pH to 1.2. All other chemicals were purchased from Sigma-Aldrich and used as received

Characterization

^{1}H NMR spectra were obtained from a Bruker AC400 Fourier Transform Spectrometer, with DMSO-d6 as the solvent. High-performance liquid chromatography (HPLC) was carried out using a Waters chromatograph equipped with a Waters 2996 variable wavelength photodiode array detector, a Waters 1525 binary HPLC pump, and a reverse phase column (100 x 4.6 mm i.d., pore size 5 μm, Thermo Scientific). All runs were performed using an isocratic gradient of water and acetonitrile (1:1 v/v) at a flow rate of 1 mL/min. Thermogravimetric analysis (TGA) was carried out using an Universal V4.5A TA instrument and heated from 25 °C to 500 °C at a rate of 10 °C/min. TGA analysis was conducted and provided by Anand Rahalker of the Muthukumar lab at University of Massachusetts Amherst.

Synthesis of polycarbonate hydrogel via thiolene click (PC and PC-1.5k)

3,6-dixoa-1,8-octanedithiol (8.6 uL, 5.2 x 10^{-2} mmol) was added to a solution of poly(MAC, MEC) (100 mg, Mn = 4,712 Da, 0.105 mmol alkene) and 2,2-dimethoxy-2-phenylacetophenone (DMPA, 0.2 eq per alkene, 5.4 mg) in DMF (100 uL). The solution was UV-irradiated (365 nm) for 5 minutes. The resulting gel (PC) was soaked and rinsed sequentially with methanol and water to remove unreacted starting material and solvent, and gel was dried via lyophilization. Gels containing longer crosslinker (PC-1.5k) were synthesized in the same manner but using PEG-dithiol (78.6 mg, Mn = 1,500 Da, 5.2 x 10^{-2} mmol) instead of 3,6-dixoa-1,8-octanedithiol.

Synthesis of polycarbonate/polyglycidol hydrogel via thiolene click (PC-PG and PC-1.5k-PG)

3,6-dixoa-1,8-octanedithiol (8.6 uL, 5.2 x 10^{-2} mmol) was added to a solution of poly(MAC, MEC) (100 mg, Mn = 4,712 Da, 0.105 mmol alkene), polyglycidol (100 mg), and 2,2-dimethoxy-2-phenylacetophenone (DMPA, 0.2 eq per alkene, 5.4 mg) in DMF (100 uL). The solution was UV-irradiated (365 nm) for 5 minutes. The resulting gel (PC-PG) was soaked and rinsed sequentially with methanol and water to remove unreacted starting material and solvent, and gel was dried via lyophilization. Gels containing longer crosslinker (PC-1.5k-PG) were synthesized in the same manner but using PEG-dithiol (78.6 mg, Mn = 1,500 Da, 5.2 x 10^{-2} mmol) instead of 3,6-dixoa-1,8-octanedithiol.

Synthesis of PTX-loaded hydrogels and encapsulation efficiency

Hydrogels were synthesized as previously described, but paclitaxel was added (10 mg paclitaxel per 100 mg poly(MAC, MEC)) to the polymer solution prior to UV irradiation. The resulting gels were soaked and rinsed with water multiple times. The washes were collected, lyophilized,

and analyzed by HPLC to determine mass of non-encapsulated paclitaxel. Encapsulation efficiency was determined using the equation:

$$\left(\frac{M_{ptx(i)} - M_{ptx(w)}}{M_{ptx(i)}}\right) \times 100\%$$

where $M_{ptx(i)}$ is the initial mass of paclitaxel added to the reaction and $M_{ptx(w)}$ is the mass of washed paclitaxel determined by HPLC.

Swelling studies

Prepared gels were soaked in deionized water or simulated gastric fluid (pH = 1.2) and allowed to swell for 24 hours. The swelled gels were then gently blotted dry before recording the swelled mass (M_{sw}), and the sample was then lyophilized to record the dry mass (M_{dry}). The percent water content post-swelling was quantified using the following equation:

$$\frac{(M_{sw} - M_{dry})}{M_{dry}} \times 100\%$$

In vitro **drug release**

The release of paclitaxel from the gels was measured in PBS (pH 7.4) or simulated gastric fluid (pH 1.2), both buffers containing Tween-80 (0.1% v/v) and stirred at 37 °C. Initial paclitaxel concentration was 0.15 mM. At each time point, the supernatant was collected and replaced with an equal volume of fresh release medium. For release studies in PBS, the supernatant was directly analyzed by HPLC. For release studies in simulated gastric fluid, the supernatant was neutralized to pH 7 with sodium bicarbonate, extracted three times with dichloromethane, organic fractions were combined, and solvent was evaporated. The resulting sample was dissolved in acetonitrile/water (1:1, v/v) and analyzed by HPLC. Samples were injected (30 uL)

to a reverse phase column (100 x 4.6 mm i.d., pore size 5 um, Thermo Scientific) using an isocratic gradient of acetonitrile and water (1:1, v/v) with a variable wavelength detector (227 nm).

Degradation Studies

An initial swelled mass (M_i) was recorded by submerging the gels in PBS (pH 7.4) for 24 hours and gently blotting dry before recording the mass. Gels were then submerged in PBS (pH 7.4) at 37 °C for the duration of the experiment. At each time point, the gels were gently blotted and a mass was recorded (M_t) before being submerged into fresh PBS (pH 7.4) at 37 °C. The percent mass remaining at each time point was quantified using the following equation:

$$\frac{M_t}{M_i} \times 100\%$$

References

1.   Lee, K.; Mooney, D., Hydrogels for tissue engineering. *Chemical Reviews* **2001,** *101* (7), 1869-1879; van der Linden, H.; Herber, S.; Olthuis, W.; Bergveld, P., Stimulus-sensitive hydrogels and their applications in chemical (micro)analysis. *Analyst* **2003,** *128* (4), 325-331.

2.   Wang, K.; Burban, J.; Cussler, E., Hydrogels as separation agents. *Advances in Polymer Science* **1993,** *110*, 67-79.

3.   Bennett, S.; Melanson, D.; Torchiana, D.; Wiseman, D.; Sawhney, A., Next-generation HydroGel films as tissue sealants and adhesion barriers. *Journal of Cardiac Surgery* **2003,** *18* (6), 494-499.

4.   Li, Y.; Tang, Y.; Narain, R.; Lewis, A.; Armes, S., Biomimetic stimulus-responsive star diblock gelators. *Langmuir* **2005,** *21* (22), 9946-9954.

5.   Hu, Z.; Xia, X.; Marquez, M.; Weng, H.; Tang, L., Controlled release from and tissue response to physically bonded hydrogel nanoparticle assembly. *Macromolecular Symposia* **2005,** *227*, 275-284.

6.   Hoare, T.; Kohane, D., Hydrogels in drug delivery: Progress and challenges. *Polymer* **2008,** *49* (8), 1993-2007.

7.   Namdeo, M.; Bajpai, S.; Kakkar, S., Preparation of a Magnetic-Field-Sensitive Hydrogel and Preliminary Study of Its Drug Release Behavior. *Journal of Biomaterials Science-Polymer Edition* **2009,** *20* (12), 1747-1761.

8.   Zhao, B.; Moore, J., Fast pH- and ionic strength-responsive hydrogels in microchannels. *Langmuir* **2001,** *17* (16), 4758-4763.

9.   Verdejo, B.; Rodriguez-Llansola, F.; Escuder, B.; Miravet, J.; Ballester, P., Sodium and pH responsive hydrogel formation by the supramolecular system calix[4]pyrrole derivative/tetramethylammonium cation. *Chemical Communications* **2011,** *47* (7), 2017-2019.

10.   Li, Z.; Shen, J.; Ma, H.; Lu, X.; Shi, M.; Li, N.; Ye, M., Preparation and characterization of pH- and temperature-responsive hydrogels with surface-functionalized graphene oxide as the crosslinker. *Soft Matter* **2012,** *8* (11), 3139-3145.

11.   Grover, G.; Lam, J.; Nguyen, T.; Segura, T.; Maynard, H., Biocompatible Hydrogels by Oxime Click Chemistry. *Biomacromolecules* **2012,** *13* (10), 3013-3017.

12.   Kumar, P.; Lakshmanan, V.; Anilkumar, T.; Ramya, C.; Reshmi, P.; Unnikrishnan, A.; Nair, S.; Jayakumar, R., Flexible and Microporous Chitosan Hydrogel/Nano ZnO Composite Bandages for Wound Dressing: In Vitro and In Vivo Evaluation. *Acs Applied Materials & Interfaces* **2012,** *4* (5), 2618-2629.

13.   Kumar, P.; Raj, N.; Praveen, G.; Chennazhi, K.; Nair, S.; Jayakumar, R., In Vitro and In Vivo Evaluation of Microporous Chitosan Hydrogel/Nanofibrin Composite Bandage for Skin Tissue Regeneration. *Tissue Engineering Part a* **2013,** *19* (3-4), 380-392.

14.   Caicco, M.; Cooke, M.; Wang, Y.; Tuladhar, A.; Morshead, C.; Shoichet, M., A hydrogel composite system for sustained epi-cortical delivery of Cyclosporin A to the brain for treatment of stroke. *Journal of Controlled Release* **2013,** *166* (3), 197-202.

15.   Chen, X.; Zhi, F.; Jia, X.; Zhang, X.; Ambardekar, R.; Meng, Z.; Paradkar, A.; Hu, Y.; Yang, Y., Enhanced brain targeting of curcumin by intranasal administration of a thermosensitive poloxamer hydrogel. *Journal of Pharmacy and Pharmacology* **2013,** *65* (6), 807-816.

16.   Payyappilly, S.; Dhara, S.; Chattopadhyay, S., The heat-chill method for preparation of self-assembled amphiphilic poly(epsilon-caprolactone)-poly(ethylene glycol) block copolymer based micellar nanoparticles for drug delivery. *Soft Matter* **2014,** *10* (13), 2150-2159.

17.   Stevens, D. M.; Tempelaar, S.; Dove, A. P.; Harth, E., Nanosponge Formation from Organocatalytically Synthesized Poly(carbonate) Copolymers. *Acs Macro Letters* **2012,** *1* (7), 915-918.

18.   Stevens, D.; Watson, H.; LeBlanc, M.; Wang, R.; Chou, J.; Bauer, W.; Harth, E., Practical polymerization of functionalized lactones and carbonates with Sn(OTf)(2) in metal catalysed ring-opening polymerization methods. *Polymer Chemistry* **2013,** *4* (8), 2470-2474.

19.   Montarnal, D.; Capelot, M.; Tournilhac, F.; Leibler, L., Silica-Like Malleable Materials from Permanent Organic Networks. *Science* **2011,** *334* (6058), 965-968.

20.   Chang, C.; Duan, B.; Cai, J.; Zhang, L., Superabsorbent hydrogels based on cellulose for smart swelling and controllable delivery. *European Polymer Journal* **2010,** *46* (1), 92-100.

21.   Zhu, K.; Hendren, R.; Jensen, K.; Pitt, C., Synthesis, properties, and biodegradation of poly(1,3-trimethylene carbonate). *Macromolecules* **1991,** *24* (8), 1736-1740.

22.   Truong, V.; Barker, I.; Tan, M.; Mespouille, L.; Dubois, P.; Dove, A., Preparation of in situ-forming poly(5-methyl-5-allyloxycarbonyl-1,3-dioxan-2-one)-poly(ethylene glycol) hydrogels with tuneable swelling, mechanical strength and degradability. *Journal of Materials Chemistry B* **2013,** *1* (2), 221-229.

23.   Song, C.; Labhasetwar, V.; Levy, R., Controlled release of U-86983 from double-layer biodegradable matrices: Effect of additives on release mechanism and kinetics. *Journal of Controlled Release* **1997,** *45* (2), 177-192.

24.   Spears, B.; Waksal, J.; McQuade, C.; Lanier, L.; Harth, E., Controlled branching of polyglycidol and formation of protein-glycidol bioconjugates via a graft-from approach with "PEG-like" arms. *Chemical Communications* **2013,** *49* (24), 2394-2396.